Optimization and Control of an Energy Management System for Microgrids

OPTIMIZATION AND CONTROL OF AN ENERGY MANAGEMENT SYSTEM FOR MICROGRIDS

BY

XIANG YU, B.Eng.

A THESIS

SUBMITTED TO THE DEPARTMENT OF ELECTRICAL & COMPUTER ENGINEERING

AND THE SCHOOL OF GRADUATE STUDIES

OF MCMASTER UNIVERSITY

IN PARTIAL FULFILMENT OF THE REQUIREMENTS

FOR THE DEGREE OF

Master of Applied Science

Master of Applied Science (2014) McMaster University

(Electrical & Computer Engineering) Hamilton, Ontario, Canada

TITLE:	Optimization and Control of an Energy Management System for Microgrids
AUTHOR:	Xiang Yu B.Eng., (Electrical Engineering) McMaster University, Hamilton, Canada
SUPERVISORS:	Dr. S. Sirouspour, Dr. A. Emadi
NUMBER OF PAGES:	xvi, 117

To my wife Anqi, daughter Fandi, parents, parents in-law and my grandparents.

Abstract

An increasing concern over environmental impacts of fossil fuels and sustainability of energy resources is leading to significant changes in the electric power systems. Decentralized power generation, in particular, is emerging as one of the most effective and promising tools in addressing these concerns.

Microgrids are small-scale electricity grids with elements of load, generation and storage. Microgrids have emerged as an essential building block of a future smart grid, and an enabling technology for distributed power generation and control. This thesis presents an optimization-based approach for the design and control of energy management systems (EMS) for electric microgrids. A linear programming formulation of power/energy management is proposed to minimize energy cost for a microgrid with energy storage and renewable energy generation, by taking advantage of time-of-use (TOU) pricing. The thesis also addresses the issue of sizing of the battery storage and solar power generation capacity by formulating and solving a mixed integer linear programming (MILP) problem. The aim of the optimization is to minimize the combined capital and electricity usage cost subject to applicable physical constraints. Several case scenarios are analyzed for grid-connected microgrids in residential, commercial and industrial settings, as well as a case of an islanded microgrid intended for a remote community.

Finally, the thesis investigates circuit level control of a microgrid with EMS. A finite state machine based control logic is proposed that enables outage ride through and smooth transition between islanded and grid connected operation. Simulation results are provided to demonstrate the effectiveness of the proposed controller under various possible scenarios.

Acknowledgements

Many thanks and appreciation to my supervisors, Dr. Shahin Sirouspour and Dr. Ali Emadi, for their guidance, support and encouragement.

Special thanks to my family for their endless love and support since they have made it possible for me to accomplish my graduate study.

Sincere gratitude to my fellow colleagues, Pawel Malysz, Yanbo Xue, Berker Bilgin, Hao Ge, Haizhong Ye, Jin Ye, Weisheng Jiang, Yinye Yang, Aochi Yang, Parampreet Toor, Adihithya Ravichandran and Guotao Lin for their help in my research.

Notation and Abbreviations

Notations and abbreviations

AEMS - Adaptive Energy Management System

CHP - Combined Heat and Power

CSI - Current Source Inverter

DERs - Distributed energy Resources

DGs - Distributed Generations

EOB - Ontario Energy Board

EV - Electric Vehicle

HVAC - Heat Ventilation and Air Conditioning

kVA - kilovolt-amperes

kW - kilowatts

kWh - kilowatts-hours

MILP - Mixed Integer Linear Program

MPC - Model Predictive Control

MPPT - Maximum power point tracing

LP - Linear Program

ICE - Internal Combustion Engine

OEB - Ontario Energy Board

PDF - Probability Density Function

PV - Photovoltaic

RES - Renewable Energy Sources

SOC - State-of-Charge

TOU - Time-of-Use

V2G - Vehicle to Grid

VSI - Voltage Source Inverter

Contents

List of Figures

Chapter 1

Introduction

1.1 Motivation

Energy and sustainability are arguably the defining issues of the 21st Century (UnitedNation, 2013). As illustrated in Figure 1.1, in the United States, the electric power sector account for 40% of the total energy consumption in the year 2010 (USEIA, 2012). In 2010, the carbon dioxide emissions by electricity power sector were 2271 million metric tons (USEIA, 2012).

The current electricity grid has been operating in essentially the same way for a century now. It is based on centralized power generation produced mostly from fossil fuels and nuclear energy that is transmitted over a long distribution network to reach consumers. Short supply of fossil fuel, increasing emissions of greenhouse gases (Armstrong, 2007), and more frequent power outages have lead to renewed efforts in developing new concepts of electric power system to facilitate a more sustainable and greener operation. Researchers and government regulators have recognized that grid decentralization is among the most effective means of tackling the problem of energy

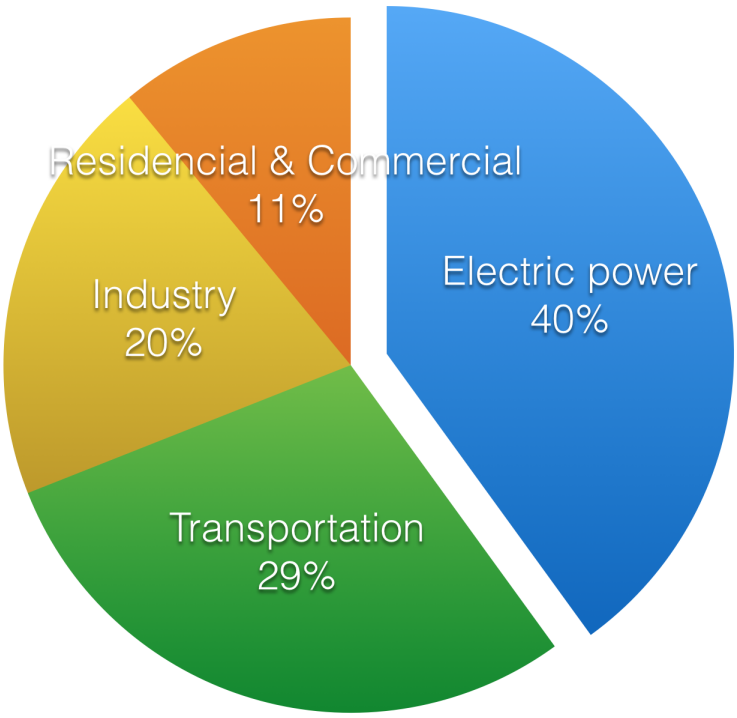

Figure 1.1: US primary energy consumption by sector in the year 2010 (USEIA, 2012).

scarcity. This can lead to transformational changes in the way we produce and consume energy helping to improve their sustainability, efficiency, security, reliability and scalability.

Generation Decentralization

Given that the efficiency of the current power system is around 30% (Lasseter, 2011), it is abundantly clearly that any effort in tackling our energy challenges must involve improvement of the efficiency of the electric power system. One way of tackling this problem is to reduce the distance between generation and demand through integration of distributed renewable energy sources such as solar and wind. This would not only lower reliance on dirty sources of energy,

but could also significantly reduce the transmission loss. Moreover, power outages cost the economy billions of dollars a year (LaCommare and Eto, 2006). Distributed renewable generation will help improve reliability of the power grid and reduce pollution and carbon emissions.

Demand-Side Control

Figure 1.2 shows the hourly energy usage in the province of Ontario, Canada in the year 2011. It is evident from the data in this figure that the electricity demand is highly time dependent. The peak load can be as much as twice of the off-peak load. The unbalanced nature of the load dramatically increases the generation cost of the system. The relatively inexpensive base-load generation cannot react fast enough to respond to rapid changes in the load during the peak time. Therefore, more expensive peak load generation and spin reserve are required for such purposes. The unbalanced load also creates problems in the transmission and distribution system, e.g. distribution transformers may over-heat during very hot summer days. Therefore it is necessary to have some degree of demand-side control in order to reduce variation between on-peak and off-peak demand, and hence lower the amount of peak power generation and spin reserve.

EV Integration

Figure 1.1 shows that the transportation sector accounts for 29% of total energy consumption in the U.S. Transportation electrification would be an essential element in any comprehensive solution to the problem of carbon emissions and climate change. However, deeper EV penetration can pose great challenges to

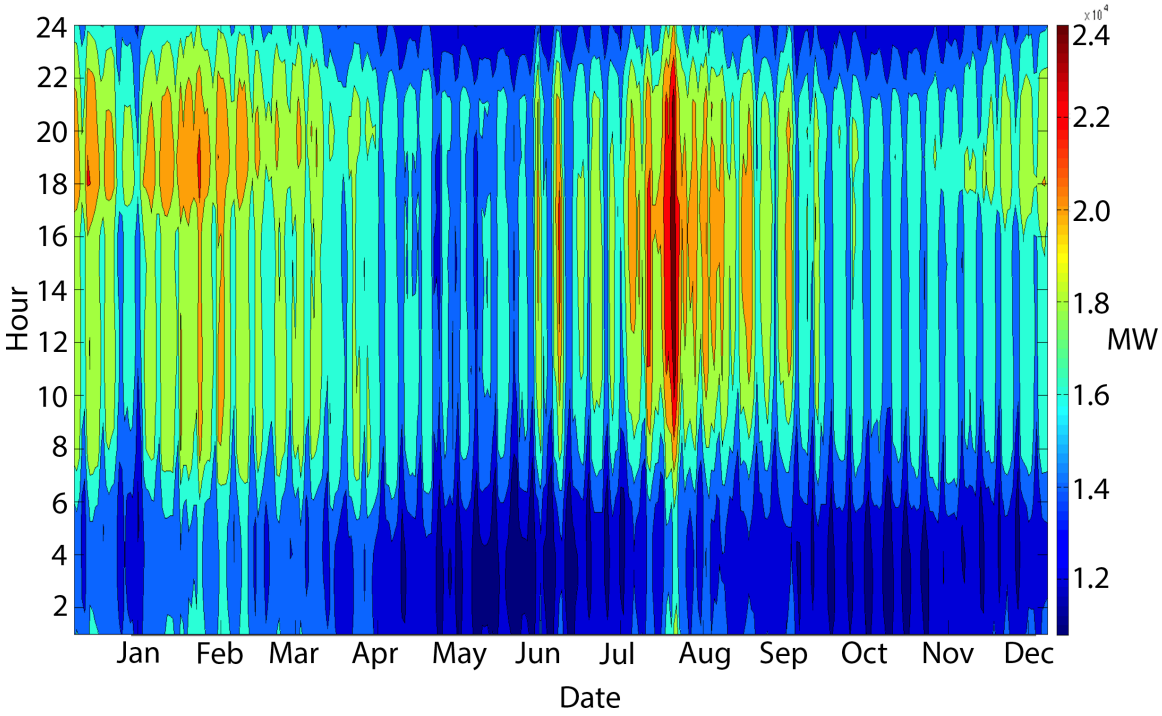

Figure 1.2: Ontario hourly energy usage, 2011 (IESO, 2013b)

the current generation and distribution system, specially to local distribution networks. Electric vehicles represent significant loads[1]. Charging EVs during the peak time can easily overload the local distribution networks, which were not designed to accommodate this extra demand. Given that it would be very costly to upgrade the existing generation capacity and distribution network, there is need for new technologies that could utilize distributed renewable energy sources reliably and add more controllability to the load.

Renewable Energy Integration

Massive integration of renewable energy generation is a must-taken step in our

[1]To charge a typical pure electrical vehicle with 24 kWh battery using Level 2 charger, it takes around 4 hours at 7 kVA. A typical Ontario utility distribution transformer's capacity is 50 kVA, which would supply 10-15 households.

efforts to reduce our carbon footprint. However, renewable sources of energy such as solar and wind are intermittent and cannot continuously provide a reliable supply of power. In fact lack of reliability is one of the main arguments of the critics of solar and wind energy. Addition of energy storage capacity to the electric grid can help alleviate some of these concerns by providing a mechanism for storing energy when is produced, and delivering it to the consumers, when is needed.

Electric microgrids with an energy management system (EMS) can help address many of the issues discussed above. Microgrids integrate distributed generations (DGs), distributed energy resources (DERs), energy storages and loads by their physical proximity for ease of control, power sharing and management. They provide electricity and other forms of energy for the benefit of the consumer. For ease of control, microgrid is treated as a single entry in the power grid and is transparent to the consumer (R. Lasseter and Stephens, 2002).

EMS is the central control unit for a microgrid, which would control the power flow among the elements of the microgrid and in relation to the external grid. At the circuit level protection and control, it ensures stable and safe operation of the microgrid, and its protection from unexpected power outages and potential faults. A residential microgrid with EMS system is shown in Figure 1.3. The system consists of a high level optimization controller which optimizes power flow to reduce energy cost, and a circuit level controller to enforce power control commands of the EMS and handle transitions and faults.

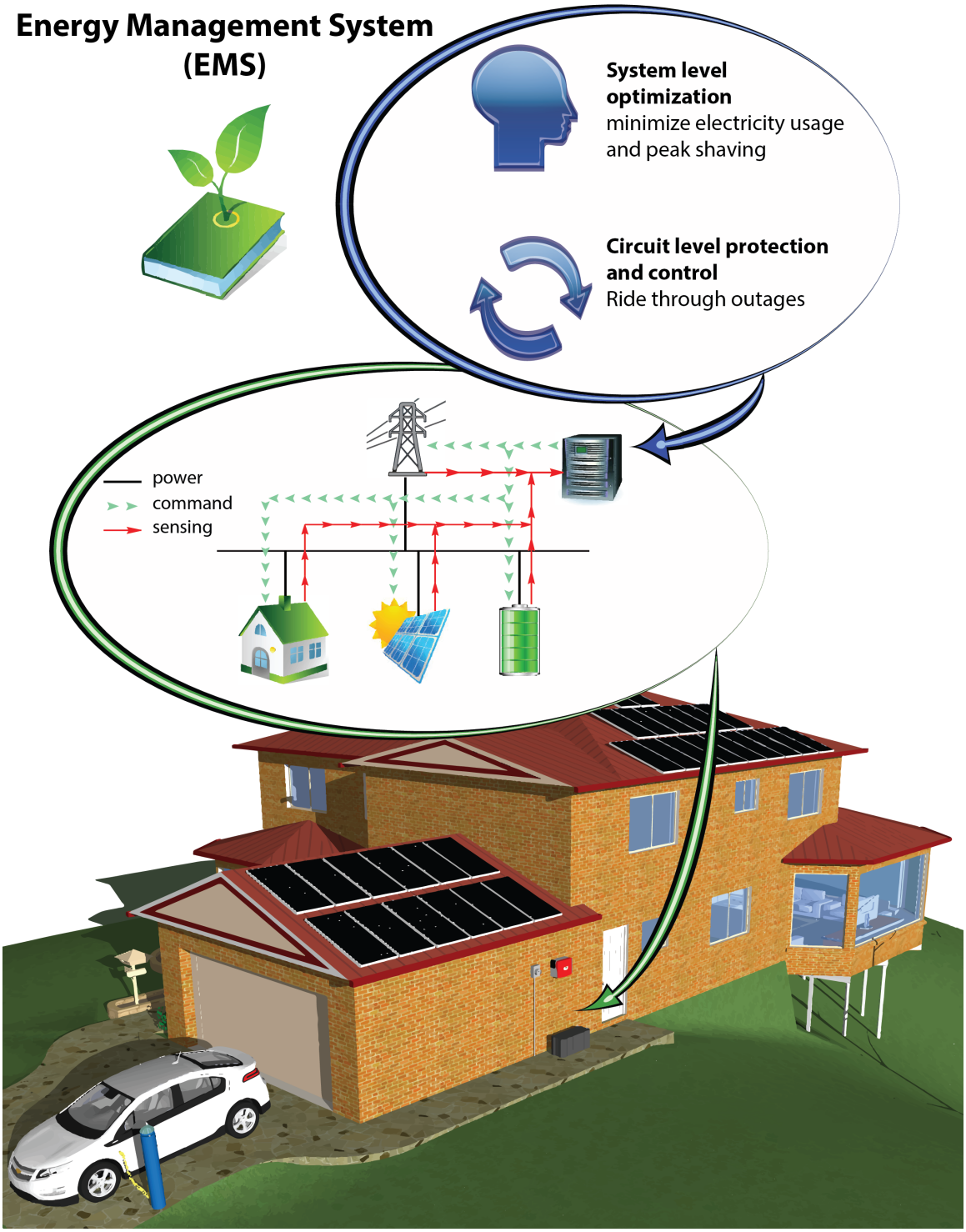

Figure 1.3: Residential microgrid with EMS

1.2 Problem Statement and Thesis Contributions

This thesis is concerned with the design, optimization, and control of electric microgrids. It studies optimal energy management, optimal component sizing, and circuit level power control in microgrid. The thesis addresses the following specific problems in electric microgrids.

Problem 1: Optimal Energy Management

With increasing adoption of renewable energy sources by individual home owners and commercial business owners, the produced energy is usually injected into the utility grid without considering demand. Most renewable energy sources, e.g. solar and wind, are not controllable sources. A microgrid with energy storage, with or without renewable energy, provides a degree of control to maximize the benefit of electricity consumer by lowering the overall cost of energy.

A simple optimization-based energy management system is proposed in this thesis for controlling the charge and discharge of a energy storage device, i.e. a battery in order to minimize the cost of electricity for the consumer. This is achieved by taking advantage of time-of-use pricing, to buy and store energy during off-peak period and to sell it back during the peak time. The EMS in commercial and industrial settings enables peak shaving, that in some cases could significantly reduce the peak demand charge for those types of customers.

Problem 2: Component Optimization for Microgrid with EMS

The prevalence of renewable energy generation and distributed energy storages is expected to increase in the power system to reduce reliance on polluting fossil fuels.

Residential, commercial, and industrial customers will gradually adopt renewable generations and distributed energy storages. However, the diversity of component type, building type and pricing regime complicates the design of EMS for such microgrids.

In the thesis, a systematic method is proposed to select component sizes, i.e. the number of battery modules and solar panels, in a microgrid with EMS. The approach is based on formulating and solving a mixed integer linear program (MILP) optimization for energy management and component selection. The proposed component sizing optimization is implemented for residential, commercial and industrial settings with consideration of different pricing schemes, e.g. Micro-FIT, net-metering, demand cost, etc. For given solar panel and battery modules with their respective capital cost and rating parameters, the component sizing optimization algorithm would calculate the optimal number of modules to maximize the customer's return on investment based on the property's actual power demand proble and the local electricity pricing regime.

Problem 3: Circuit Level Protection and Control

The microgrid with EMS requires a circuit level controller to enforce the power flow decisions, handle transitions among modes of operation, and protect against faults. Power flow control and sharing between power electronics based energy sources are implemented using the well-known droop control method. Power outage and grid instability are of great concern to customers who require a reliable uninterrupted supply of power. The low-level microgrid controller with EMS proposed in this thesis would provide a ride through capability for the microgrid. The microgrid would switch to an islanded mode when grid power is not available and use local generation

and energy storages to continue the supply of power. After grid power recovers, the microgrid with EMS would detect that event and re-synchronize with the grid before the reconnection. The whole process is autonomous and transparent to the customer.

1.3 Thesis Organization

The rest of the thesis is organized as follows. Chapter 2 reviews the literature on microgrids and their control strategies. This is followed by a system level optimization study for residential microgrames in Chapter 3. Chapter 4 explores system level optimization for commercial and industrial micro grids. Circuit level modelling and control of a microgrid with EMS are investigated in Chapter 5. The thesis is concluded in Chapter 6 where some possible directions for future work are also discussed.

1.4 Related Publications

- Yu, X. E., Xue, Y., Sirouspour, S., and Emadi, A. (2012, June). Microgrid and transportation electrification: A review. In Transportation Electrification Conference and Expo (ITEC), 2012 IEEE (pp. 1-6).

  Yu, X. E., Sirouspour, S., and Emadi, A. (2014, June). Optimization-based Components Sizing for Microgrid. In Transportation Electrification Conference and Expo (ITEC), 2014 IEEE(submitted).

Chapter 2

Literature Review

This chapter is divided into five sections. The first section introduces the electricity grid and microgrid concept. The second and third section deal with microgrid control and optimization-based control strategies for microgrids. The fourth section introduces microgrid and its components modelling. The final section focuses on existing energy management that are currently commercialized.

2.1 Electricity grid, Microgrid, and Distributed Generation

The concept of microgrid is not new. In fact back in the 18th century, Thomas Edison's first utility system was an isolated grid powered by a generator close to the load, what we may call today a microgrid. Over time electricity overtook steam and major hydro and fossil fuel energy sources were harvested, resulting in massive expansion of electric power grids covering large territories. In the 1920s, electric grids started

to be connected in an effort to achieve better performance and reliability by peak load sharing and power backup (Borbely and Kreider, 2001). The electric grids of the 20th century distribute massive amount of electricity generated by large power generation stations mostly from fossil fuels to remotely located load centers. The energy is delivered by one-way transmission and distribution systems to the end consumers without knowledge of energy cost and on-peak/off-peak information (Arnold, 2011). This system is neither sustainable nor is reliable. The fuel-to-end consumer efficiency is only around 30% (Lasseter, 2011). A 2006 study shows that the total cost of power outage throughout the US for the entire year was over 100 billion dollars in 2006 (LaCommare and Eto, 2006). Security issues, finite supply of fossil fuels, the increasing difficulty of extracting, and unstable fuel prices have caused international concerns threatening the world economy. Decentralization of electricity generation using alternative energy sources can address of some of these challenges. Wind turbine, photovoltaic (PV), and combined heat and power (CHP), are typical sources of DG. In the DG model, local generation and local consumption completely eliminate the loss due to long distance transmission and distribution. In addition, the by-product heat can be used for heating. Higher efficiency can be achieved by using multi-generation to co-generate heating, cooling etc. (Chicco and Mancarefla, 2009). However, the control of a large number of DGs can become quite challenging. To address this problem, the Consortium for Electrical reliability Solutions (CETRS) introduced the concept of modern microgrid in the US in late 1990s (Lasseter, 2001). Several control schemes for microgrids are briefly discussed below.

2.2 Microgrid Modelling

(Armstrong *et al.*, 2009) introduce a method to model electrical load for typical Canadian household, which does not include Heat Ventilation and Air Conditioning (HVAC). They classify a typical Canadian household into three clusters, low usage, medium usage and high usage. For each cluster, a 5 minute interval model is derived. The probabilistic load profile is generated from lighting, and typical household appliance with the consideration of seasonal factor and each load heuristic usage factor. Although no conclusion can be made by looking at each single usage profile, after averaging a large number of such usage profiles, the resulting curve is quite smooth. They use this model and compare its predictions with actual data from 7 Quebec homes. The result shows similarity in the aspect of typical peaks and total yearly consumption. Modelling and analysis of power electronics based microgrid under autonomous operation is proposed by (Pogaku *et al.*, 2007). The model is detailed to converter control loop level; high frequency switching is not modelled. A sensitivity analysis is also presented to improve overall system stability. Distributed energy sources, e.g. solar panel, wind turbine, fuel cell and microturbine are modelled with their corresponding power electronics interface to microgrid by (Kariniotakis *et al.*, 2005). Both steady state and dynamic behaviour are studied in the paper.

A simple circuit based battery model is presented by (Olivier Tremblay, 2009). This model is suitable for modelling the charging and discharging behaviour of different type of batteries, i.e. lithium-ion, lead-acid, etc. The author of (Villalva *et al.*, 2009) present a model of solar panel and a method to determine key parameters from manufacture provided data sheet. It could model the output characteristics of solar panel under different temperature and solar irradiance. Some main distributed

energy sources, e.g. wind turbine, diesel generation and batteries packs, are modelled with their power electronics interface under microgrid environment by (Yubing *et al.*, 2008). Matlab/simulink based simulation is also provided with steady state and dynamic characteristics.

2.3 Microgrid Control

Supply and Demand Control

Generation in a microgrid could be classified either as dispatchable or non-dispatchable. Typical dispatchable or controllable energy generators are internal combustion engine(ICE) generator, battery, super capacitor and flywheel. Most of renewable sources like wind and PV are non-dispatchable due to the uncontrollability of sun and wind. The power electronics inverters acting as the interface between DG and microgrid play an important role in controlling the generation to meet the power demand of the load. Loads in the microgrid should be prioritized by their importance and sensitivity. In case of blackout and scheduled islanding operation of microgrid, when supply is not sufficient for all the loads, load shedding or a scheduled time-shift is necessary for the operation of non-critical loads in order to balance the supply/demand (Katiraei *et al.*, 2008; Zamora and Srivastava, 2010).

Droop Control

A microgrid often contains multiple DGs. Frequency droop control and voltage droop control allow for power sharing and voltage regulation of the microgrid without the need for a complicated communication scheme among its elements (Lasseter, 2002;

Katiraei and Iravani, 2006). Droop control strategies are well studied in system balancing and the control of real and reactive power in microgrid in grid connected and islanded mode (Barklund *et al.*, 2008; Mohamed and El-Saadany, 2008; Sao and Lehn, 2008; Majumder *et al.*, 2009). A microgrid containing PV, wind turbine, CHP and electronically connected synchronous generators is an inertia-less system. In bulk energy systems, the transitional power due to newly added load is generated by the inertia of the system. In microgrids, energy storage elements such as batteries, super-capacitors, and fly-wheels are required to create the needed inertia in the system. A microgrid control strategy based on droop control with UPS is discussed in (Guerrero *et al.*, 2009). In (Li and Kao, 2009), Li et al. propose an accurate power control strategy for microgrids to cover an uncontrollable scenario of the droop controller.

Decentralized Control

Decentralized control tends to provide the autonomy to the DGs and controllable load in the microgrid in order to supply the demand without compromising the performance of the microgrid (Zamora and Srivastava, 2010; Katiraei *et al.*, 2008). The authors of (Dimeas and Hatziargyriou, 2005) propose a multiagent system to control the power exchange between DG, microgrid and utility grid; their approach allows the microgrid to operate in the market and make local decisions with minimum information about the environment. An adaptive decentralized controller is proposed by (Mohamed and El-Saadany, 2008) to implement power sharing between parallel converter based energy sources. A microgrid control scheme is studied by (Wang *et al.*, 2008), in which, both load power sharing and active/reactive power sharing among the energy sources are covered.

Centralized Control

Centralized control is a top down control strategy for microgrid operation (Tsikalakis and Hatziargyriou, 2008). The microgrid central controller maintains the optimal operation of local production based on the pricing information. It focuses on the grid connected mode to optimize power exchange with the grid (Katiraei *et al.*, 2008). The authors of (Hatziargyriou *et al.*, 2005) discuss the centralized microgrid control system to maximize economic benefit in exchange of power between microgrid and utility grid by controlling the activity of distributed generators in microgrid. A centralized optimization and dispatch model is developed by (DING *et al.*, 2009) for a group of microgrid to minimize the cost of grid operation.

2.4 Optimization-based Control Strategies for Microgrids

(Chakraborty *et al.*, 2007) proposed a novel microgrid system called Distributed Intelligent EMS(DIEMS), which could learn the energy production pattern and predict and optimize the economic cost. Hourly predictions are implemented by a neural-network which utilizes the climate information such as solar radiation, temperature, pressure and relative humidity to predict the energy production and consumption. The optimization algorithm consists of a linear program (LP). Both running and idle cost of solar system and wind system are considered. Energy storage device optimization is based on a heuristic charging and discharging decision, with 90% charging and discharging efficiency. This heuristic method would decide the end of day energy level and power rating with the consideration of maximize battery life. The end of day

energy level and power rating of energy storage device are then passed on to the LP optimization. (Mohamed and Koivo, 2007) proposed a control strategy for a isolated microgrid, consisting of solar panels, wind turbine, battery storage, micro turbine, diesel generator and fuel cell. They employed a nonlinear multi-objective optimization algorithm to minimize economic cost and emissions (eg. NO_X, SO_2 and CO_2). The authors also provided a model to calculate wind and solar power output from solar irradiance and wind speed.

(Morais *et al.*, 2010) proposed an optimized control dispatch system for microgrid based MILP optimization. Their microgrid is comprised of solar PV panels, wind turbine, fuel cell, battery pack and controllable load. The optimization algorithm uses a set of linear objectives. Storage energy and power limit are used in defining constrains for the optimization. (Youli *et al.*, 2009) perform simulations to study the reliability, economic and environmental impact of a microgrid in Japan. Their study consists of 186 households with micro hydro power (up to 160 kW), solar PV system (up to 30kW), wind power (up to 660 kW) and a large central battery storage system (1800 kWh). They obtain the power demand profile from historical data, and predict production for each generating unit. Their storage control strategy is to charge the battery when there is energy surplus, and discharge it when short on generation. (Parisio and Glielmo, 2011) propose a Model Predictive Control (MPC) in combination with Mixed Integer Linear Programming (MILP) optimization based control approach for microgrids. Their energy storage model includes charging and discharging efficiencies and charge degradation model. They also consider time-varing buying and selling prices and quadratic cost for fuel based generators. They consider critical and controllable loads; controllable load is treated as a penalty cost during

the optimization. (Pawel Malysz, 2013) propose a MILP based rolling horizon optimization and control method for microgrids. The power saving is achieved by solving a MILP based optimization problem over a rolling horizon. This algorithm also considers the economic benefits, battery usage cost, and grid power profile. Performance is optimized by utilizing a battery incremental red-zone power rates method that the algorithm can run in real time.

2.5 Existing Energy Management Systems

Kyocera Corporation (Kyocera, 2013) has developed an EMS system by controlling the power of roof top solar PV and lithium-ion battery. The EMS regulates the energy flow between energy sources, load and utility grid. At on-peak period, the EMS would use the battery stored power first before buying power from the grid. DENSO Corporation (LaRose, 2013) has developed a home energy management system (HEMS) with optional battery pack. Energy usage is more visible with a home energy monitor and smartphone application, and the user could remotely turn on/off a particular appliance. EV charging can be scheduled by HEMS to utilize cheaper electricity during nighttime. If optional energy pack is installed, peak shifting is enabled during on-peak period. SMA Solar technology AG (SMA, 2013) has introduced a backup power system which can work as add-on to existing PV plants. It could switch to islanded stand-alone power supply when there is a grid failure. Due to the existence of PV plants, a relatively smaller battery could be used. On-site auxiliary generation is also supported by this system. Nokia Siemens (NSN, 2013) has proposed a stand-alone emission free mobile broadcast station. The energy sources in this system are solar PV and wind turbine with deep cycle battery pack and fuel cell in case

neither solar and wind are available . The controller has a built-in control strategy for decentralized control; it also has the connection to a central data management system.

Chapter 3

Residential EMS System Level Study

In this chapter, energy management system configuration for a residential property is studied. The first section of this chapter reviews the electricity pricing policy for residential houses in the province of Ontario, Canada. The second section looks at the power profile for a typical residential house. The third section presents a sample formulation of the optimization problem for home energy management along with an example of its application. The last section discusses the formulation of an optimization problem for selection of the size of components in a home energy management system. Four scenarios of components sizing under different Time-of-Use (TOU) pricing schemes are presented in this chapter.

3.1 Pricing Regime and Power Profile

In Ontario, there are two major pricing regimes. One is for residential and small business users, and the other is for medium to large commercial and industrial users.

1. Residential and small business users are subject to a TOU pricing scheme, shown in Figure 3.1. In this system, the consumers are charged based on the day of the week and hour of the day for their electricity usage. The Ontario Energy Board has set the current electricity rates at 12.9 C/kWh for on-peak, 10.9 C/hWh for mid-peak,and 7.2 C/kWh for off-peak. Weekends are considered off-peak. The time of use charge is obtained from OEB (2013).

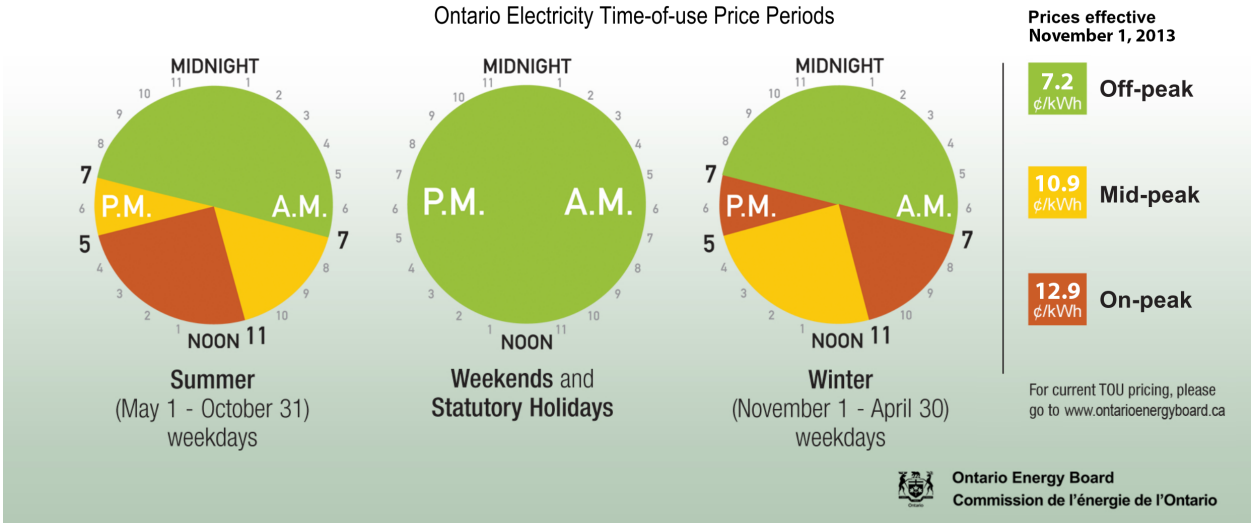

Figure 3.1: Ontario electricity TOU pricing, OEB (2013)

Other than the TOU price scheme, there are other cost components for the residential costumers, including delivery charges, regulatory charges, debt retirement charge and HST. Some charges are based on adjusted usage, with a

TOU charge adjustd to metered usage

		TOU (¢ / kWh)	Adjustment factor	Adjusted TOU (¢ / kWh))
Electricity	on-peak	12.900	1.078	13.906
	mid-peak	10.900	1.078	11.750
	off-peak	7.200	1.078	7.762

Delivery, regulatory and debt retirement charge adjusted to metered usage

	Usage charge (¢ / kWh))	Adjustment factor	Adjusted Usage charge (¢ / kWh)	Fixed Charge ($ / month)
Delivery				
Distribution service charge ($ / month)				16.500
Distribution volume charge (metered usage - ¢ / kWh)	2.528	1.000	2.528	
Transmission charge (adjusted usage - ¢ / kWh)	1.196	1.078	1.289	
Smart metering entity charge ($ / month)				0.790
Regulatory charge				
Standard supply service administration charge ($/month)				0.250
Rural rate protection charge (adjusted usage - ¢/kWh)	0.120	1.078	0.129	
Wholesale market service rate (adjusted usage - ¢/kWh)	0.440	1.078	0.474	
Debt retirement charge (metered usage - ¢/kWh)	0.700	1.000	0.700	
Total			**5.121**	**17.540**

Total usage and fix electricity charge

		Adjusted TOU	Delivery, Regulatory and retirement	HST	Total
Usage charge (¢ / kWh)	**on-peak**	13.906	5.121	2.474	21.501
	mid-peak	11.750	5.121	2.193	19.064
	off-peak	7.762	5.121	1.675	14.557
Fixed Charge ($ / month)			17.540	2.280	19.820

Figure 3.2: Electricity rate calculation for urban high density residential household, HydroOne (2013a,b)

adjustment factor 1.078 (HydroOne, 2013a,b). The rate calculation for an urban high density residential house based on metered usage is presented in Figure 3.2. These numbers will be used in the rest of the thesis in various example scenarios..

2. Medium and large business are those with power demand of more then 50 kW (or approximately $2,000 per month electricity usage) IESO (2013a). Their electricity bill is mainly based on two factors: the energy consumed and peak demand. Energy consumption is the accrual power supplied and used by the consumer, measured in kilowatts-hours (kWh). If the business has a interval meter, they would pay the Ontario hourly energy price, same as theTOU price. Based on the total consumption, the customer also pays for line loss, and global adjustments. Peak demand charges are based on the highest electric demand reading during the billing period, which is measured in kilowatts(kW) or kilovolt-amperes(kVA). For example, if the peak demand charge rate is $6 per kW, and the peak power demand of a business is 50kW, the charge would be 50kW x $6 = $300. This charge also includes the transmission and distribution cost of electricity.

3.2 Residential House Power Profile

A residential house located in Ancaster, Ontario is chosen for study in this chapter. This is a $2500 ft^2$ single detached house, with unfinished basement, living room and kitchen on the first floor and 4 bed rooms on the second floor. The heating and range use natural gas. A list of the electrical loads is given in Table 3.1.

Device	Power (kW)	Quantity	Total power (kW)
Dryer	2.88	1	2.88
Washer	0.84	1	0.84
Dishwasher	1.044	1	1.044
Fridge	0.78	1	0.78
Microwave	1.5	1	1.5
Toaster	0.85	1	0.85
Electric Range	2.5	4	10
Furnace	1.44	1	1.44
Air condition	4.4	1	4.4
Lighting	0.06	33	1.98
TV	0.3	2	0.6
Computer	0.3	3	0.9

Table 3.1: A Typical household electrical load in Ontario

To study the energy usage profile of this particular house, the hourly electricity usage profile for 12 month period from June 1, 2012 to June 1 2013 was obtained. Figure 3.3 shows the energy usage for one week (Sunday-Saturday), July 2 to July 8, in hot summer plotted in red line and one week, Feb 20 - Feb 27, in cold winter plotted blue line. The data in the figure shows a single peak in late afternoon in summer days and two peaks in winter days in the power demand profile. The electricity load in weekends is significantly higher than that in weekdays for this family. This can be attributed to the fact that the residents spend most of their time at home during

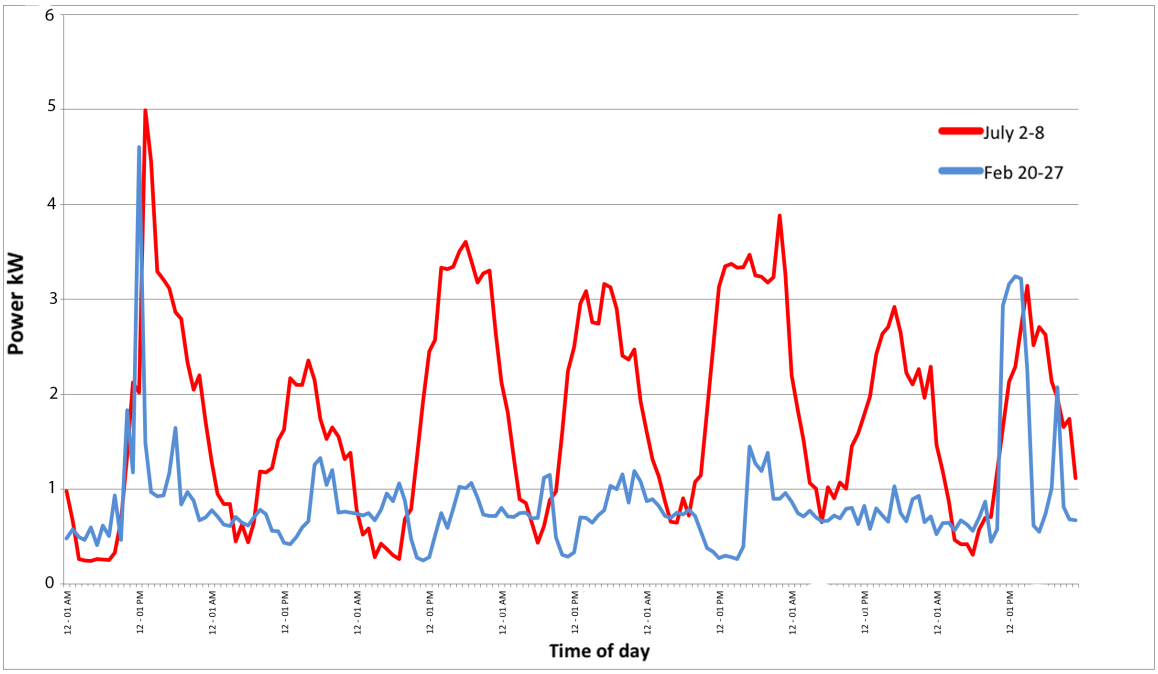

Figure 3.3: Hourly power usage for a week in summer and winter

weekends. Laundry, dishwashing and entertainment devices would be all in use. This could also explain the power spikes in Sunday afternoon.

Figure 3.4 shows the Probability Density Function (PDF) of hourly electricity energy usage obtained from the whole year data. The mean hourly consumption is 0.7471 kWh.

A number of energy related components could be added to this house to create a residential microgrid. The concept is demonstrated in Figure 3.5, where solar panels are installed on top of the roof, and a grid tie converter and battery pack are installed beside the electric meter. An EV with Level 2 [1]charging station is also considered. Other possible components include wind turbines, fuel cells or ultra-capacitors.

[1]Typical Level 2 charging station need installation of 208/240V with maximum current 80A.

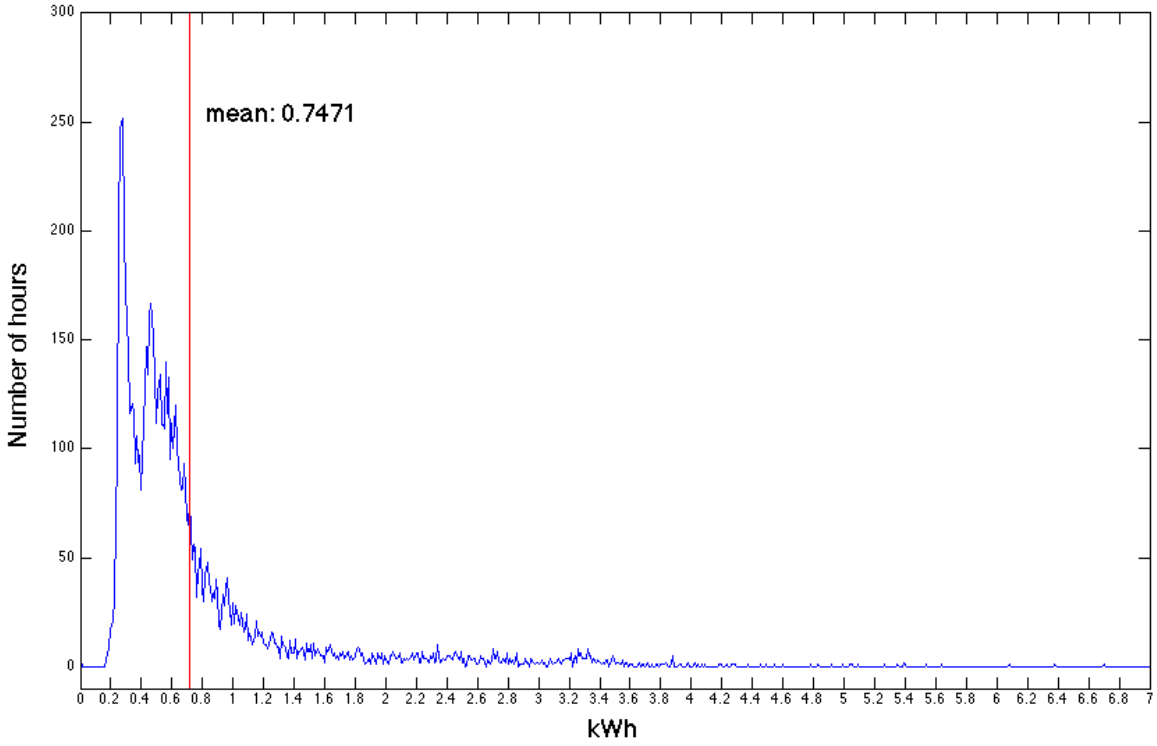

Figure 3.4: PDF plot of hourly power usage of a year for a residential house located in Ancaster, Ontario, Canada

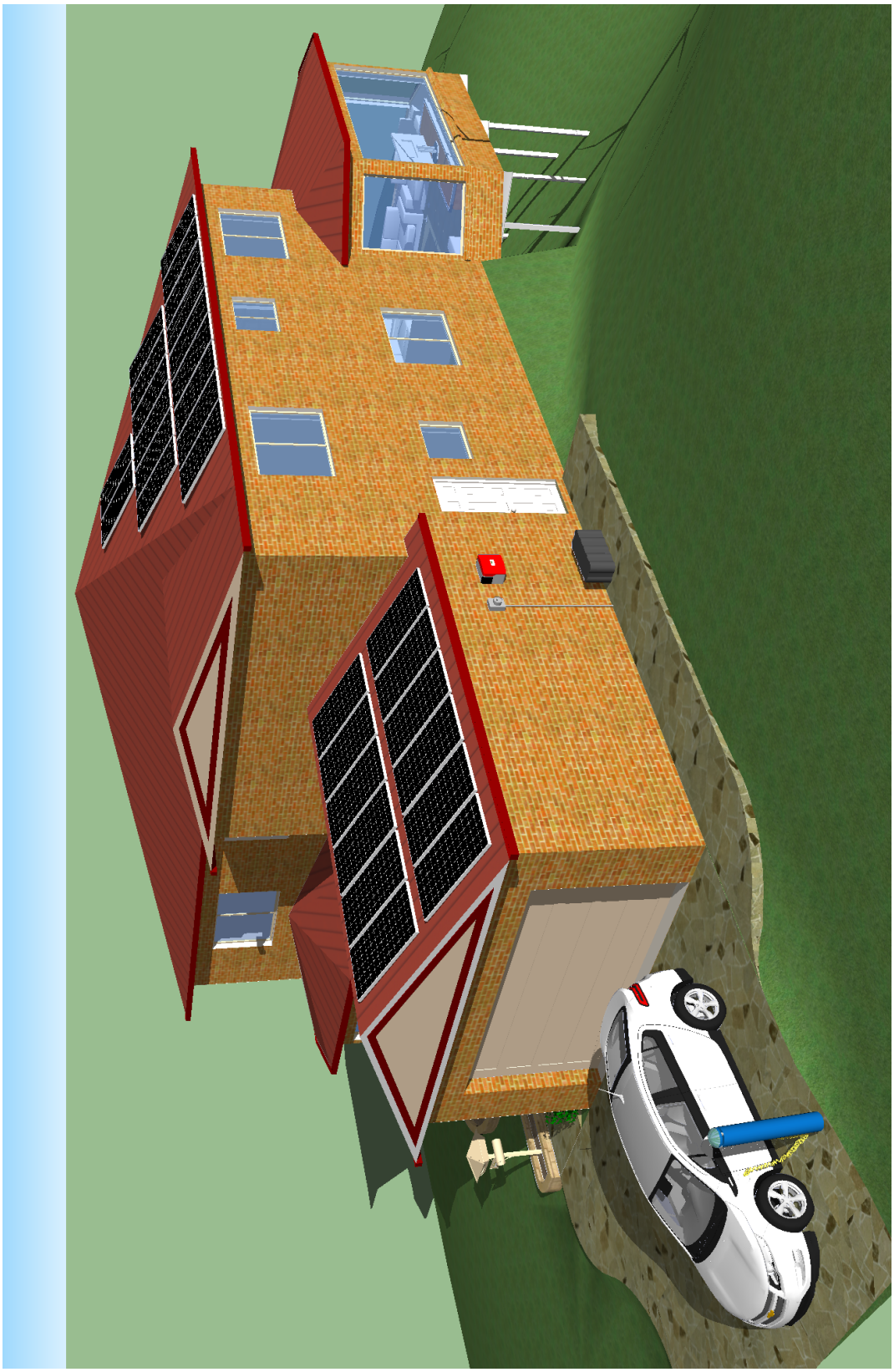

Figure 3.5: A residencial microgrid

3.3 System Level Study of Home Energy Management System

An EMS enables residential home owner to lower their electricity cost by reducing their demand from the grid during the peak period through the use of storage. It can also help integrate renewable sources of energy into the grid in an effective way. This section presents a linear programming based method for making optimal charge/discharge decisions for the battery storage in a residential microgrid.

3.3.1 Optimization Problem Formulation for Controlling Storage Activities

The battery storage charge/discharge activities are the solution to the following linear programming problem

$$\min_x(\mathbf{C_{TOU}^T P_S}) \tag{3.1}$$

$$x = [\mathbf{P_S}, E_0]^T$$

subject to

$$-P_S^{\max} \leq P_{Si} \leq P_S^{\max} \quad i \in [1, N_h] \tag{3.2}$$

$$0 \leq \sum_{i=1}^{k} P_{Si} + E_0 \leq E_{bat} \quad k \in [1, N_h] \tag{3.3}$$

$$-P_G^{\max} 1_{N_h} \leq \mathbf{P_G} = \mathbf{P_D} + \mathbf{P_S} \leq P_G^{\max} 1_{N_h} \tag{3.4}$$

$$\mathbf{1}^T \mathbf{P_S} = \mathbf{0} \tag{3.5}$$

where

$N_h \in \Re$: number of hours in the time horizon.

$\mathbf{C_{TOU}} \in \Re^{\mathbf{N_h}}$: vector of TOU cost in $\$/kW$.

$\mathbf{P_S} \in \Re^{\mathbf{N_h}}$: battery storage input or output power.

$E_0 \in \Re$: initial energy level of the battery.

$\mathbf{P_D} \in \Re^{\mathbf{N_h}}$: power demand of the household.

$\mathbf{P_G} \in \Re^{\mathbf{N_h}}$: power at the point of common coupling to the grid.

$P_G^{\max} \in \Re$: maximum power allowed at the common point of coupling.

$P_S^{\max} \in \Re$: maximum power rating of the battery.

$E_{bat} \in \Re$: capacity of battery.

Note that, assuming the buying/selling price of electricity from/to the grid is the same, the actuarial electricity cost is

$$\mathbf{C_{TOU}^T P_G} \tag{3.6}$$

Since the grid power $\mathbf{P_G}$ is given by

$$\mathbf{P_G} = \mathbf{P_D} + \mathbf{P_S} \tag{3.7}$$

and $\mathbf{P_D}$ is independent of the decision variables, the cost objective used in the optimization is chosen as in Eq 3.1 as opposed to the actual cost of the electricity. Note that in the above formulation, a positive $\mathbf{P_S}$ means charging and negative $\mathbf{P_S}$ denotes discharging of the battery. There are limits on charge and discharge power rates of the battery, as in Eq 3.2. The battery also has minimum and maximum allowable energy levels as shown in Eq 3.3. Buying and selling power from/to the grid is limited by the line capacity constrains as in Eq 3.4. The equality constrain in Eq 3.5 ensures

the battery would return to the same energy level after a 24 hour period of usage.

3.3.2 Case Study - Residential Home

The residential house used in this case study is the one mentioned in Section 3.1.3. The hourly energy consumption data for this house was obtained from Hydro One. The case study here focused on the second week of July in 2011. It is assumed that a battery, $E_{bat} = 15kWh$, is used with a maximum output power rating, $P_S^{\max} = 3kW$. The battery charge/discharge activities were determined by solving the optimization problem in Eq 3.1 - 3.5. The optimization was run at one hour time step for the whole week. The maximum power rating for a typical residential house is 100A, with a safety factor of 80% to the maximum power rating, $P_g^{\max} = 9.6kW$. The simulation results are illustrated in Figure 3.6. From this graph, it can be clearly seen that the some of the peak load is shifted to off-peak period, and the demand curve is smoothed as the result by utilizing the energy storage element. The electricity costs with and without EMS are given in Table 3.2. The data in this table includes all applicable charges in Figure 3.2. In this case, the EMS with energy storage yields a saving of 21.5%, compared to the case where the house is directly connected to the grid. The optimization was solved in Matlab 2012 using MILP solver LPSolve 5.5.

From Figure 3.7, it could be seen that there are some unnecessary battery activities. Penalizing charge/discharge activities as in (Pawel Malysz, 2013), would smoothen the battery power profile.

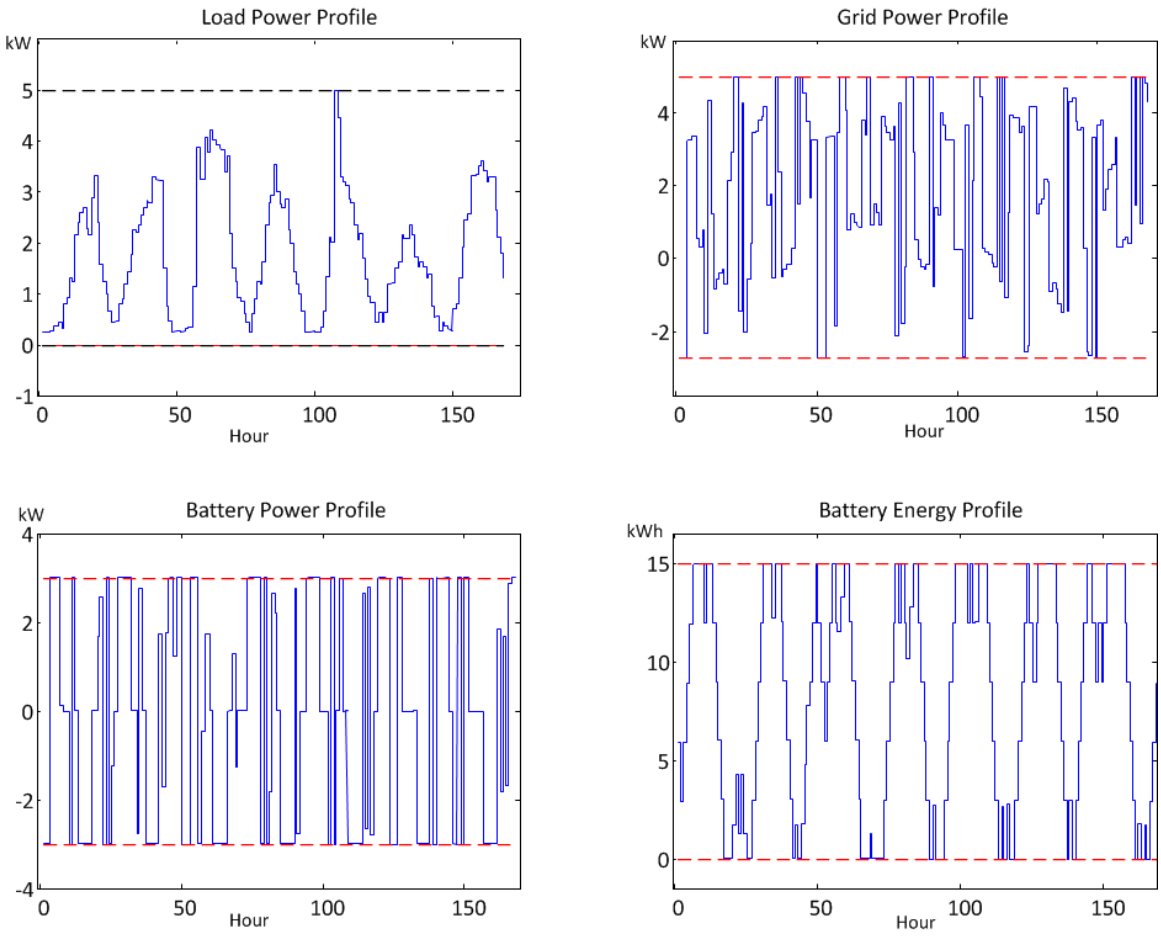

Figure 3.6: Linear programming based electricity usage optimization for residential house by controlling battery activities: (a) power demand profile of the house, without EMS, (b) grid power profile using EMS, (c) battery energy profile, (d) battery power profile; $P \leq 0$ means discharge of battery

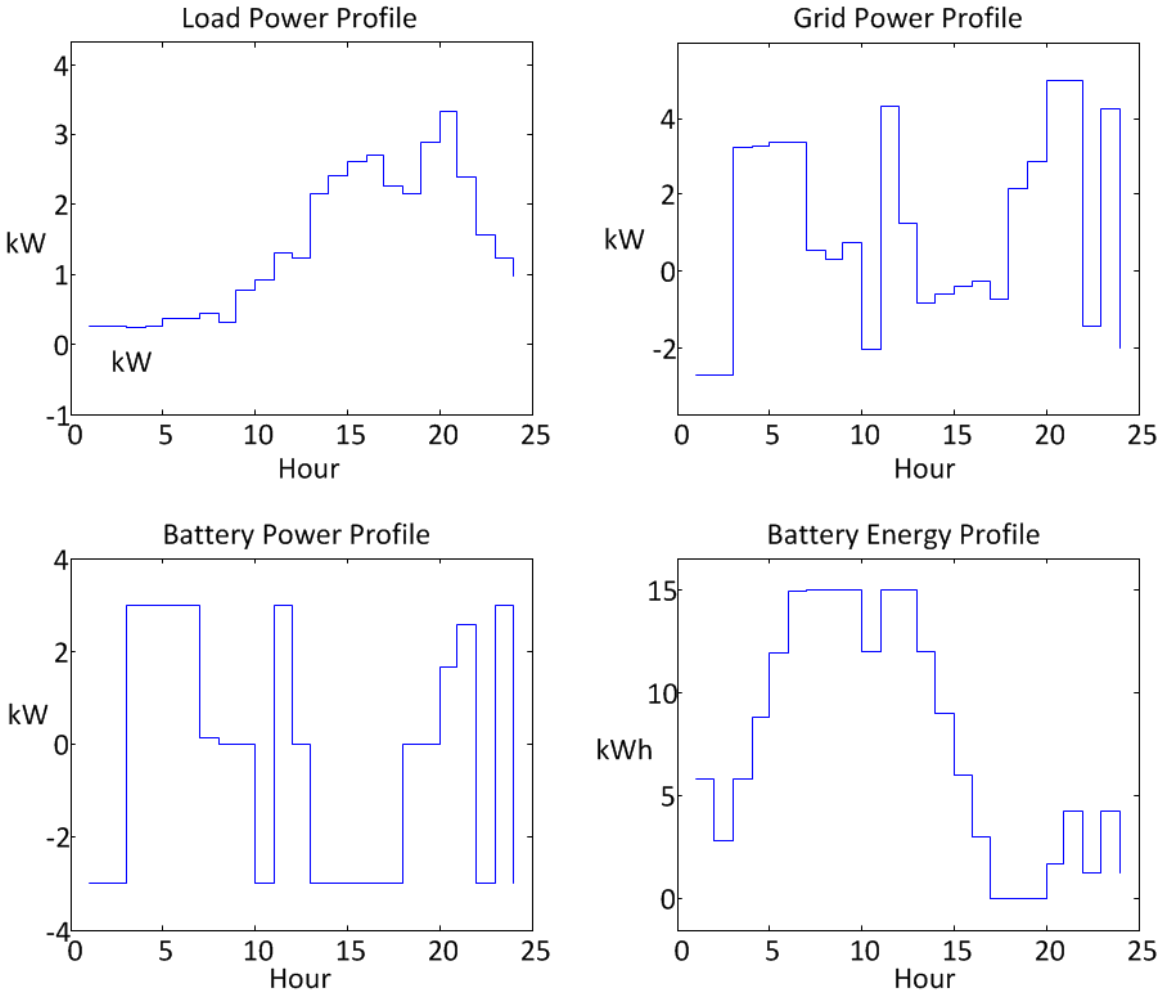

Figure 3.7: A 24-hour period plot of Figure 3.6 : (a) power demand profile of the house, without EMS. (b) grid power profile using EMS.(c) battery energy profile, (d) battery power profile; $P \leq 0$ means discharge of battery

Electricity Cost without EMS($)	55.693
Electricity Cost with EMS ($)	48.448
Cost saving ($)	7.245
Percentage saving (%)	14.9%

Table 3.2: Linear programming based electricity usage optimization result for residential house

3.4 Components Sizing Optimization

An important question that a home owner would face before upgrading to a green smart home concerns sizing of the system components to maximize economic benefit. In this section, an optimization problem is formulated to help determine an optimal system configuration in terms of component sizes. Several pricing scenarios are considered in sizing the components.

3.4.1 Case 1 - Current TOU Pricing with Micro-Fit

Micro-Fit is an Ontario energy program designed for individuals who want to sell clean power to the grid with a guaranteed price and fair return on their investment. Clean power includes sun, wind, hydro and bioenergy which is 10 kW or less (OPA, 2013). In this case, the power pricing regime is assumed to be net metering with current TOU price for battery and household load. The power generated by solar array is fed directly to the grid with the Micro-fit program pricing, which is currently at 39.6 cents/kWh (OPA, 2013).

The task of determining components size could be formulated as a mixed integer linear programming (MILP).

$$\min_{x}(C_{sol}n_{sol} + C_s n_s + C_{TOU}^T \mathbf{P_s} + (\mathbf{C}_{Micro-FIT}^T \mathbf{P_{sol}})n_{sol}) \tag{3.8}$$

$$x = [\, n_{sol} \quad n_s \quad E_s^0 \quad \mathbf{P_s} \,]^T \tag{3.9}$$

subject to

$$-n_s {P_s}^{\max} \leq P_{s_k} \leq n_s {P_s}^{\max}, \quad k \in [1, N_h] \tag{3.10}$$

$$-P_g^{\max} \leq P_{s_k} + n_{sol} P_{sol_k} + P_{d_k} \leq P_g^{\max}, \quad k \in [1, N_h] \tag{3.11}$$

$$0 \leq \sum_{j=1}^{k} P_{s_j} + E_s^0 \leq n_s E_s^{\max} \quad , \quad k \in [1, N_h] \tag{3.12}$$

$$1^T \mathbf{P_s} = \mathbf{0} \tag{3.13}$$

$$0 \leq n_{sol} \leq n_{sol}^{max} \tag{3.14}$$

where

$E_s^0 \in \Re$: initial energy level of the battery.

$\mathbf{P_{sol}} \in \Re^{\mathbf{N_h}}$: solar panel power profile.

$E_s^{max} \in \Re$: capacity of battery.

$n_{sol} \in \Re$: number of solar panel.

$n_{sol}^{max} \in \Re$: maximum number of solar panel allowed by physical condition.

$n_s \in \Re$: number of battery unit.

$C_{sol} \in \Re$: capital cost of solar panel.

$C_s \in \Re$: capital cost of each battery pack.

$\mathbf{C_{Micro-FIT}} \in \Re^{\mathbf{N_h}}$: Micro-FIT pricing in $\$/kW$.

The rest of the variables have been defined earlier.

Note that the number of solar panels is limited by the space available for their installation, as shown in Eq. 3.14. Table 3.3 shows the calculation of the capital cost of installing and operating a solar array system. The numbers were obtained from a experienced contractor.

Solar panel cost($/W)	2
Inverter cost ($/W)	0.65
Labor and installation cost ($/W)	1.5
Total capital cost ($/W)	4.15
Life of solar system (years)	20
Annual interest rate (%)	3%
Monthly capital cost ($/W)	0.023

Table 3.3: solar capital cost calculation

The capital cost of batteries can be calculated as follows. The cost of a Trojan IND17-6V, 6.54kWh battery is about $1400 CAD. The rated life at 50% depth of discharge(DOD) is 2800 cycles, and at 80% DOD is 1500 cycles. Assuming that the battery is cycled at 80% DOD once per day, the estimated capital cost of each battery unit is 1400/1500 x 30 = 28 $/month.

The case study here focuses on the month of July in 2011. It is assumed that Trojan IND17-6V, 6.54kWh battery modules with a maximum output power rating of 1.1kW and Conergy 235P-60 solar panel modules with a maximum output power rating of 235W panel are selected. The solar panel power profile was obtained from Burlington Hydro for the same period of time as the residential usage data. It is also assumed a maximum of 27 solar panels can be installed at this particular location. The monthly cost of each solar panel in this optimization is assumed to be $3.5, and the monthly cost for each battery module is assumed to be $11[2]. The optimization was run for the whole month. The results are given in Table 3.4

The cost saving of battery backed solar panel system with EMS is listed in Table 3.5. With the components selected for this house, the monthly cost is $35.5 instead

[2]The current cost of the battery is $32 per month based on its retail price. In order to demonstrate this optimization algorithm with a non-zero result for the number of battery modules, it is assumed that there is $21 subsidy from utilities or government.

Device	Part number	Quantity	Total power (kW)	Total Energy (kWh)
Solar Panels	Conergy 235P-60	27	6.12	N/A
Battery	Trojan IND17-6V	5	5.5	32.7

Table 3.4: Optimal system configuration- component sizing with Micro-fit pricing

of $58 cost. The monthly devices capital cost is calculated as 27 x 3.5 + 5 x 11 = $149.5.

Electricity cost, pure load ($)	58
Solar Array revenue ($)	-116
Battery with EMS revenue ($)	-56
Total monthly solar capital cost ($)	94.5
Total monthly battery capital cost ($)	55
Total monthly cost ($)	35.5

Table 3.5: Monthly cost/revenue for optimal configuration - component sizing with Micro-fit pricing

The optimized power/energy profiles with optimally selected component sizes are illustrated in Figure 3.8. From this graph, it can be clearly seen that the maximum power rating at the point of common coupling to the grid is effectively utilized to buy power at off-peak period and sell power during on-peak period.

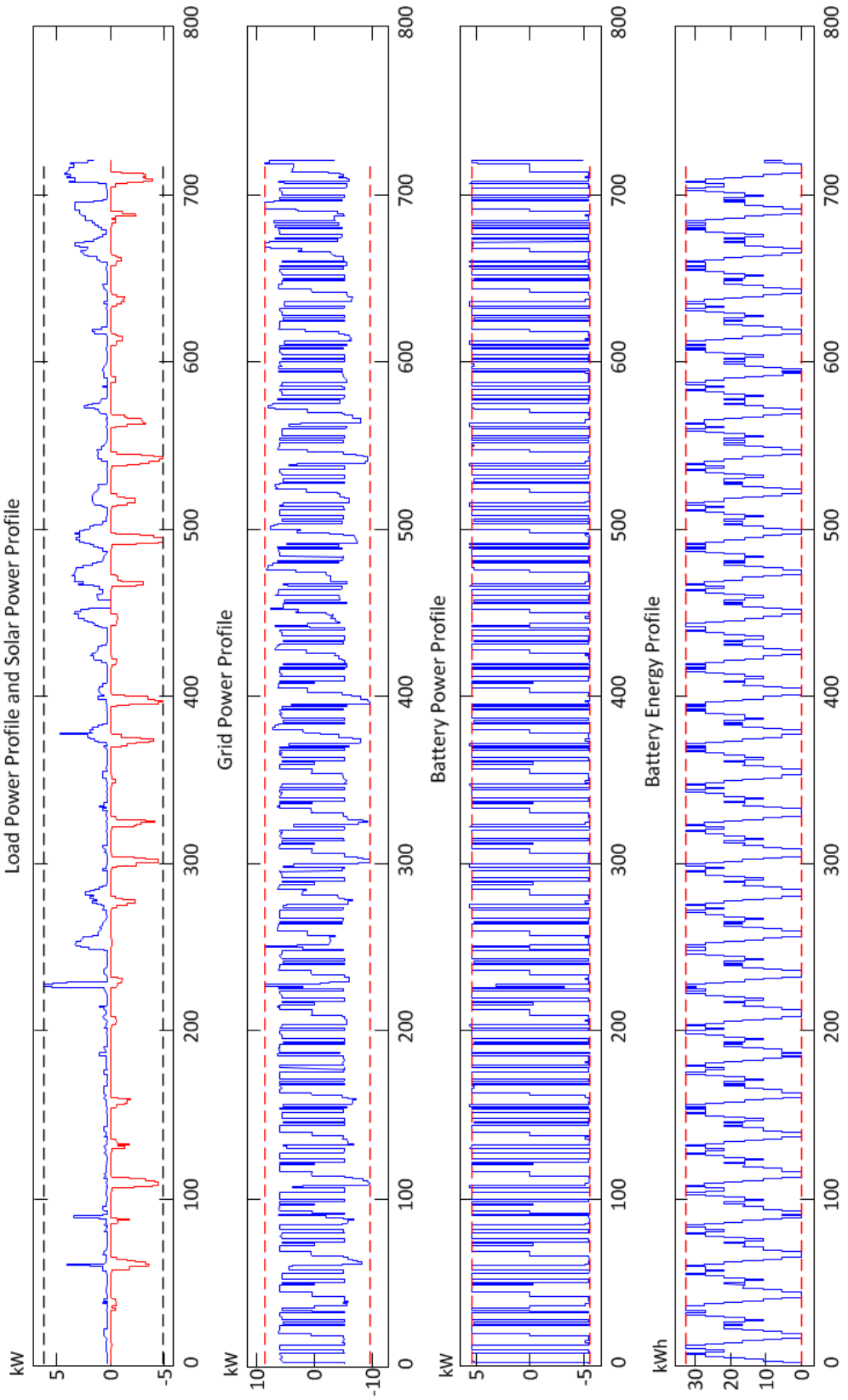

Figure 3.8: MILP-based component sizing optimization to maximize revenue - component sizing with Micro-fit pricing a) Load power profile and solar array power profile b) Grid power profile after optimization c) Battery power profile d) Battery energy profile

The battery backed solar array system with EMS would not only benefit the individual home owner by reducing their monthly electricity bill, but it also adds another dimension for utility companies to perform demand-side control. Therefore, it would make sense for the utilities to subsidize the capital cost of installing such system.

3.4.2 Case 2 - Future TOU Price

Since the capital cost of solar panels and batteries is trending down and the TOU prices are expected to increase, a second case study was considered that assumes net metering with TOU price increased by a factor of three; Micro-Fit program was not utilized in this case. The other assumptions made in the previous case are also valid here.

With these assumptions, the components sizes can be determined by solving the following MILP optimization

$$\min_x(C_{sol}n_{sol} + C_s n_s + \mathbf{C_{TOU}}^{\mathbf{T}}\mathbf{P_s} + (\mathbf{C_{TOU}}^{\mathbf{T}}\mathbf{P_{sol}})\mathbf{n_{sol}}) \tag{3.15}$$

$$x = [\, n_{sol} \quad n_s \quad E_s^0 \quad \mathbf{P_s} \,]^T \tag{3.16}$$

subject to

$$-n_s P_s^{\max} \leq P_{s_k} \leq n_s P_s^{\max}, \quad k \in [1, N_h] \tag{3.17}$$

$$-P_g^{\max} \leq P_{s_k} + n_{sol}P_{sol_k} + P_{d_k} \leq P_g^{\max}, \quad k \in [1, N_h] \tag{3.18}$$

$$0 \leq \sum_{j=1}^{k} P_{S_j} + E_s^0 \leq n_s E_s^{\max} \quad , \quad k \in [1, N_h] \tag{3.19}$$

$$1^T\mathbf{P_s} = 0 \tag{3.20}$$

$$0 \leq n_{sol} \leq n_{sol}^{max} \tag{3.21}$$

All variables have been defined earlier.

The first scenario assumes a monthly cost of \$3.5 per solar panel and \$32 per battery module. The energy consumption data is exactly the same as that in the previous case.

The optimization was run for the whole month. The results are presented in Table 3.6.

Device	Part number	Quantity	Total power (kW)	Total Energy (kWh)
Solar Panels	Conergy 235P-60	27	6.21	N/A
Battery	Trojan IND17-6V	7	7.7	45.78

Table 3.6: Optimal system configuration - component sizing with future pricing(1)

The cost saving of battery backed solar panel system with EMS is listed in Table 3.7. With the components selected for this house, the monthly cost has been reduced to \$153.5 from \$174 cost.

Electricity cost, pure load (\$)	174
Solar Array revenue (\$)	-106
Battery with EMS revenue (\$)	-233
Total monthly solar capital cost (\$)	94.5
Total monthly battery capital cost (\$)	224
Total monthly cost (\$)	153.5

Table 3.7: Monthly cost/revenue for optimal configuration - component sizing with future pricing(1)

The optimized power or energy profiles for each component are illustrated in Figure 3.9. From this graph, it can be clearly seen that the maximum power rating at the point of common coupling to the grid is effectively utilized to buy power at off-peak period and sell power during on-peak period.

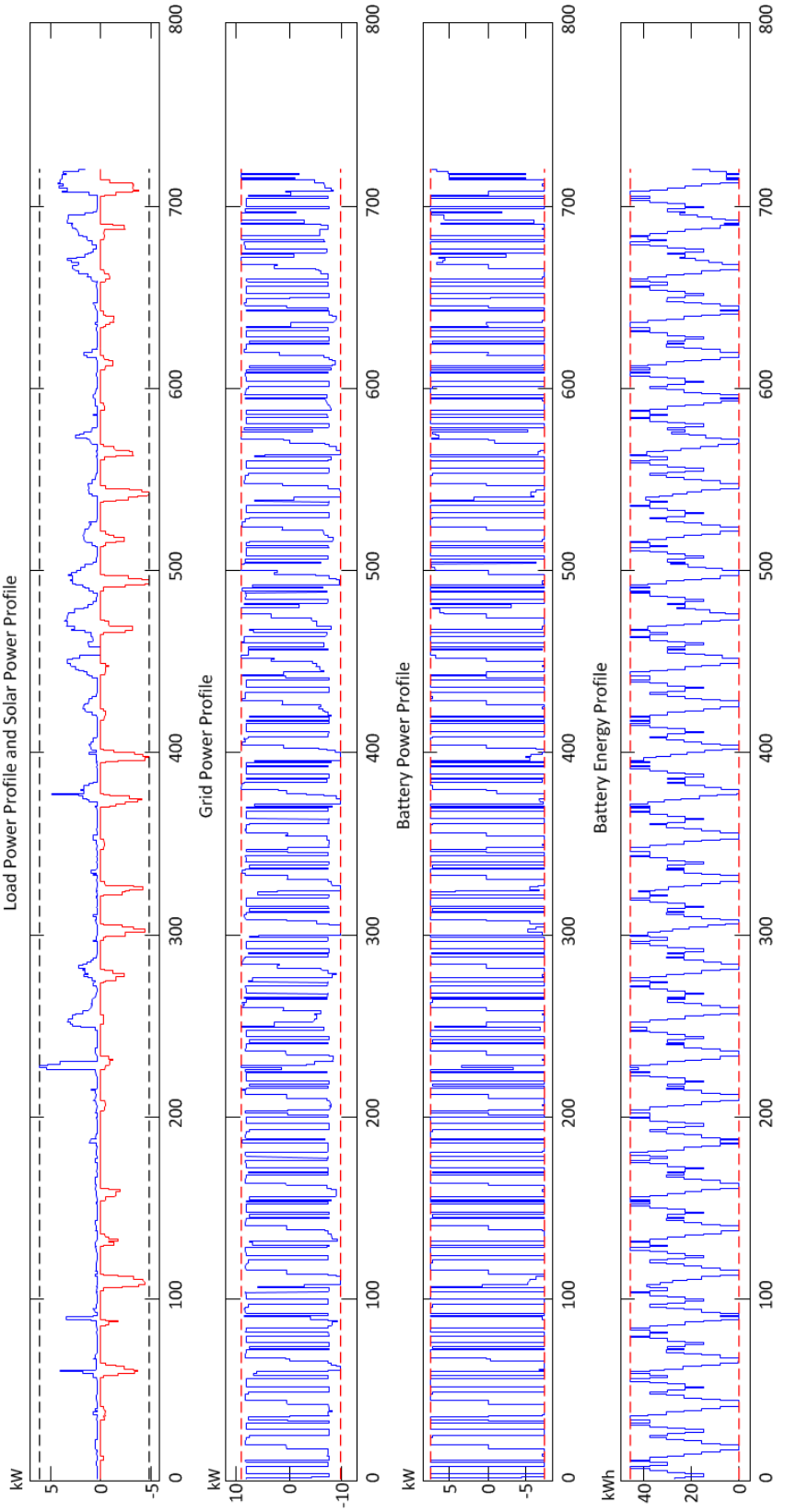

Figure 3.9: MILP-based component sizing optimization to maximize revenue - with future pricing(1). a) Load power profile and solar array power profile b) Grid power profile after optimization c) Battery power profile d) Battery energy profile

In the next scenario, the monthly capital cost of battery unit is reduced to $25 per battery module at sometime in the future.

The optimization was run for the whole month. The results of optimization are given in Table 4.10.

Device	Part number	Quantity	Total power (kW)	Total Energy (kWh)
Solar Panels	Conergy 235P-60	16	3.68	N/A
Battery	Trojan IND17-6V	10	11	65.4

Table 3.8: Optimal system configuration- component sizing with future pricing(2)

The cost saving of battery backed solar panel system with EMS is listed in Table 4.11. With the components selected for this house, the monthly cost is $93 instead of $174 cost.

Electricity cost, pure load ($)	174
Solar Array revenue ($)	-63
Battery with EMS revenue ($)	-324
Total monthly solar capital cost ($)	56
Total monthly battery capital cost ($)	250
Total monthly cost ($)	93

Table 3.9: Monthly cost/revenue for optimal configuration - component sizing with future pricing(2)

The optimized power or energy profiles for each component are illustrated in Figure 4.10. The result shows that the grid power profile is optimized to take advantage of the TOU price to maximize savings.

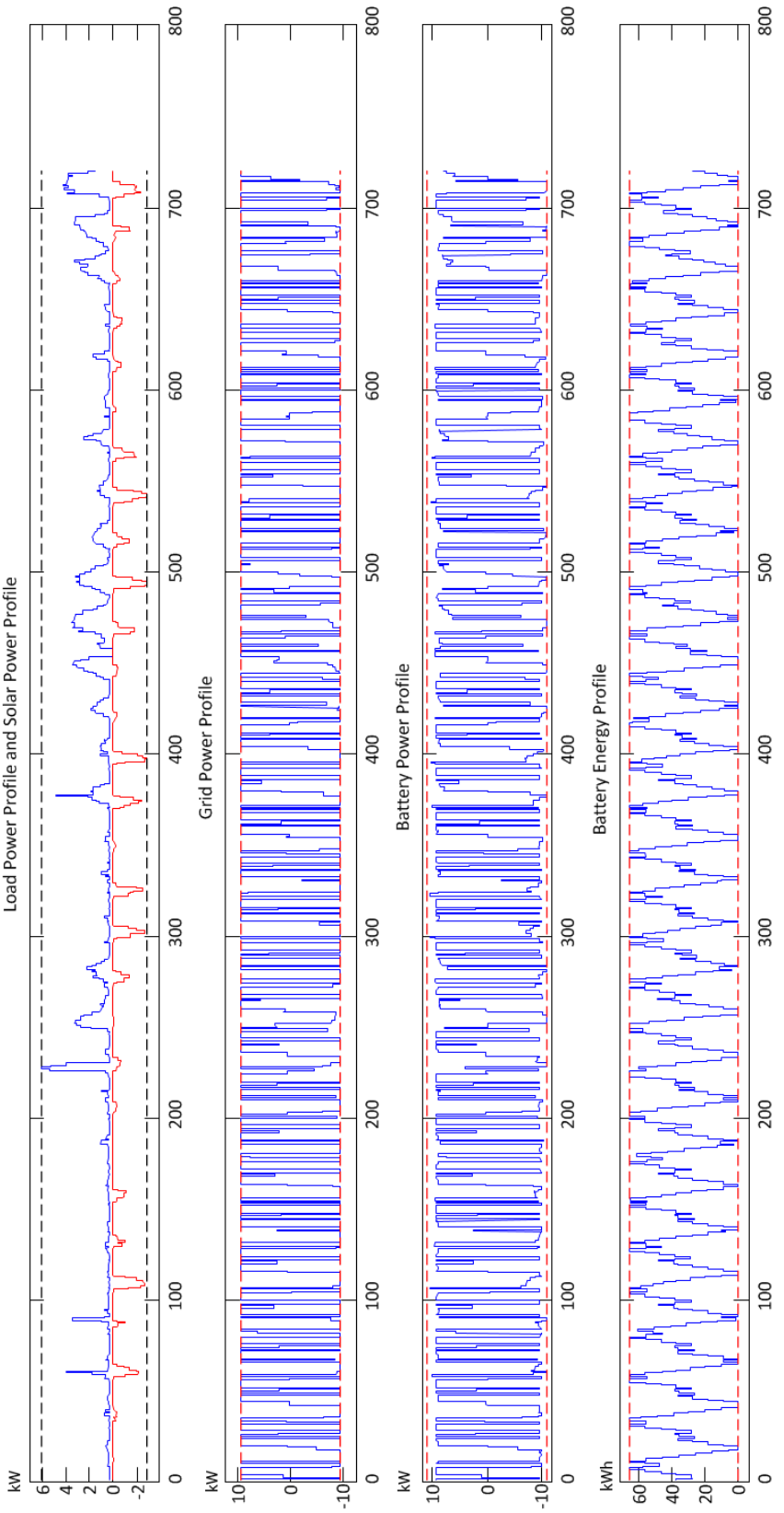

Figure 3.10: MILP-based component sizing optimization to maximize revenue - with future pricing(2). a) Load power profile and solar array power profile b) Grid power profile after optimization c) Battery power profile d) Battery energy profile

3.4.3 Case 3 - Future TOU Price Buy-in Only

The cases assumes that the user would not be able to sell power back to the grid. The other assumptions made in the previous case are still valid here.

With the above assumption, the number of component modules can be determined as the solution to the following linear programming problem

$$\min_x((\mathbf{C_{TOU}}^T\mathbf{P_{sol}} + C_{sol})n_{sol} + C_s n_s + \mathbf{C_{TOU}}^T\mathbf{P_g^+}) \tag{3.22}$$

$$x = [\, n_{sol} \quad n_s \quad \mathbf{P_s} \quad E_s^0 \quad \mathbf{P_g^+} \,]^T \tag{3.23}$$

subject to

$$-n_s{}_s^{\max} \leq \mathbf{P_{s_k}} \leq n_s P_s^{\max}, \quad k \in [1, N_h] \tag{3.24}$$

$$-P_g^{\max} \leq \mathbf{P_{s_k}} + n_{sol}\mathbf{P_{sol_k}} + \mathbf{P_{d_k}} \leq P_g^{\max}, \quad k \in [1, N_h] \tag{3.25}$$

$$0 \leq \sum_{j=1}^{k} \mathbf{P_{s_j}} + E_s^0 \leq n_s E_s^{\max} \quad , \quad k \in [1, N_h] \tag{3.26}$$

$$1^T\mathbf{P_s} = 0 \tag{3.27}$$

$$\mathbf{P_s} + n_{sol}\mathbf{P_{sol}} + \mathbf{P_d} \leq \mathbf{P_g^+} \tag{3.28}$$

$$0 \leq n_{sol} \leq n_{sol}^{max} \tag{3.29}$$

where

$\mathbf{P_g^+} \in \Re^{\mathbf{N_h}}$: inbound grid power flow in $\$/kW$.

The rest of variables have been defined earlier.

The positive grid power $\mathbf{P_g^+}$ has its upper bound and lower bound

$$\mathbf{0_{N_h}} \leq \mathbf{P_g^+} \leq \mathbf{P_g^{max}}\mathbf{1_{N_h}}$$

The capital cost of solar panel and battery is the same as the previous case. The optimization was run for the whole month. The results are given in Table 3.10.

Device	Part number	Quantity	Total power (kW)	Total Energy (kWh)
Solar Panels	Conergy 235P-60	27	6.21	N/A
Battery	Trojan IND17-6V	1	1.1	6.54

Table 3.10: Optimal system configuration with future pricing and buy-in only

The cost saving of battery backed solar panel system with EMS is listed in Table 3.11. With the components selected for this house, the monthly cost is reduced to \$171.5 from \$174.

Electricity cost, pure load ($)	174
Solar Array revenue ($)	-106
Battery with EMS revenue ($)	-16
Total monthly solar capital cost ($)	94.5
Total monthly battery capital cost ($)	25
Total monthly cost ($)	171.5

Table 3.11: Cost saving for optimal configuration with future pricing and buy-in only

The optimized power or energy profiles for each component are illustrated in Figure 3.11. From this graph, it can be clearly seen that the grid power profile is optimized in a way that both consuming/feedback power from/to the grid are being minimized.

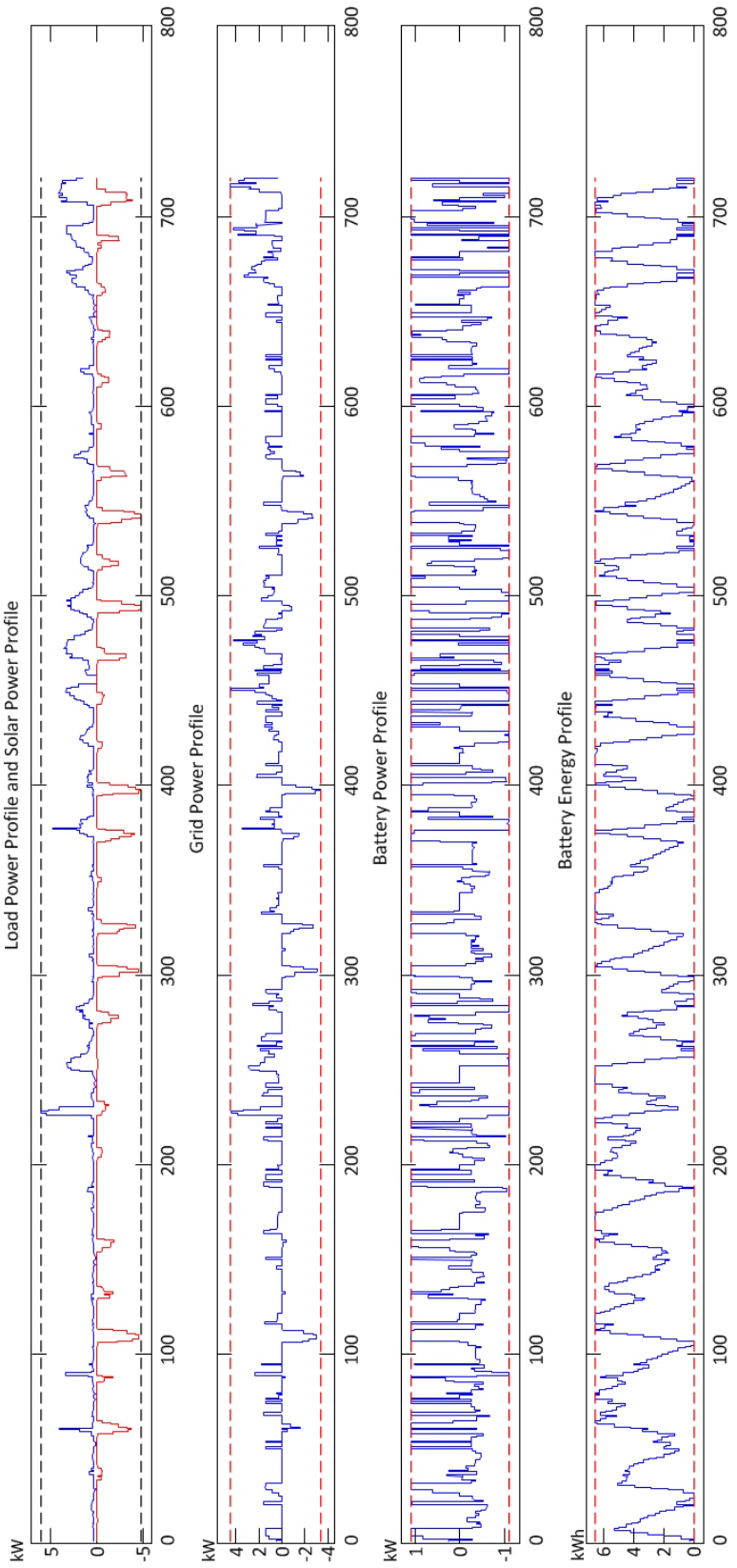

Figure 3.11: MILP-based component sizing optimization to maximize revenue - with future pricing buy-in only. a) Load power profile and solar array power profile b) Grid power profile after optimization c) Battery power profile d) Battery energy profile

3.4.4 Islanding Operation for Remote Homes

This case considers a scenario in which the microgrid is isolated from the grid, i.e. islanded mode operation. This would be typical of remote communities which would not have access to the grid and have to rely on on-site generation for their electricity needs. Renewable energy sources like solar and wind alone may not meet the actual demand all the time, given the variability in weather conditions. An energy storage device such as a battery will help provide a reliable supply of power to an islanded microgrid with solar and wind energy.

Optimization Formulation

The optimal number for each energy sources and storages are obtained by solving the following mixed integer linear programming problem

$$\min_x (n_{sol}C_{sol} + n_{wind}C_{wind} + n_{si}C_{si}) \qquad i \in [1, N_s] \tag{3.30}$$

$$x = [\, n_{sol} \quad n_{wind} \quad n_{si} \quad E_s^0 \quad \mathbf{P_{si}} \,]^T \qquad i \in [1, N_s] \tag{3.31}$$

subject to

$$-n_{si}P_{si}^{\max} \leq \mathbf{P_{si_k}} \leq n_{si}P_{si}^{\max} \quad i \in [1, N_s] \;, \quad k \in [1, N_h] \tag{3.32}$$

$$0 \leq \sum_{j=1}^{k} \mathbf{P_{Si_j}} + E_{si}^0 \leq n_{si}E_{si}^{\max} \quad i \in [1, N_s] \quad , \quad k \in [1, N_h] \tag{3.33}$$

$$1^T\mathbf{P_{si}} = 0 \qquad i \in [1, N_s] \tag{3.34}$$

$$n_{sol}\mathbf{P_{sol}} + n_{wind}\mathbf{P_{wind}} + \sum_{j=1}^{i} \mathbf{P_{Sj}} \leq -\mathbf{P_d} \qquad i \in [1, N_s] \tag{3.35}$$

$$-n_{sol}1^T\mathbf{P_{sol}} - n_{wind}1^T\mathbf{P_{wind}} \leq \max\left(-1^T\mathbf{P_{sol}}, -1^T\mathbf{P_{wind}}\right) + 1^T\mathbf{P_d} \tag{3.36}$$

where

$E_s^0 \in \Re$: initial energy level of energy storage module.

$N_s \in \Re$: number of different kinds of energy storages.

$\mathbf{P_{sol}} \in \Re^{N_h}$: solar panel power profile.

$\mathbf{P_{wind}} \in \Re^{N_h}$: wind turbine power profile.

$E_s^{max} \in \Re$: capacity of energy storage module.

$n_{wind} \in \Re$: number of wind turbines.

$n_s \in \Re$: number of energy storage units.

$C_{sol} \in \Re$: capital cost of each solar panel.

$C_{wind} \in \Re$: capital cost of each wind turbine.

$C_s \in \Re$: capital cost of each energy storage module.

$\mathbf{P_{sol}}$ and $\mathbf{P_{wind}}$ are always negative, which means generation. The total power supplied by solar, wind and energy storage must exceed the demand as in Eq 3.35. Total electricity generation is bounded to prevent over generation as in Eq 3.36.

The example considered is a remote community of 21 households, without grid connection. Wind and solar are energy sources of energy for this microgrid. Three types of energy storage device with the power and energy ratings in Table 3.12 are considered in this study.

Device	Unit power rating (kW)	Unit energy rating (kWh)	Unit cost $
Solar Panels	0.25	N/A	550
Wind turbine	0.8	N/A	2000
Energy storage 1	1	5	850
Energy storage 2	10	0.1	6000
Energy storage 3	30	2.5	2000

Table 3.12: Unit rated values and cost of equipments for remote village

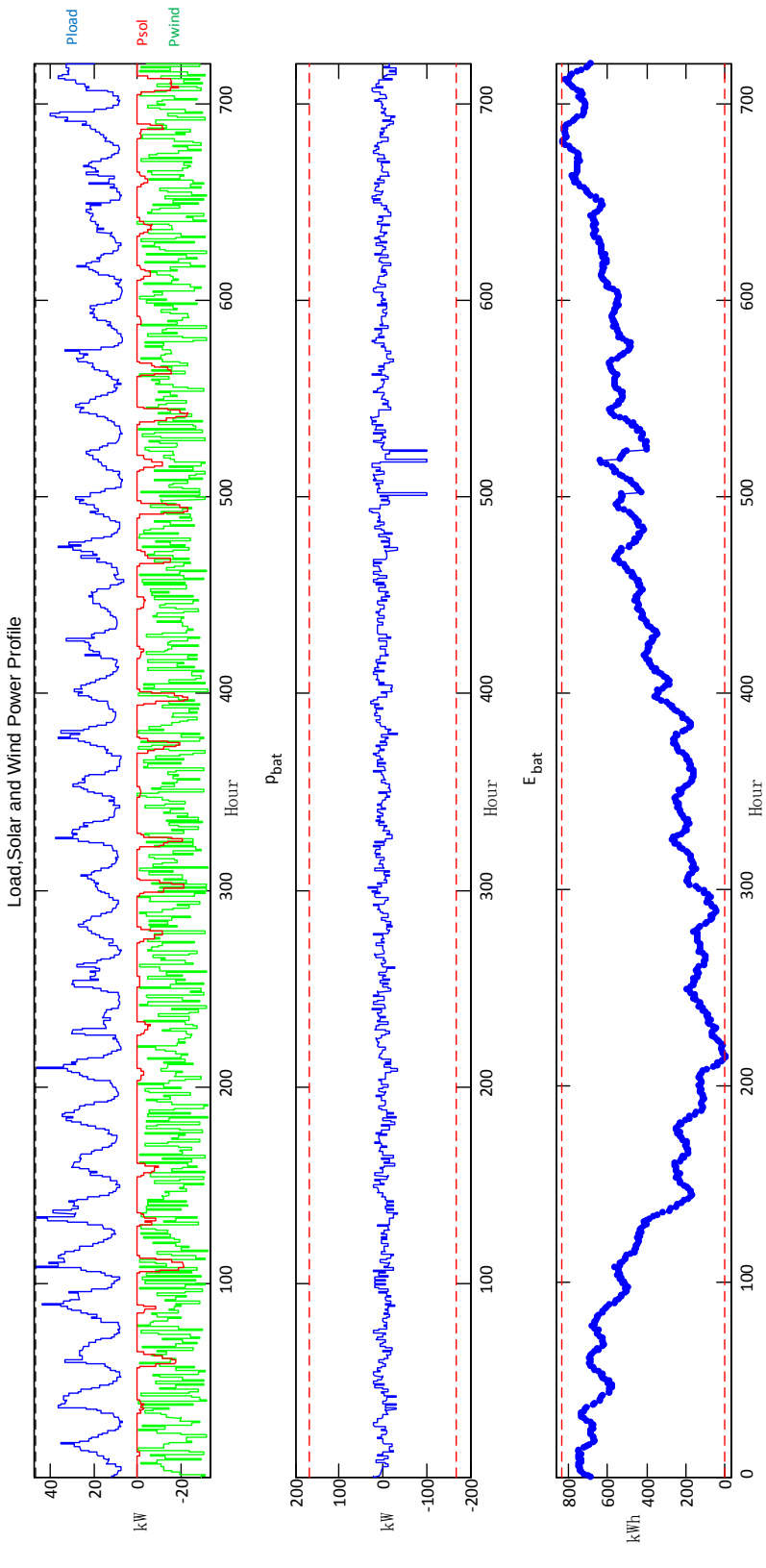

Figure 3.12: An islanded microgrid for a remote community. a) Load, solar and wind power profile b) energy storage power profile c) energy storage energy profile

The results are given in Table 3.13.

Device	Number of units	Total Cost
Solar Panels	130	65,000
Wind turbines	40	80,000
Energy storage 1	167	143,650
Energy storage 2	0	0
Energy storage 3	0	0
Total		288,650

Table 3.13: Number of units after optimization

The optimization result suggests the minimum number of each device to power up this community. The system cost for each house is 288,650 / 21 = 13,745. There are three types of energy storages available. Only the first one is chosen by the optimization, since the capital cost and energy rating of the other two energy storages are not suitable for this community. Also note from the above figure that there are a lot of energy storages are added to this system. Compared to the maximum power rating, the actuarial power usage level of the energy storage is much lower. From the storage energy profile graph, it can be seen that energy is shifting from the beginning to the end of the month. The reason causing this result is that there is no energy sink for excessive energy generated nor a dispatchable generator, e.g. a diesel generator.

Chapter 4

Commercial and Industrial EMS System Level Analysis

In this chapter, energy management for commercial and industrial settings is studied. Power profile for a typical commercial building is presented in the first section. The second section presents the power profile for a typical industrial site. The third section introduces a sample formulation of the optimization problem for commercial and industrial energy management system along with an example of each commercial and industrial application. The last section discusses the formulation of an optimization problem for sizing of components in commercial and industrial energy management systems. Five scenarios of component sizing with different pricing regimes are presented in this chapter.

4.1 Commercial Building Power Profile

Examples of commercial buildings are office buildings, warehouses and retail stores. The electricity usage patterns of commercial buildings have been analyzed by the US department of energy. The major usages of energy in a commercial building are listed in Table 4.1.

Purpose	Usage (Quadrillion Btu)	Percentage (%)
Lighting	3.69	26.4
Space Heating	0.88	6.3
Space Colling	2.60	18.6
Ventilation	1.66	11.9
Refrigeration	1.21	8.6
Water Heating	0.28	2.0
Electronics	0.81	5.8
Computers	0.66	4.7
Cooking	0.07	0.5
Other	2.13	15.2
Total	13.99	100

Table 4.1: 2010 Commercial energy usage split (DOE, 2012)

For this study, the hourly energy usage profile of a commercial building in Burlington, Ontario, for the period January 1 to December 31, 2012 was obtained from Burlington Hydro. Figure 4.1 shows the energy usage for a month, July 2 to August 1, plotted in red and Feb 20 - March 19, plotted in blue. Both monthly data plots start on Sunday and end on Saturday. The figure shows a single peak appears late afternoon in summer days and two peaks in winter days. The electricity load in weekdays is significantly higher than that in weekends for this commercial building. This can be attributed to the fact that the people spend most of their time in the office during working hours in weekdays. Note that, from Table 4.1, lighting, space cooling

and ventilation account for more than 50% of the electricity load.

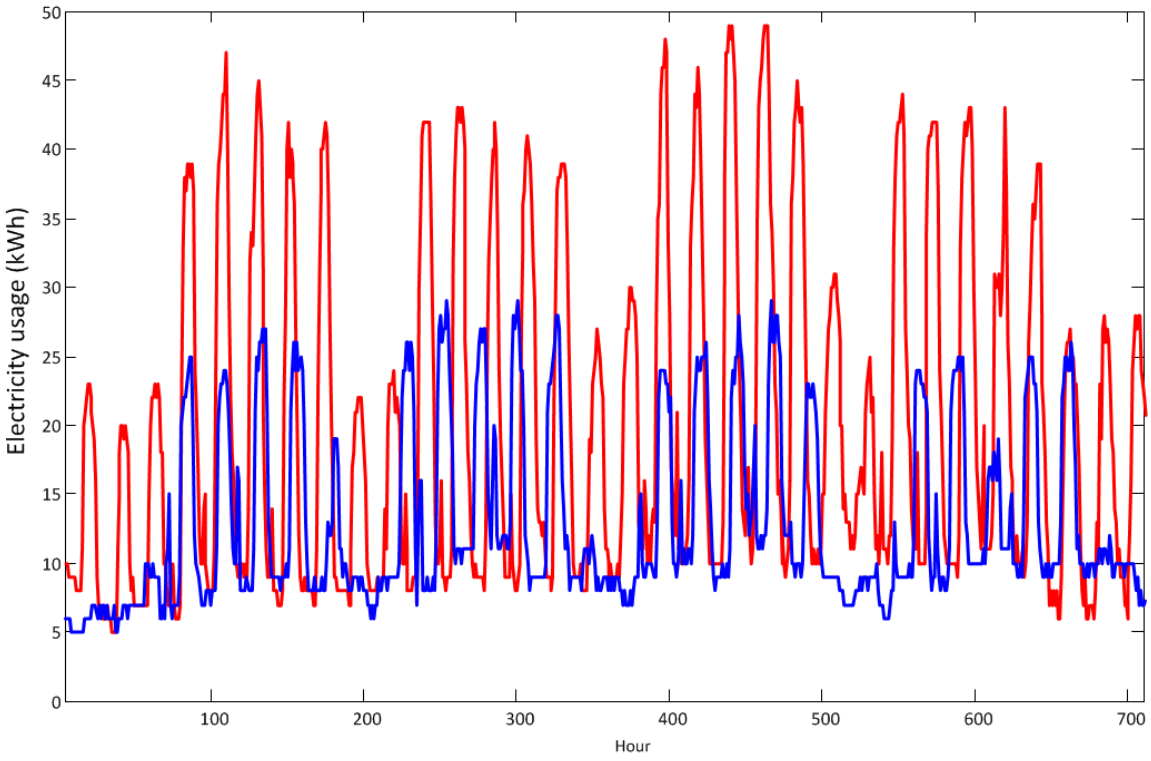

Figure 4.1: Commercial building hourly power usage for a month in summer and winter

Figure 4.2 shows the Probability Density Function (PDF) of hourly electricity energy usage obtained from the whole year data. The mean hourly consumption is 13.98 kWh, with peak demand 50kW. As mentioned in Chapter 3, medium and large electricity consumers are also charged for peak demand. Peak demand charge used in this chapter is \$6 per kW. As shown in the figure, there are not many hours with energy usage higher than 35kWh. Therefore, it is ideal for energy management system to reduce the peak and smoothen the grid power profile in order to reduce total electricity cost. Compared to residential power usage profile, a commercial building's power profile has a more consistent pattern with seasonal and weekly cycles.

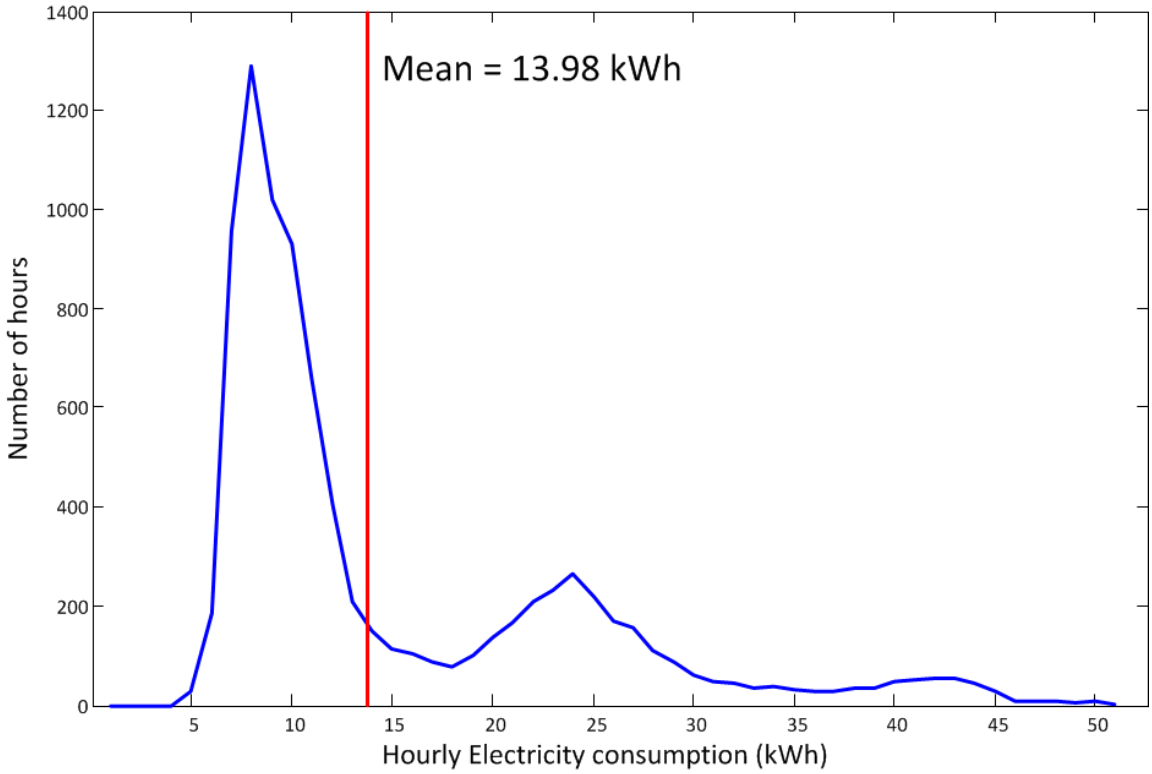

Figure 4.2: Probability density function of annual energy usage for a commercial building

4.2 Industrial Building Power Profile

The electricity usage in an industrial building is mainly for industrial production, e.g. motor drive, lighting and other industrial load. The hourly electric energy usage profile of an industrial building in Burlington, Ontario, for the period January 1, 2012 to December 31 2013 was obtained from Burlington Hydro. A weekly usage cycle can be clearly identified from this data. For weekdays, there are electrical loads which run 24 hours a day, and peak load only appears during working hours. For weekends, the load drops significantly, with some peaks occurring during the day. There is no significant load variation between summer and winter for this industrial plant, since

HVAC and lighting only accounts for a small portion of the total load.

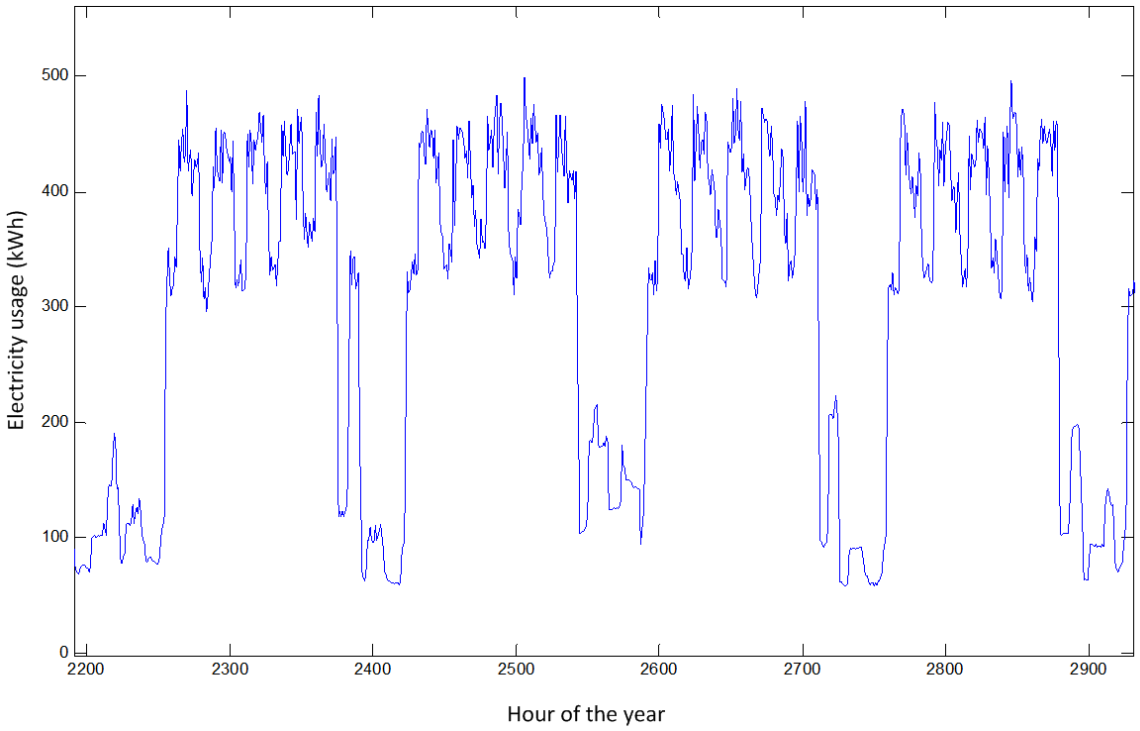

Figure 4.3: Industrial building hourly power usage for a month

The probability density function of the hourly energy demand for this building is shown in Figure 4.4. The mean usage is 335 kWh and the maximum demand is 630kWh.

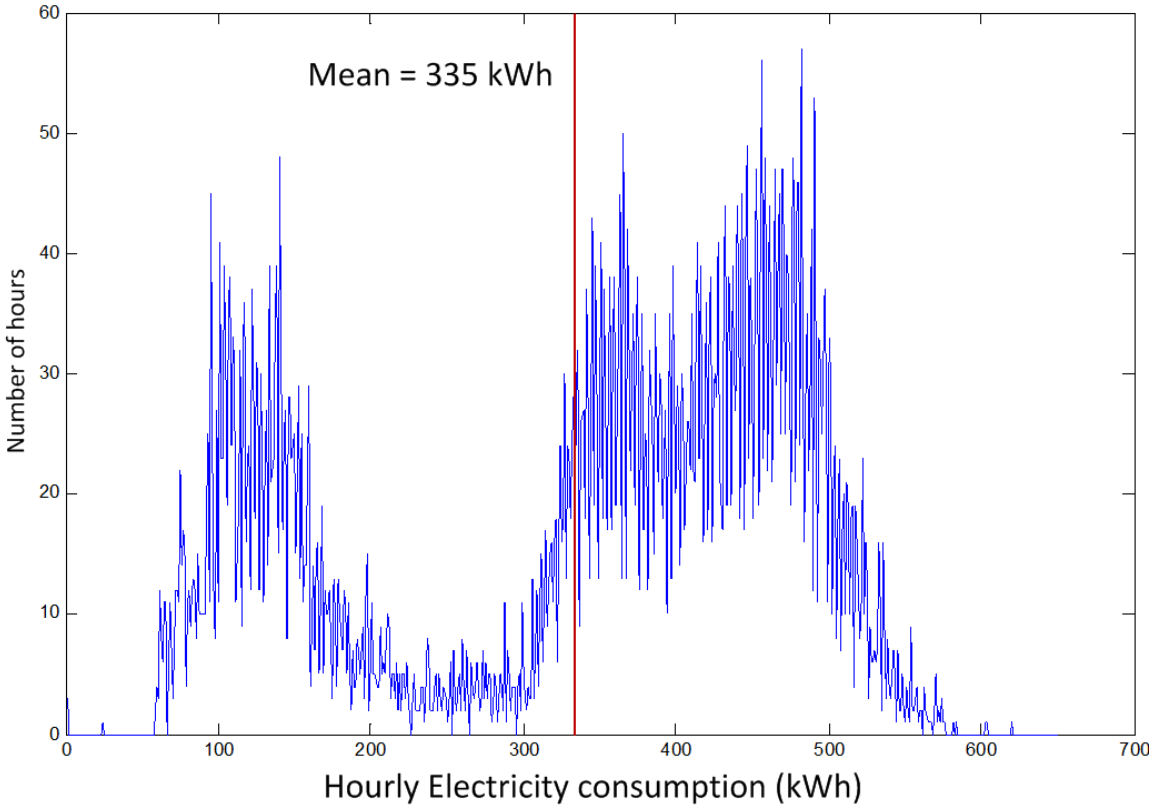

Figure 4.4: Industrial building probability density function of annual power usage

4.3 Power Usage Optimization for Commercial and Industrial Setting

In this section, an EMS system with energy storage for commercial and industrial settings is studied. In addition to the TOU price, a peak demand charge needs to also be considered in this case.

4.3.1 Optimization Formulation

The battery storage charge/discharge activities are solution to the following linear programming problem

$$\min_x(\mathbf{C_{TOU}}^T\mathbf{P_s} + C_{dem}P_g^{\max}) \tag{4.1}$$

$$x = [\mathbf{P_s}, E_0]^T$$

subject to

$$-P_s^{\max} \leq \mathbf{P_s} \leq P_s^{\max} \tag{4.2}$$

$$0 \leq \mathbf{P_s} + E_0 \leq E_{bat} \quad k \in [1, N_h] \tag{4.3}$$

$$-P_g^{\max}1_{N_h} \leq \mathbf{P_g} = \mathbf{P_d} + \mathbf{P_s} \leq P_g^{\max}1_{N_h} \tag{4.4}$$

$$\mathbf{1}^T P_s = 0 \tag{4.5}$$

where

$N_h \in \Re$: number of hours in the time horizon under study.

$\mathbf{C_{TOU}} \in \Re^{\mathbf{N_h}}$: TOU cost in $\$/kW$.

$C_{dem} \in \Re$: peak demand charge.

$\mathbf{P_s} \in \Re^{\mathbf{N_h}}$: battery storage input or output power.

$E_s^0 \in \Re$: initial energy level of the battery.

$\mathbf{P_d} \in \Re^{\mathbf{N_h}}$: net demand of the electricity load.

$P_g^{\max} \in \Re$: maximum power allowed at the common point of coupling.

$P_s^{\max} \in \Re$: maximum power rating of the battery.

$E_{bat} \in \Re$: capacity of battery.

Note that in the above formulation, a positive $\mathbf{P_s}$ means charging and negative $\mathbf{P_s}$

denotes discharging of the battery. There are limits on charge and discharge power rates of the battery, as in Eq 4.2. The battery also has minimum and maximum allowable energy levels as shown in Eq 4.3. Buying and selling power from/to the grid is limited by the constraints in Eq 4.4. The constraint in Eq 4.4 ensures the battery would return to the same energy level after a 24 hour period of usage. The optimization problem was solved in Matlab 2012b using MILP solver LPSolve 5.5.

4.3.2 Case Study - Commercial Building

Current TOU net metering pricing with demand charge is used in this case. No solar system is presented in this case. The electricity usage data is obtained from Burlington Hydro (Burlington, Ontario). 30 days hourly realtime data is used in the simulation,i.e. see Figure 4.5 (a). It is assumed that a 70 kWh battery unit is used with a maximum output power rating of 10kW. Maximum allowed grid power is $P_g^{\max} = 100kW$. The capital cost of equipments is not considered in this example.

The optimization was run for the whole month. The simulation results are given in Figure 4.5. From this graph, it can be clearly seen that the some of the peak load is shifted to off-peak period, and the demand curve is smoothed as a result of utilizing the energy storage element. The peak demand is reduced from 30kW to 20kW.

The electricity costs with and without EMS are given in Table 4.2. In this case, EMS with energy storage yields a saving of 14.5%, compared to the case where the building is directly connected to the grid.

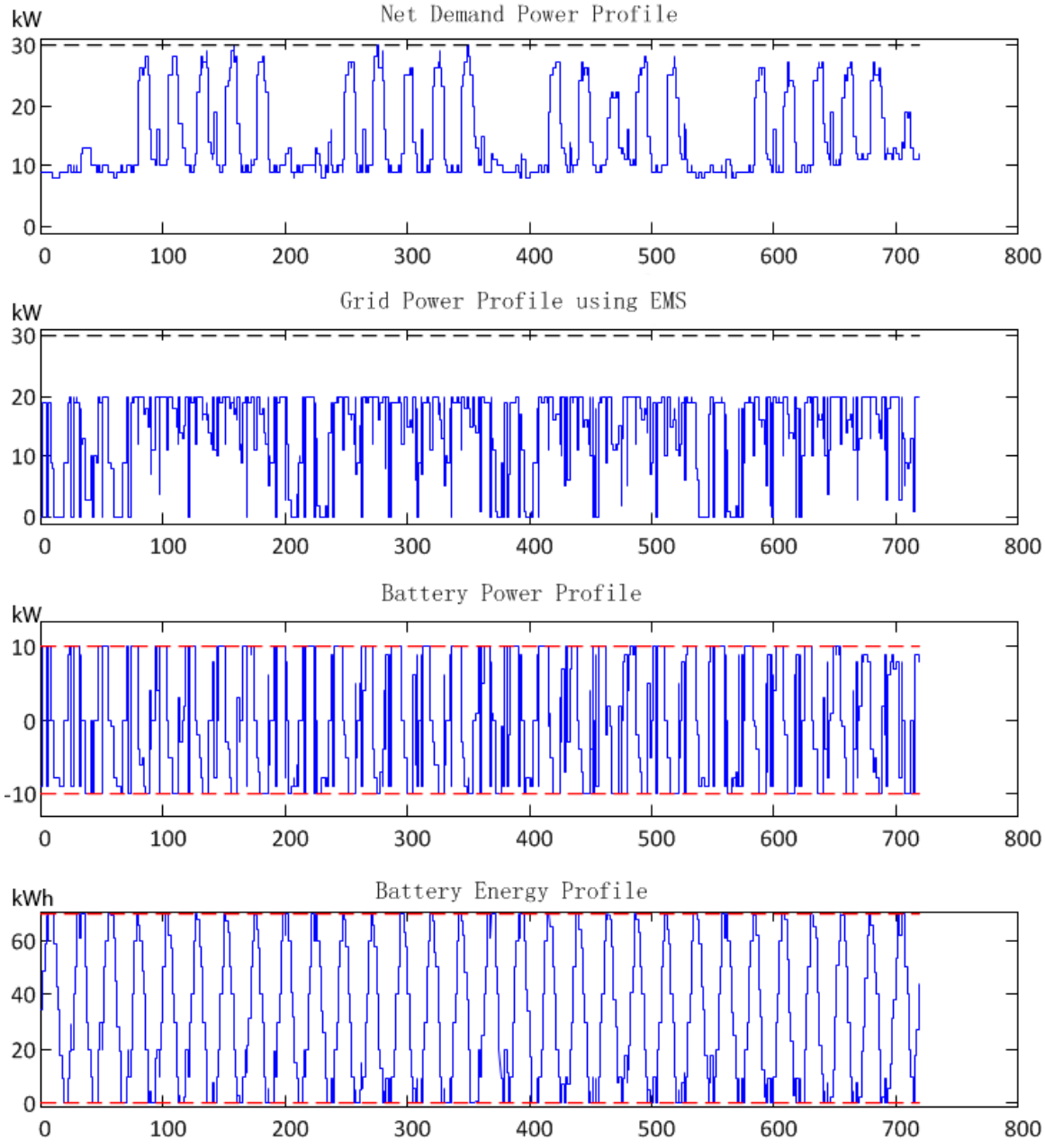

Figure 4.5: Commercial TOU with demand charge optimization, (a) power net demand power profile, (b) grid power profile with EMS, (c) battery power profile, (d) battery energy profile

Electricity Cost without EMS($)	1171.96
Electricity Cost with EMS ($)	1000.4
Demand charge saving ($)	60
TOU charge saving ($)	111.56
Total saving ($)	171.56
Percentage saving (%)	14.5%

Table 4.2: Electricity saving with EMS for commercial building

4.3.3 Case Study - Industrial Site

Other then specified conditions, the simulation is the same as the previous case. The industrial building electricity usage data was obtained from Burlington Hydro (Burlington, Ontario). 30 days hourly data in Figure 4.6 (a) was used in the optimization. The microgrid is assumed to be equipped with a 600 kWh battery used with a maximum output power rating of 100kW. The power rating to the grid is $P_g^{\max} = 1000kW$.

The results of the optimization are presented in Figure 4.6. It can be seen from this data that on-peak power consumption is reduced and the demand curve is smoothed as a result of utilizing the energy storage element in an optimal way. Peak demand is reduced from 510kW to 465kW.

The electricity costs with and without EMS are given in Table 4.2. In this case, the EMS with energy storage yields a saving of 5.71%, compared to the case where the building is directly connected to the grid.

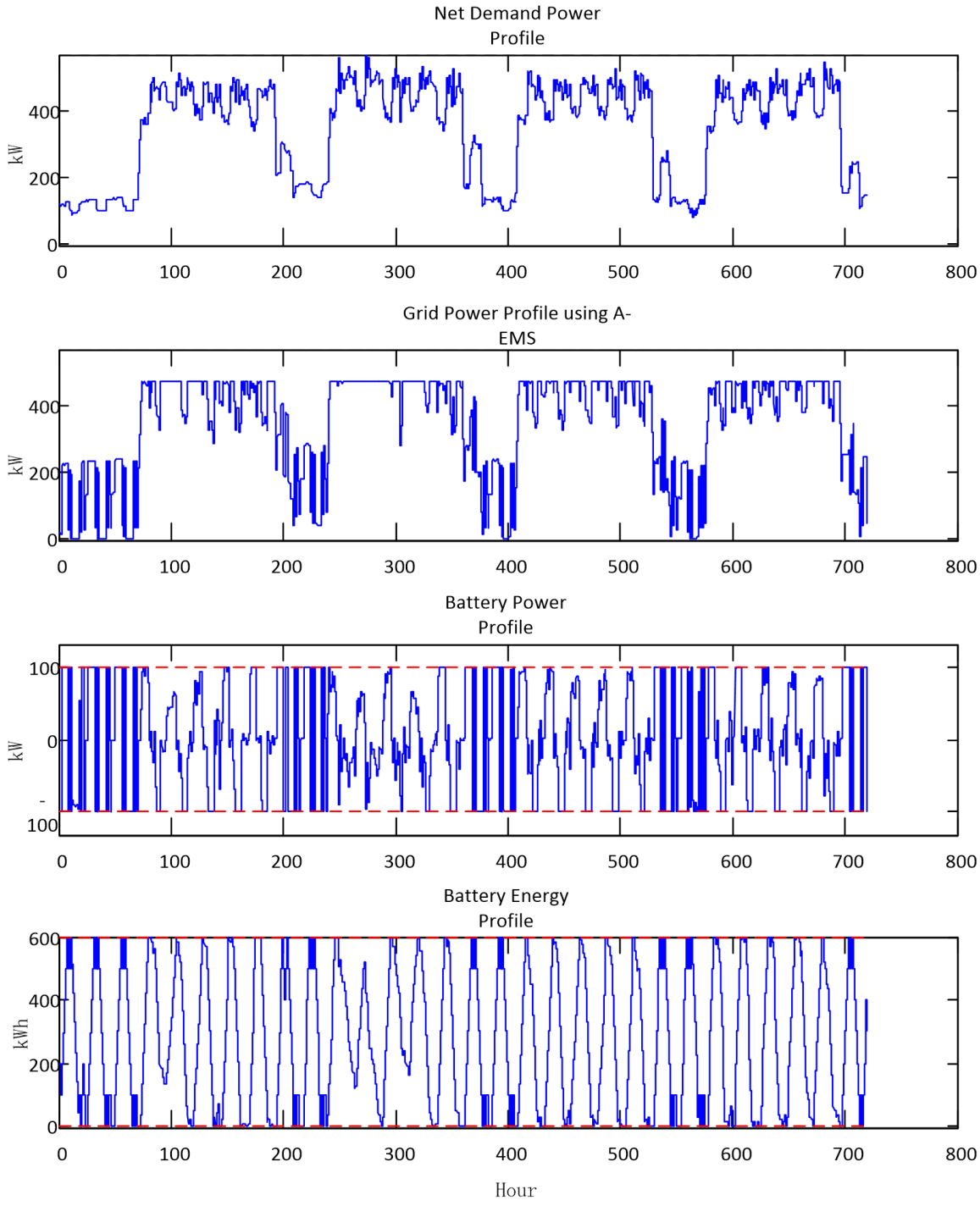

Figure 4.6: Industrial TOU with demand charge optimization, (a) power net demand power profile, (b) grid power profile with EMS, (c) battery power profile, (d) battery energy profile

Electricity Cost without EMS($)	26282
Electricity Cost with EMS ($)	24781
Demand charge saving ($)	587
TOU charge saving ($)	914
Total saving ($)	1501
Percentage saving (%)	5.71%

Table 4.3: Electricity saving with EMS for industrial setting

4.4 Components Sizing Optimization

In this section, an optimization problem is formulated to help determine an optimal system configuration in terms of component sizing. Several pricing regimes are considered in sizing components.

4.4.1 Current TOU price and Micro-fit with Demand Charge

The power pricing regime is assumed to be net metering with current TOU price for household load and micro-fit price for solar power in this optimization. For most of the commercial and industrial building, demand charge would apply to their bill. Therefore, The task of determining components size could be formulated as a mixed integer linear program optimization.

$$\min_x(C_{sol}n_{sol} + C_s n_s + \mathbf{C_{TOU}}^T\mathbf{P_s} + (\mathbf{C}^T_{Micro-FIT}\mathbf{P_{sol}})n_{sol} + C_{dem}P_g^{peak}) \tag{4.6}$$

$$x = [\, n_{sol} \quad n_s \quad E_s^0 \quad \mathbf{P_s} \quad P_g^{peak} \,]^T \tag{4.7}$$

subject to

$$-n_s P_s^{\max} \leq \mathbf{P_{s_k}} \leq n_s P_s^{\max}, \quad k \in [1, N_h] \tag{4.8}$$

$$-P_g^{\max} \leq P_{s_k} + n_{sol} P_{sol_k} + P_{d_k} \leq P_g^{\max}, \quad k \in [1, N_h] \tag{4.9}$$

$$0 \leq \sum_{j=1}^{k} P_{S_j} + E_s^0 \leq n_s E_s^{\max} \quad , \quad k \in [1, N_h] \tag{4.10}$$

$$1^T P_s = 0 \tag{4.11}$$

$$n_{sol} \leq n_{sol}^{max} \tag{4.12}$$

where

$E_s^{max} \in \Re$: capacity of battery.

$n_{sol} \in \Re$: number of solar panel.

$n_{sol}^{max} \in \Re$: maximum number of solar panel allowed by physical condition.

$n_s \in \Re$: number of battery unit.

$P_g^{peak} \in \Re$: peak power demand.

$C_{sol} \in \Re$: capital cost of solar panel.

$\mathbf{C_{Micro-FIT}} \in \Re^{\mathbf{N_h}}$: Micro-FIT pricing in $\$/kW$.

The rest of the variables have been defined earlier in the thesis.

The commercial building used in this case study is the one mentioned in Section 4.3.2. It is assumed that Trojan IND17-6V, 6.54kWh battery module with a maximum output power rating of 1.1kW and Conergy 235P-60 solar panel module with a maximum output power rating of 235W are used here and in the rest of the thesis. Solar panel power profile was obtained from Burlington Hydro for the same period of time as the electricity usage data. Monthly cost of each solar panel in this optimization is assumed to be $3.5, and the monthly cost for each battery module is assumed to be $25. Moreover, $P_g^{\max} = 100kW$. $n_{sol}^{max} = 200$

The cost saving of installing EMS is listed in Table 4.5. With the components

Device	Part number	Quantity	Total power (kW)	Total Energy (kWh)
Solar Panels	Conergy 235P-60	200	39.95	N/A
Battery	Trojan IND17-6V	18	19.8	117.72

Table 4.4: Optimal number of component modules for a commercial building with Micro-fit

selected for this building, the monthly electricity cost is reduced to $1168 from $1180.

Electricity cost, pure load ($)	1180
Solar Array revenue ($)	-724
Battery with EMS TOU revenue ($)	-312
Demand charge revenue ($)	-126
Total monthly solar capital cost ($)	700
Total monthly battery capital cost ($)	450
Total monthly cost ($)	1168

Table 4.5: Monthly electricity cost and revenue for commercial building with Micro-fit

The optimized power and energy profiles for each components are illustrated in Figure 4.7. The data shows that the peak power demand at the point of common coupling to the grid is significantly reduced and the on-peak power consumption is minimized.

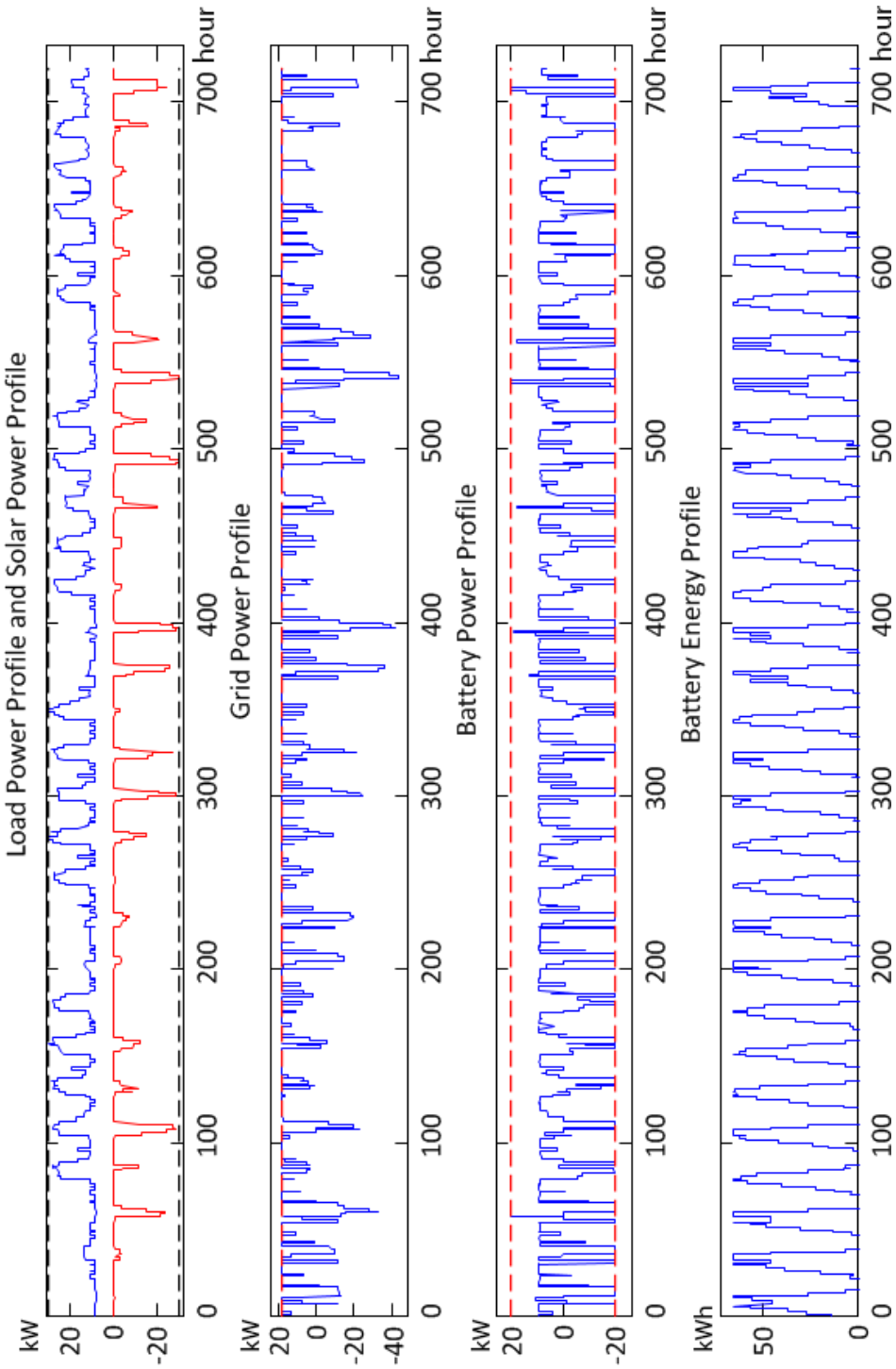

Figure 4.7: Commercial building optimization Micro-fit, a) Load power profile and solar array power profile b) Grid power profile after optimization c) Battery power profile d) Battery energy profile

4.4.2 Future TOU Price with Demand Charge

A different TOU price and demand charge are used in this case, by increasing the current prices by a factor of three. The pricing regime is assumed to be net metering only.

$$\min_x(C_{sol}n_{sol} + C_s n_s + \mathbf{C_{TOU}}^T\mathbf{P_s} + (\mathbf{C}_{TOU}^T\mathbf{P_{sol}})n_{sol} + C_{dem}P_g^{peak}) \tag{4.13}$$

$$x = [\, n_{sol} \quad n_s \quad E_s^0 \quad \mathbf{P_s} \quad P_g^{peak} \,]^T \tag{4.14}$$

subject to

$$-n_s P_s^{\max} \leq \mathbf{P_{s_k}} \leq n_s P_s^{\max}, \quad k \in [1, N_h] \tag{4.15}$$

$$-P_g^{\max} \leq P_{s_k} + n_{sol}P_{sol_k} + P_{d_k} \leq P_g^{\max}, \quad k \in [1, N_h] \tag{4.16}$$

$$0 \leq \sum_{j=1}^{k} P_{S_j} + E_s^0 \leq n_s E_s^{\max} \quad , \quad k \in [1, N_h] \tag{4.17}$$

$$1^T P_s = 0 \tag{4.18}$$

$$n_{sol} \leq n_{sol}^{max} \tag{4.19}$$

where all variables has been previously defined in the thesis.

Example - Commercial Setting

Monthly cost of each solar panel in this optimization is assumed to be $3.5, and the monthly cost for each battery module is assumed to be $25. The optimization was run for 30 days with 1 hour time step. The results are given in Table 4.10.

The cost saving of installing EMS is listed in Table 4.11. With the components

Device	Part number	Quantity	Total power (kW)	Total Energy (kWh)
Solar Panels	Conergy 235P-60	200	47	N/A
Battery	Trojan IND17-6V	20	22	130.8

Table 4.6: Optimal number of component modules for a commercial building microgrid with future pricing

selected for this building, the monthly electricity cost is $3217 instead of $3541 cost.

These cost saving is pure electrical and no capital cost is include in these numbers.

Electricity cost, pure load ($)	3541
Solar Array revenue ($)	-786
Battery with EMS revenue ($)	-549
Demand charge revenue ($)	-189
Total monthly solar capital cost ($)	700
Total monthly battery capital cost ($)	500
Total monthly cost ($)	3217

Table 4.7: Cost saving for optimal configuration for commercial building with future pricing

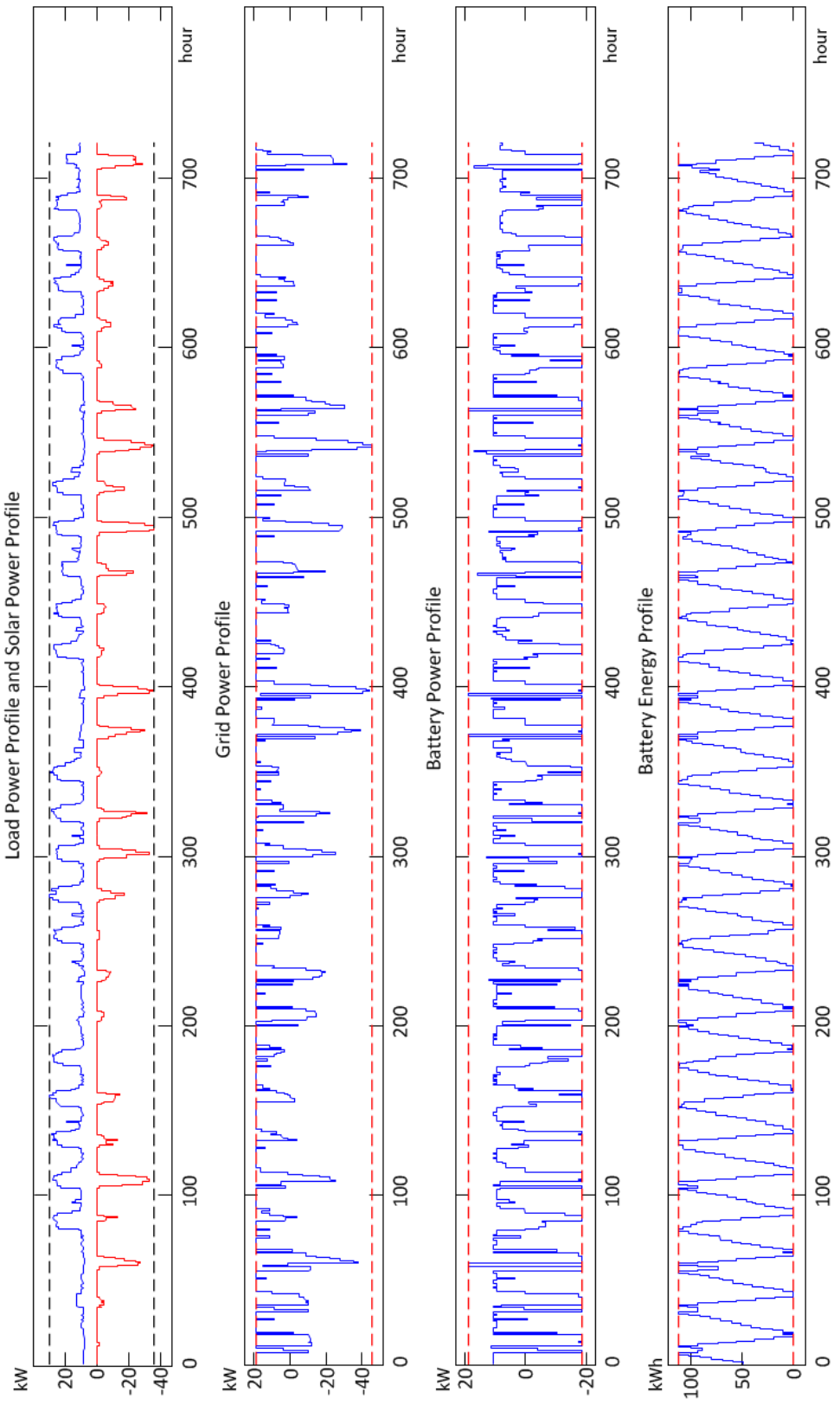

Figure 4.8: MILP-based component sizing optimization to maximize revenue for commercial setting with future pricing. a) Load power profile and solar array power profile b) Grid power profile after optimization c) Battery power profile d) Battery energy profile

Example - Industrial Setting

As in the previous example, monthly cost of each solar panel is assumed to be $3.5, and the monthly cost for each battery module is assumed to be $25. The maximum number of solar panel is 2000 and $P_g^{\max} = 1000kW$.

The optimization was run for the whole month. The results are given in Table 4.8.

Device	Part number	Quantity	Total power (kW)	Total Energy (kWh)
Solar Panels	Conergy 235P-60	2000	47	N/A
Battery	Trojan IND17-6V	134	18.7	111.18

Table 4.8: Optimal number of component modules for an industrial microgrid with future pricing

The cost saving of installing EMS is listed in Table 4.9. With the components selected for this building, the monthly electricity cost is reduced to $57,201 from $76,166. The optimized power or energy profiles for each component are illustrated

Electricity cost, pure load ($)	76,166
Solar Array revenue ($)	-13,328
Battery with EMS revenue ($)	-7,279
Demand charge revenue ($)	-1,358
Total monthly solar capital cost ($)	7,000
Total monthly battery capital cost ($)	3,350
Total monthly cost ($)	64,551

Table 4.9: Cost saving for optimal configuration for industrial setting with future pricing

in Figure 4.9. It is evident from this graph that peak power demand at the point of common coupling to the grid is significantly reduced and the on-peak power consumption is minimized.

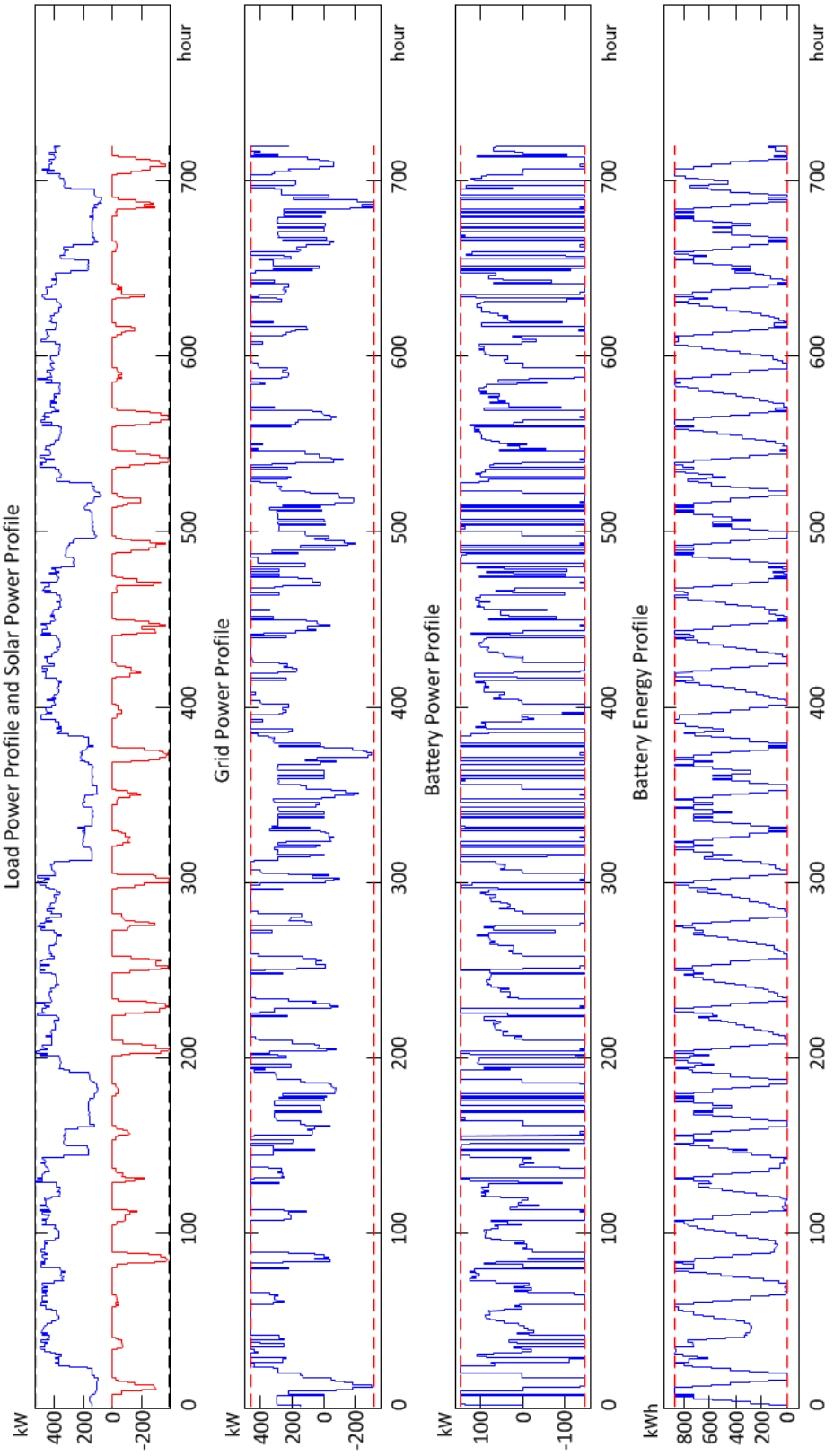

Figure 4.9: MILP-based component sizing optimization to maximize revenue for industrial setting with future pricing. a) Load power profile and solar array power profile b) Grid power profile after optimization c) Battery power profile d) Battery energy profile

4.4.3 Future TOU Price Buy-in Only with Demand Charge

Taking a step further from the previous case, the assumption in this case is that selling power back to the grid is not rewarded.

With the above assumption, the following MILP optimization can provide the optimal solution for the number of component modules.

$$\min_x((\mathbf{C_{TOU}}^T\mathbf{P_{sol}} + C_{sol})n_{sol} + C_s n_s + C^{dem}P_g^{peak} + \mathbf{C_{TOU}}^T\mathbf{P_g^+}) \tag{4.20}$$

$$x = [\, n_{sol} \quad n_s \quad E_s^0 \quad \mathbf{P_s} \quad P_g^{peak} \quad \mathbf{P_g^+}\,]^T \tag{4.21}$$

subject to

$$-n_s{}_s^{\max} \leq \mathbf{P_{s_k}} \leq n_s P_s^{\max}, \quad k \in [1, N_h] \tag{4.22}$$

$$-P_g^{\max} \leq \mathbf{P_{s_k}} + n_{sol}\mathbf{P_{sol_k}} + \mathbf{P_{d_k}} \leq P_g^{\max}, \quad k \in [1, N_h] \tag{4.23}$$

$$0 \leq \sum_{j=1}^{k} \mathbf{P_{s_j}} + E_s^0 \leq n_s E_s^{\max} \quad , \quad k \in [1, N_h] \tag{4.24}$$

$$1^T\mathbf{P_s} = 0 \tag{4.25}$$

$$\mathbf{P_s} + n_{sol}\mathbf{P_{sol}} + \mathbf{P_d} \leq \mathbf{P_g^+} \tag{4.26}$$

$$n_{sol} \leq n_{sol}^{max} \tag{4.27}$$

where

$C_s \in \Re$: capital cost of each battery pack.

$\mathbf{P_g^+} \in \Re^{\mathbf{N_h}}$: inbound grid power flow in $\$/kW$.

The positive grid power $\mathbf{P_g^+}$ has its upper bound and lower bound

$$\mathbf{0_{N_h}} \leq \mathbf{P_g^+} \leq \mathbf{P_g^{max}} \mathbf{1_{N_h}}$$

Example - Commercial Setting

One month is chosen as the optimization horizon with 1 hour time step. The simulation results are given in Table 4.10.

Device	Part number	Quantity	Total power (kW)	Total Energy (kWh)
Solar Panels	Conergy 235P-60	200	47	N/A
Battery	Trojan IND17-6V	11	12.1	71.94

Table 4.10: Optimal list of components for commercial setting with buy-in only

The cost saving of installing EMS is listed in Table 4.11. With the components selected for this building, the monthly electricity cost is reduced to $3256 from $3541.

Electricity cost, pure load ($)	3541
Solar Array revenue ($)	-786
Battery with EMS revenue ($)	-248
Demand charge revenue ($)	-226
Total monthly solar capital cost ($)	700
Total monthly battery capital cost ($)	275
Total monthly cost ($)	3,256

Table 4.11: Cost saving for optimal configuration for commercial setting with buy-in only

The optimized power or energy profiles for each component are illustrated in Figure 4.10. From this graph, it can be clearly seen that the grid power profile is optimized in a way that both consume/feed power from/to the grid are being limited to a range between 0 and the optimized maximum peak demand(kW). The battery

activity is optimized to store any excessive energy and discharge it to supply peak load, when needed.

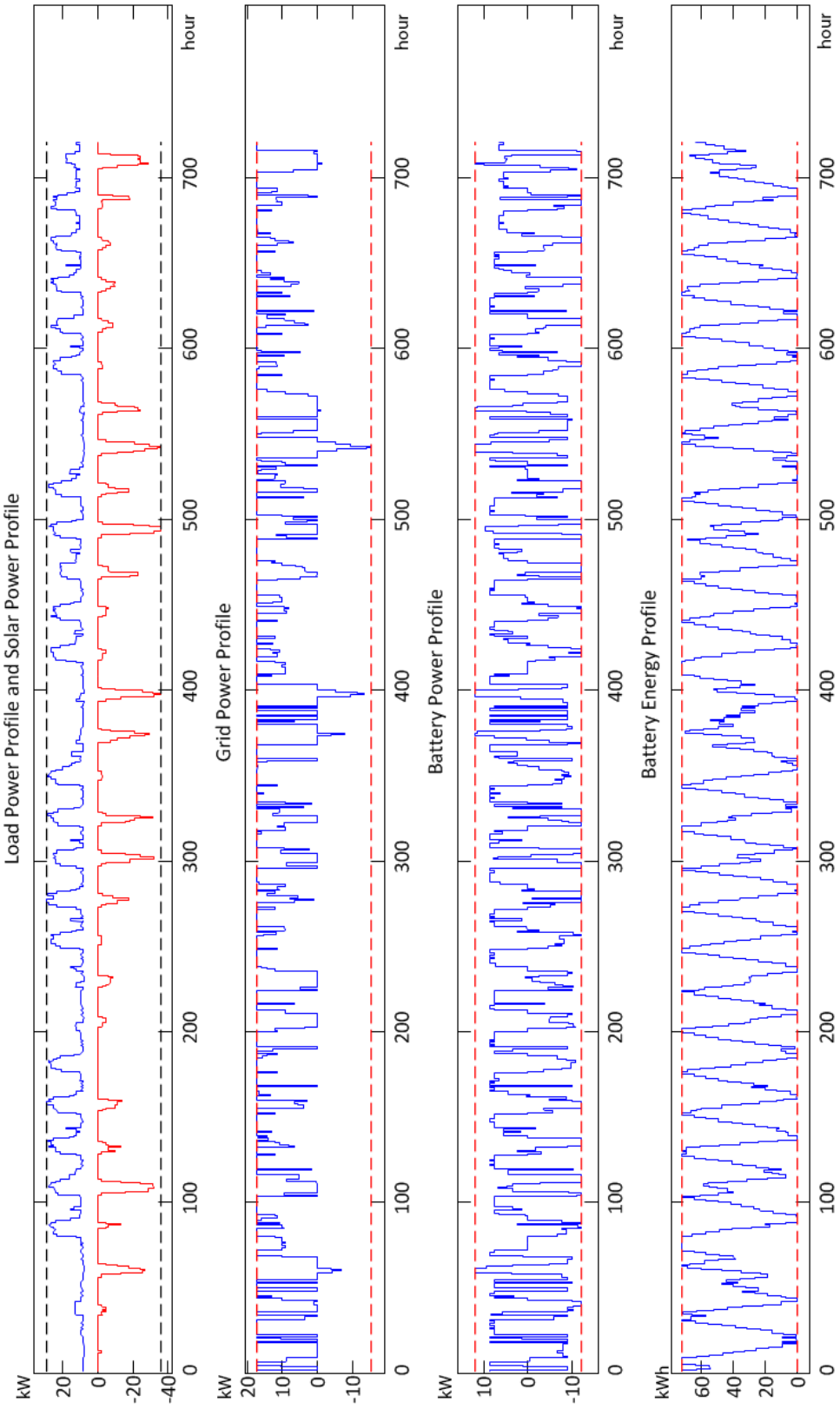

Figure 4.10: MILP-based component sizing optimization to maximize revenue for commercial setting with buy-in only. a) Load power profile and solar array power profile b) Grid power profile after optimization c) Battery power profile d) Battery energy profile

Example - Industrial Setting

The optimization was run for the whole month. The results are given in Table 4.12.

Device	Part number	Quantity	Total power (kW)	Total Energy (kWh)
Solar Panels	Conergy 235P-60	2000	470	N/A
Battery	Trojan IND17-6V	63	69.3	412.02

Table 4.12: Optimal list of components for industrial microgrid with buy-in only price

The cost saving of installing EMS is listed in Table 4.13. With the components selected for this building, the monthly electricity cost is reduced to $70,613 from $76,166.

Electricity cost, pure load ($)	76,166
Solar Array revenue ($)	-10,662
Battery with EMS revenue ($)	-1,589
Demand charge revenue ($)	-1,877
Total monthly solar capital cost ($)	7,000
Total monthly battery capital cost ($)	1,575
Total monthly cost ($)	70,613

Table 4.13: Cost saving for optimal configuration for industrial microgrid with buy-in only price

The optimized power or energy profiles for each component are illustrated in Figure 4.11. From the grid power profile, the optimization tends to limit the grid power between 0 and the optimized peak demand (kW).

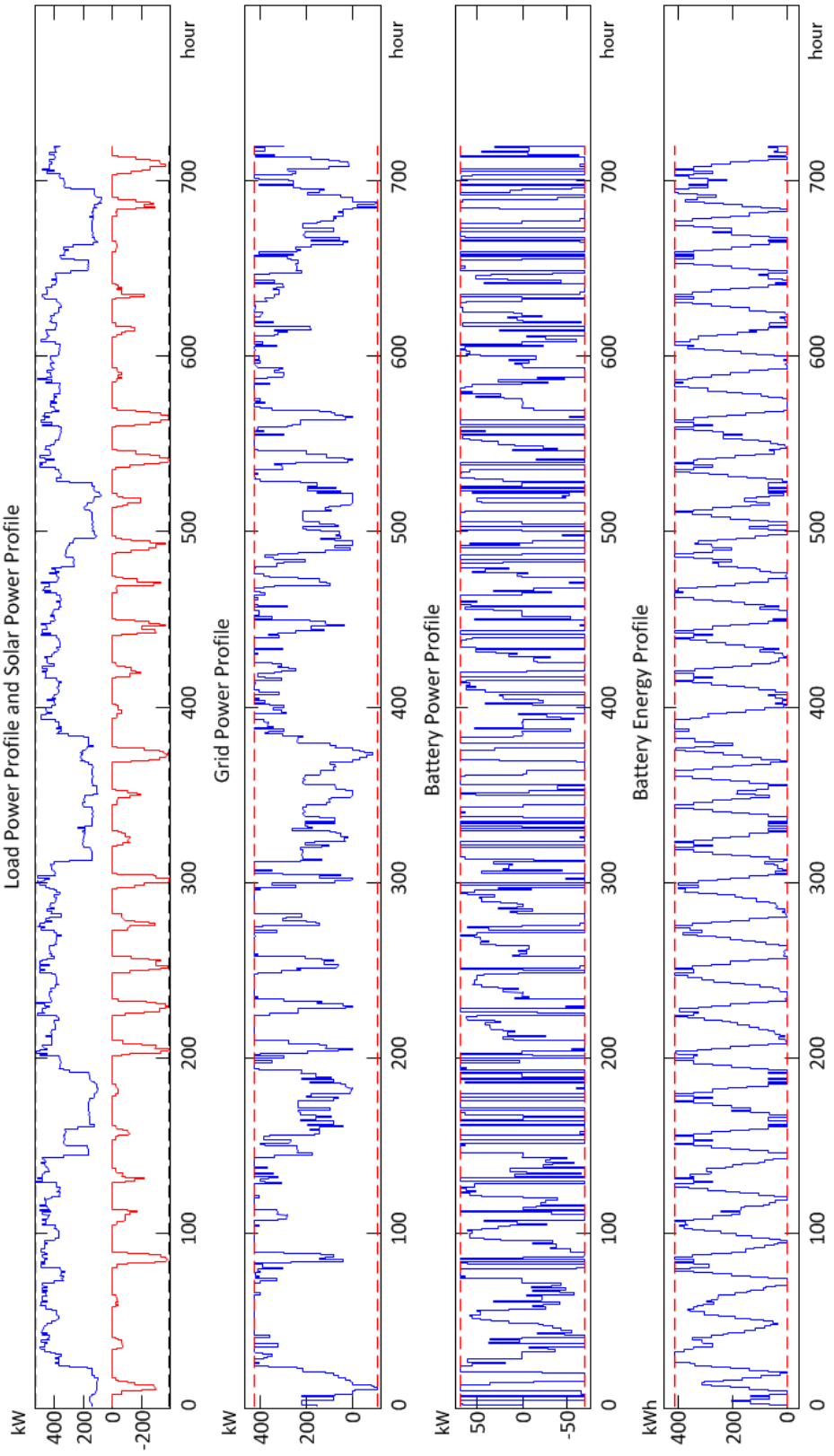

Figure 4.11: MILP-based component sizing optimization to maximize revenue for industrial setting with buy-in only price. a) Load power profile and solar array power profile b) Grid power profile after optimization c) Battery power profile d) Battery energy profile

Chapter 5

Circuit Level Modelling and Control

In this chapter, circuit-level modelling and control of the energy management system for an AC microgrid is studied. The first section looks at modelling of solar panel. The second section presents a model of lead acid battery. The third section presents a converter model and its control module in EMS for battery control. The fourth section discusses the modelling of grid-tie inverter and its control scheme for solar panels. The fifth section introduces the central control unit for the EMS system. The last section presents several scenarios of the circuit level operation of a microgrid with EMS.

5.1 Solar Panel

Solar panel is the device that converts sunlight to electric current. The basic unit of a solar array is solar cell, as shown in Figure 5.1.

Figure 5.1: Solar cell

It is common to connect solar cells in parallel and series to form a solar array or panel. A commonly used model for an ideal solar panel, e.g. see (Villalva *et al.*, 2009), is given by

The voltage-current characteristic of an ideal single solar cell is given by

$$I = I_{PV,cell} - \underbrace{I_{0,cell}\left[\exp\left(\frac{qV}{akT}\right) - 1\right]}_{I_d} \tag{5.1}$$

where

I: Output current of the solar cell

V: Terminal voltage of the solar cell

$I_{PV,cell}$: Current generated by incident light, which is directly proportional to sun irradiation

I_d: Shockley diode equation

$I_{0,cell}$: Reverse saturation or leakage current of diode

q: Electro charge ($1.60217646 \times 10^{-19} C$)

k: Boltzmann constant ($1.3506503 \times 10^{-23} J/K$)

T: Temperature of p-n junction in Kelvin

a: Diode ideality constant

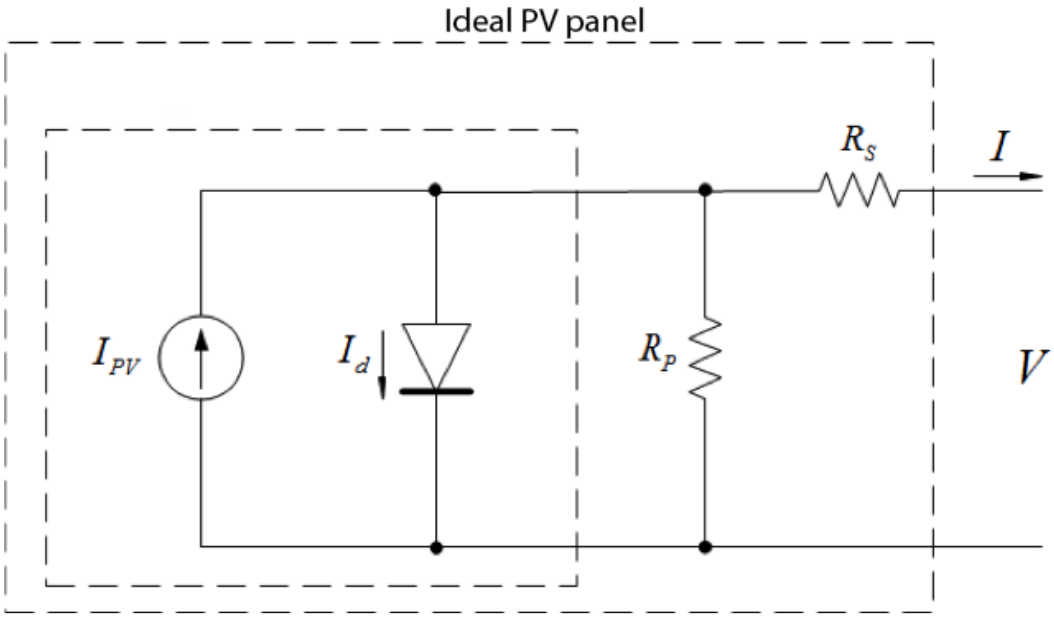

Figure 5.2: Circuit model of an ideal solar panel

Based on the single diode model in Eq. 5.1, one could derive a mathematical model for a solar panel or solar array, as shown in Figure 5.2, comprising of N_S cells in series and N_P series in parallel as

$$I = I_{PV} - I_0 \left[\exp\left(\frac{V + R_s I}{V_t a}\right) - 1\right] - \frac{V + R_s I}{R_p} \tag{5.2}$$

$$V_t = N_S k T/q \tag{5.3}$$

$$I_0 = I_{0,cell} N_P \tag{5.4}$$

$$I_{PV} = I_{PV,cell} N_P \tag{5.5}$$

where

I_{PV}: PV current of solar panel

I_0: Saturation current of solar panel

R_S: Equivalent series resistant

R_P: Equivalent parallel resistant

V_T: Thermal voltage of the solar array

N_S: Number of solar cells connected in series

N_P: Number of solar cells connected in series

Generally, the value of R_S is very small. One could reasonably simplify the equation by assuming $R_S = 0$. R_P is normally very large and can be assumed infinity for practical purposes.

Therefore, equation 5.2 could be simplified as:

$$I = I_{PV} - I_0 \left[\exp\left(\frac{V}{V_t a} \right) - 1 \right] \tag{5.6}$$

Usually, I_{PV} is not provided by solar panel manufactures. But since the parallel resistant is generally high and the series resistant is low, the following approximation can be made for practical purposes

$$I_{PV} \approx I_{SC} \tag{5.7}$$

where

I_{sc}: Short-circuit current of the solar array

I_{PV} at all different temperature and irradiation levels can be determined from

$$I_{PV} = (I_{PV,n} + K_I \Delta_T) \frac{G}{G_n} \tag{5.8}$$

where

$I_{PV,n}$: PV current generated at nominal condition

K_I: Sensitivity of the PV current to the changes in the temperature

Δ_T: Deviation from nominal temperature in Kelvin

G: Actual solar irradiation

G_n: Nominal solar irradiation

In (Villalva *et al.*, 2009), the diode saturation current of solar array is approximated by

$$I_0 = \frac{I_{sc,n} + K_I \Delta_T}{\exp((V_{oc,n} + K_V \Delta_T)/aV_t) - 1} \tag{5.9}$$

$I_{sc,n}$: Nominal short-circuit current of the solar array

K_V: Sensitivity coefficient of of open-circuit voltage with respect to temperature

$V_{oc,n}$: Nominal open-circuit voltage of the solar array

The above parameters are generally available from solar array manufacturer data sheets.

5.2 Lead Acid Battery

Battery models can be mainly divided in to three types, namely experimental, electrochemical and electric circuit models. In this thesis, a circuit based model from (Olivier Tremblay, 2009) is adopted to represent the battery. This model considers state of charge and has been verified experimentally.

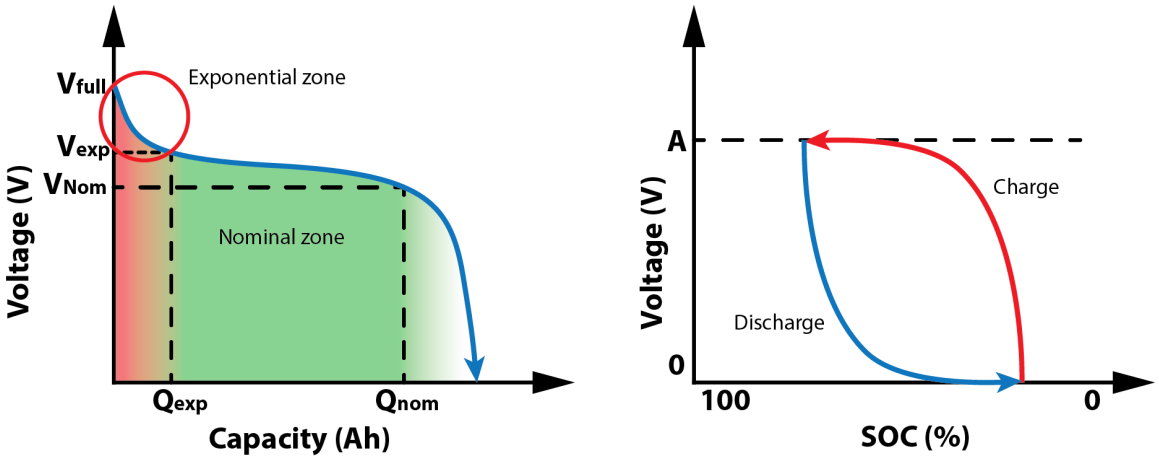

Figure 5.3: (a) Typical lead acid battery discharge curve, (b) Hysteresis phenomenon at exponential zone for lead-acid battery (Olivier Tremblay, 2009)

A typical discharge curve of a lead acid battery is shown in Figure 5.3. The horizontal axis represents the capacity or SOC of the battery, and the vertical axis represents the terminal voltage. Moreover, V_{full} is the fully charged voltage; V_{exp} is the voltage at the end of exponential zone; V_{nom} is the voltage at the end of nominal zone. Note that charge Q would actually decrease when moving along the horizontal axis. The exponential zone for charging and discharging shown in Figure 5.3 (a) has a hysteresis behaviour for lead-acid battery as shown in Figure 5.3 (b).

The charging and discharging model of the lead-acid battery could be summarized as follows (see Figure 5.4).

Discharge:

$$V_{batt} = E_0 - R \cdot i - K\frac{Q}{Q - it} \cdot (it + i^*) + V_{Exp}(t) \tag{5.10}$$

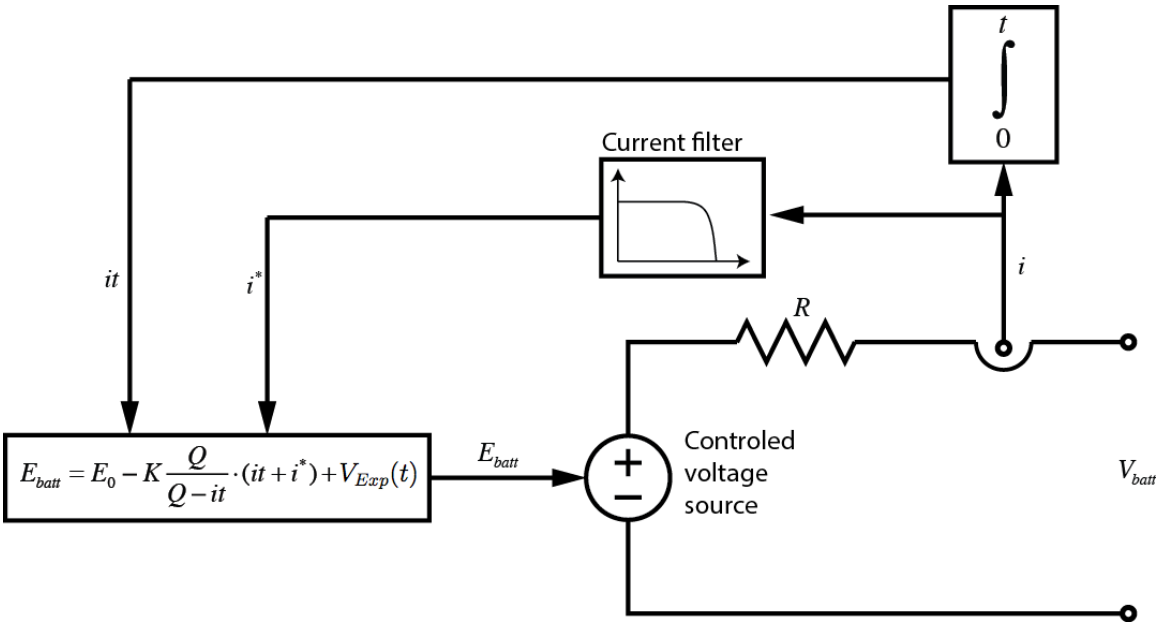

Figure 5.4: Discharge battery model(Olivier Tremblay, 2009)

Charge:

$$V_{batt} = E_0 - R \cdot i - \underbrace{K\frac{Q}{it - 0.1 \cdot Q} \cdot i^*}_{PolarizationResistance} - \underbrace{K\frac{Q}{Q - it} \cdot it}_{PolarizationVoltage} + V_{Exp}(t) \tag{5.11}$$

$$\dot{V_{Exp}}(t) = B \cdot |i(t)| \cdot (-V_{Exp}(t) + A \cdot u(t))$$

where

V_{batt}: Battery Voltage (V)

E_0: Battery Constant Voltage (V)

K: Polarisation Constant$(V/(Ah))$ or Polarization Resistance (Ω)

Q: Battery Capacity (Ah)

it: $\int idt$, Actual Battery Charge (Ah)

i: Battery Current (A)

i^*: Filtered Current (A)

A: Exponential zon amplitude (V)

B: Exponential zon time constant inverse (Ah^{-1})

$V_{Exp}(t)$: Exponential zone voltage (V)

Note that for exponential zone voltage, $u(t) = 1$ represents charge and $u(t) = 0$ represents discharge. Experimental data shows that there exists a voltage slow dynamic behaviour for a current step response. In (Olivier Tremblay, 2009), the author proposed a low-pass filtered current to flow through polarization resistance to solve the algebraic loop problem in Matlab Simulink.

The voltage of a lead-acid battery increases exponentially when battery is almost fully charged. This characteristic could be modelled by the polarization resistance as

$$PolarizationResistance = K\frac{Q}{it - 0.1 \cdot Q}$$

In charging mode, the polarization resistance term mimics the behaviour of a rapidly increasing voltage until the battery is almost fully charged, $it = 0$. However experimental data shows that the polarization resistance does not go to infinity and there is a 10% shift in the battery capacity..

5.3 Energy Storage Control with Bi-directional DC-AC Inverter

The bi-directional DC-AC converter in the simulation is modeled as a single stage H-bridge converter as shown in Figure 5.5. The left hand side is the DC side, connected to the battery pack. The right hand side is the AC side, connected to the microgrid bus.

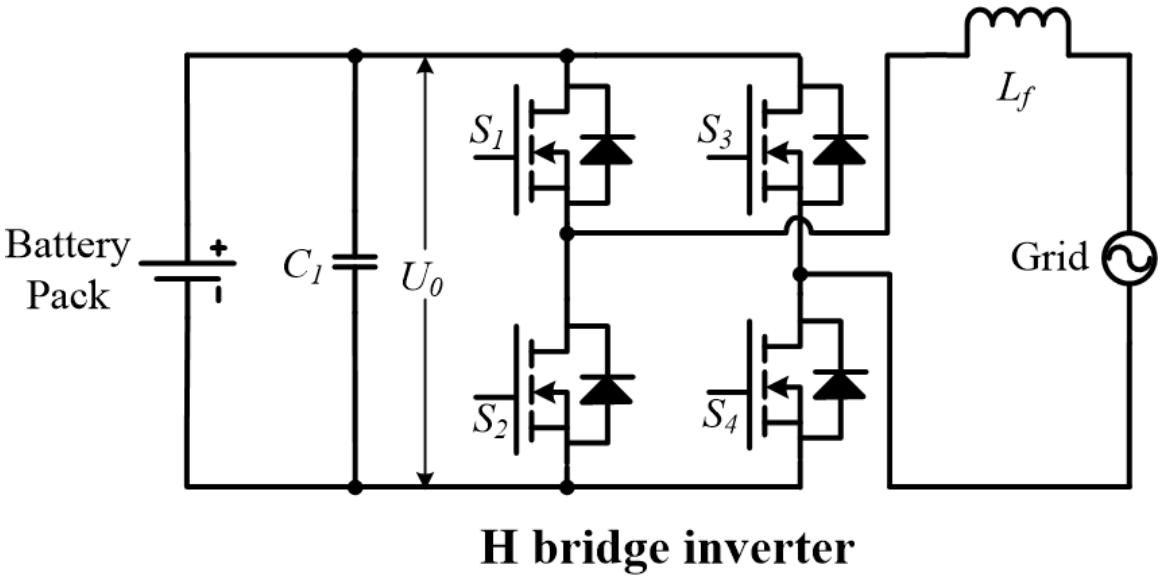

Figure 5.5: H-bridge DC-AC bidirectional converter

Figure 5.6 shows a typical H bridge inverter with a capacitor at the DC side and an inductor at the AC side. This converter is controlled to operate in all three modes (see section 5.5) of the microgrid. Most of the time, the converter is operated in grid connected mode, in which case, the microgrid voltage and frequency are set by the grid. The inputs of the control logic are the desired active power P and reactive power Q which are provided by he system-level energy management optimization algorithm.

The role of the DC/AC converter is to ensure that battery packs supply the required power to the microgrid. The converter operated in this mode is controlled to be a voltage source converter (VSC), which includes an inner current loop and an outer voltage loop.

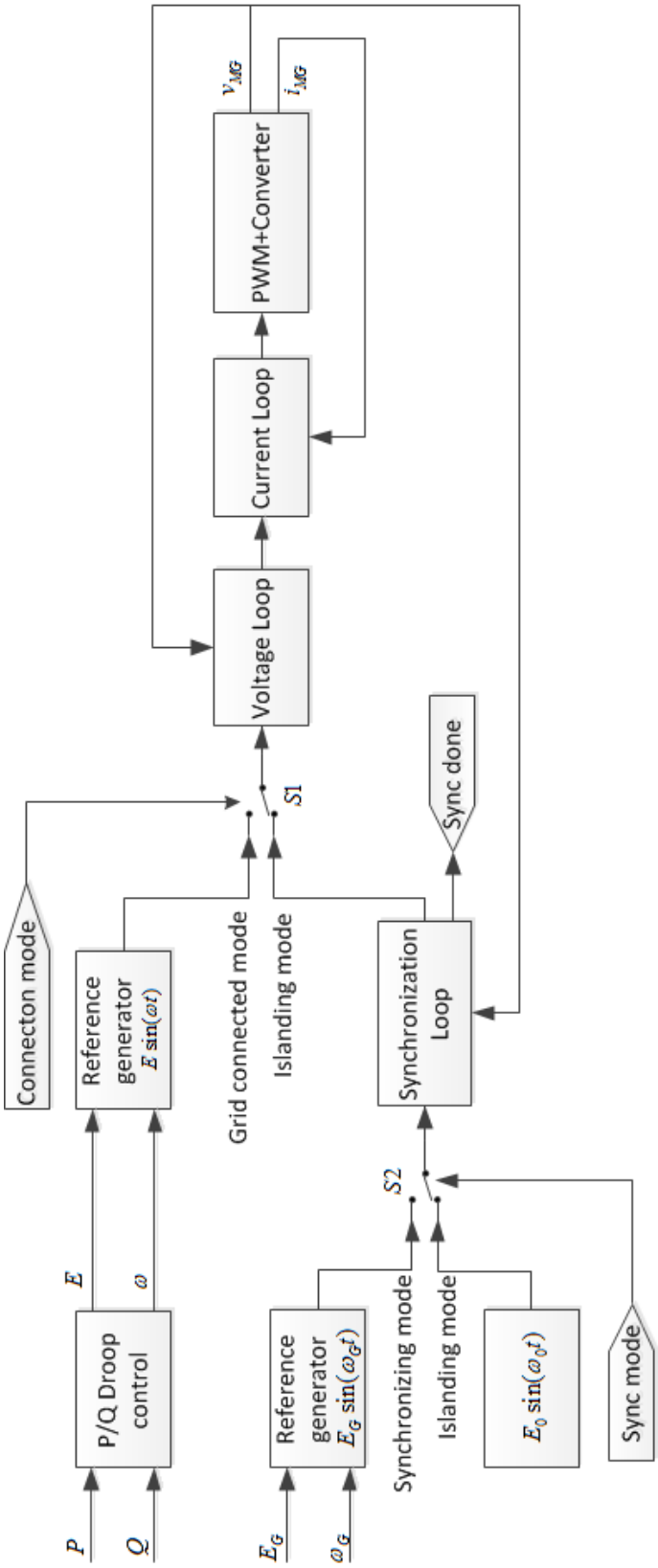

Figure 5.6: Bi-directional DC-AC converter control logic

The control signal P and Q are converted to E and ω by P/Q droop controller (De Brabandere *et al.*, 2007) as

$$E = E^* - G_Q(s)(Q - Q^*) \tag{5.12}$$

$$\omega = \omega^* - G_P(s)(P - P^*) \tag{5.13}$$

As shown in Figure 5.7, E and ω are the output voltage amplitude and frequency, respectively and E^* and ω^* are corresponding reference values. P, Q, P^*, and Q^* are active and reactive power and their references. $G_P(s)$ and $G_Q(s)$ are the droop control transfer functions. The purpose of using this droop method is to mimic the behaviour of a synchronous machine. When the system frequency drops, all generators connected to this system increase active power.

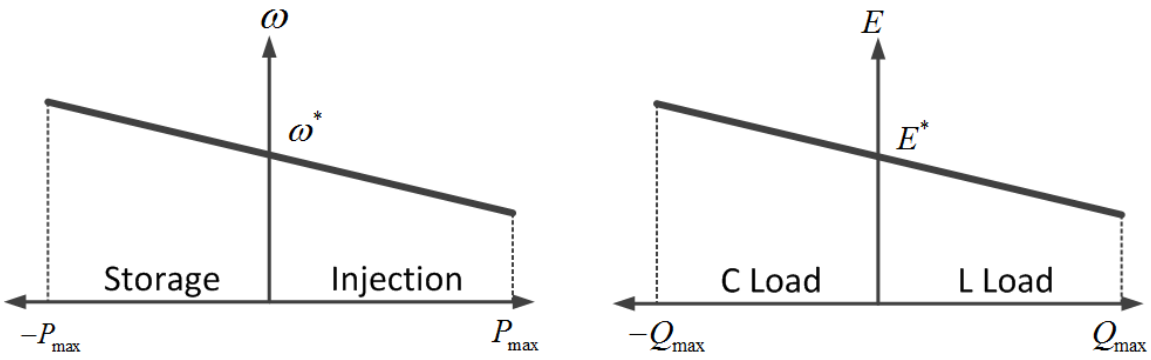

Figure 5.7: P/Q droop control function

When the converter operates in islanding mode, there is no external voltage reference and the internal voltage reference $E_0 sin(\omega_0 t)$ will be used. In islanding mode, the function of this converter is to maintain the voltage amplitude and frequency of the microgrid.

At the moment when the grid power recovers, the amplitude and frequency of

the microgrid voltage may not be synchronized with the utility grid. Therefore, a synchronization loop is required to ensure a proper transition to grid connected mode. The synchronization loop consists of a phase-lock loop and a PI controller. It adjusts the microgrid's voltage amplitude and frequency by the maximum allowable deviation. The two voltage wave forms are compared over a rolling window. When the error is smaller then a threshold value, the converter is ready to switch to grid-connected mode.

5.4 Two Stage DC-AC inverter with MPPT

Maximum power point tracking (MPPT) is a method widely used for extraction of the maximum power out of solar arrays, e.g. see (Esram and Chapman, 2007). A typical solar panel power-voltage characteristics is shown in Figure 5.8. There is one maximum power output point for each curve. The curve is changing according to solar irradiance and temperature, etc. Therefore the MPPT would have to continuously search for the maximum power point. The so-called perturbation & observation method is used in the thesis simulations for MPPT (Femia *et al.*, 2005).

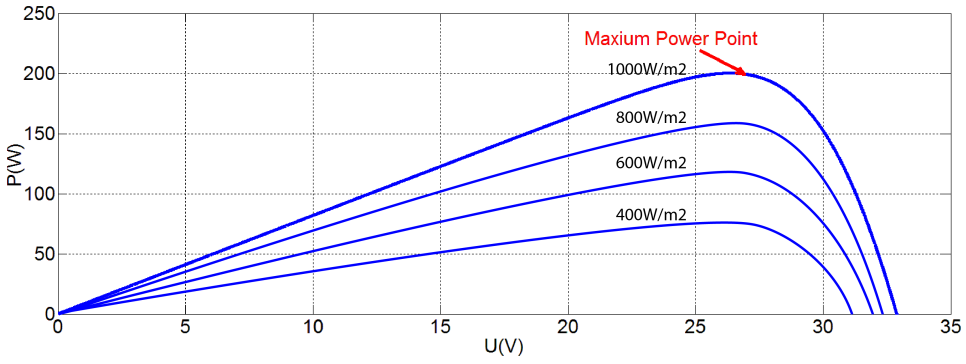

Figure 5.8: PV array electrical characteristics as a function of solar irradiance

The MPPT algorithm is built into the two stage DC-AC grid-tie inverter as shown in Figure 5.9. The left hand side is the solar array, followed by the a boost DC-DC converter. The two stages are linked by a DC link capacitor C_{link}. The output stage is a H-bridge inverter with LCL filter.

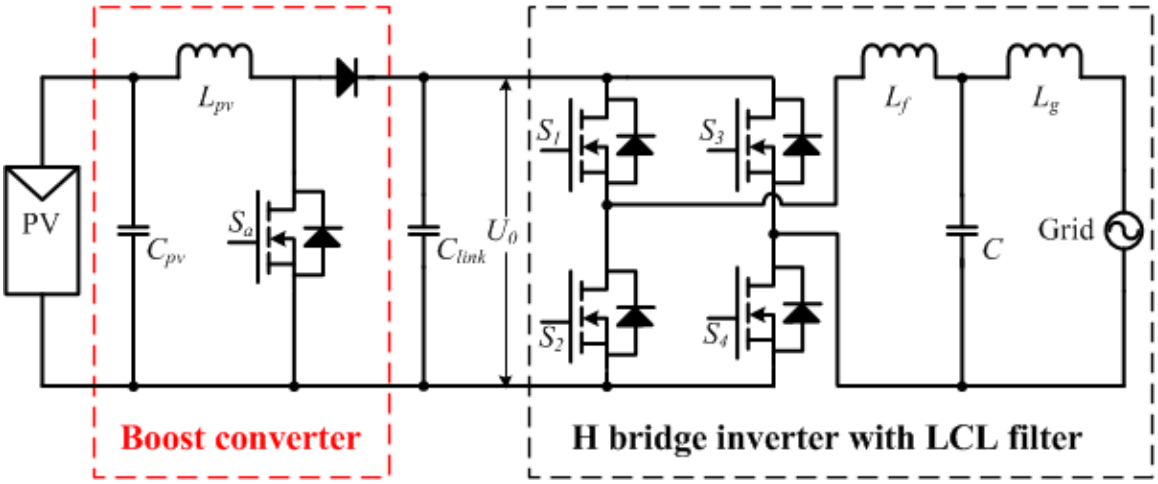

Figure 5.9: Architecture of PV grid-tie inverter

The control strategy of the converter is shown in Figure 5.10. The voltage and current of the solar array are measured and passed to the MPPT module. The perturbation & observation method is used to find I_{ref}. The current loop compares I_{ref} and I_{PV}, and passes the error to a PI controller to generate the reference for PWM. Generally speaking, the boost stage is responsible for finding the maximum power point and drawing the current from the solar array accordingly.

The H-bridge DC-AC stage consists of an outer voltage loop and an inner current loop. U_{link_ref} is the desired DC link voltage, shown as U_0 in Figure 5.9. The function of this stage is to control the DC side voltage so it would track its reference U_{link_ref}. On the AC side, the output voltage is governed by the grid voltage. The output current is proportional to the power of the solar array.

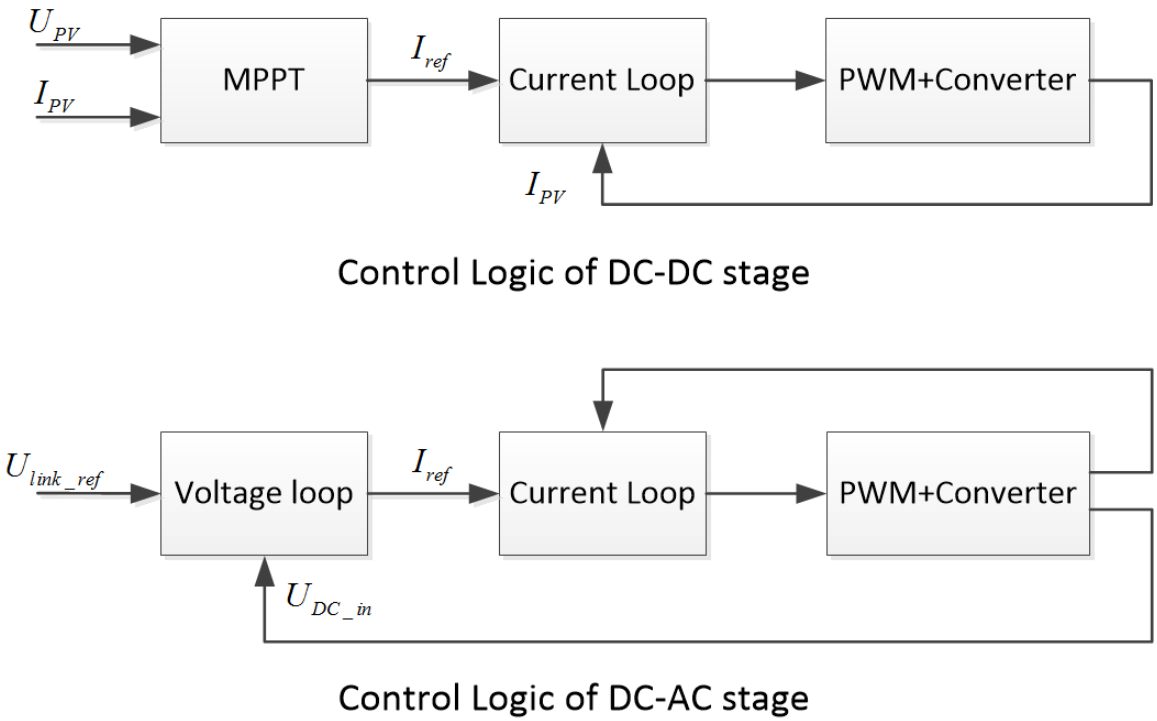

Figure 5.10: Grid-tie converter control architecture

5.5 Central Control Unit

5.5.1 Controller Implementation

In this thesis, the operation of a grid-connected microgrid with EMS is classified into five main operating modes, described below. Circuit level control schematics is shown in Figure 5.11.

1. **Grid-connected mode** : This is the normal mode of operation and most of the time, the microgrid operates in grid connected mode. In this mode, the microgrid bus voltage is determined by the utility grid. The solar grid-tie inverter is a current source inverter(CSI), which injects current to the microgrid. The battery pack is also controlled as CSI. The high-level controller of EMS would

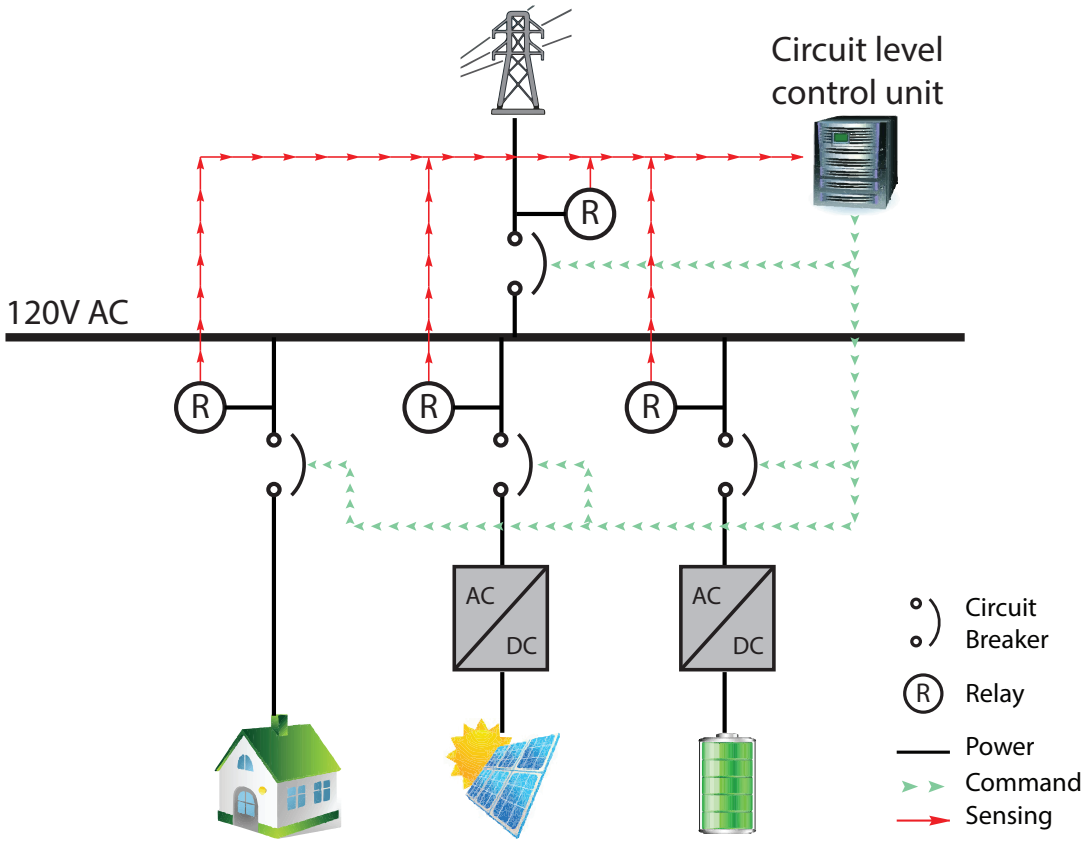

Figure 5.11: Circuit level control schematics

command the low-level EMS inverter to either charge or discharge the battery to achieve the desired charge/discharge power.

2. **Grid-only mode** : In case the battery or EMS inverter has a malfunction or is under service, the controller would open the breaker connecting the EMS to the microgrid, and enters a Grid-only operation mode. The rest of the devices should operate under the same condition as the grid connected mode.

3. **Islanding mode** : This mode could also be called battery-only mode. When the utility grid is down or suffering voltage instability, EMS could detect the

incident and open the grid transfer switch. The microgrid is isolated from the utility grid and operates in islanding mode. In this mode, the EMS inverter is operated as voltage source inverter (VSI) instead of CSI, which means the microgrid bus voltage is governed by the EMS inverter. The main function of EMS in this mode is to maintain the microgrid voltage and frequency, and power balance between generation and consumption.

4. **Synchronization mode** : This is a transition from the islanding to grid connected mode. When the microgrid operates in the islanding mode, its voltage and frequency are determined by an internal reference. Before switching to grid connected mode, EMS would ensure that the magnitude, frequency and phase of the microgrid and grid are the same.

5. **Outage mode** : This system enters this mode when both utility grid and EMS battery packs are out of power. In this mode, the EMS control unit is still active and monitors the system with reserved power, preparing for switching to the correct mode when power comes back on either from the battery or utility grid.

To implement the above functionality, a finite state machine controller is designed as shown in Figure 5.13. The state variables are the state of utility grid transfer switch, EMS breaker and grid power indicator.

Utility grid transfer switch has three states, Closed(C), Fault opening(F), and Manual opening(M). The transfer switch has build-in relay which senses utility grid current and voltage. In case of grid power outage and voltage instability, the transfer switch would trip from C to F. The M state represents the case where a maintenance

staff opens the switch manually. The EMS could direct the transfer switch to reclose from F to C when a fault is cleared, but not from M to C.

The EMS breaker has the same three states. Grid power indicator has two values: Grid has power and stable(Y), grid is power off or unstable(N).

Each blue box in Figure 5.13 represents a state of the microgrid. The three letters represent the state of EMS breaker, grid transfer switch and grid power indicators respectively. For example, CFN means EMS breaker is closed, grid transfer switch is at fault condition and grid has no power.

The red circles represent the modes of the system, which include groups of states with similar meaning.

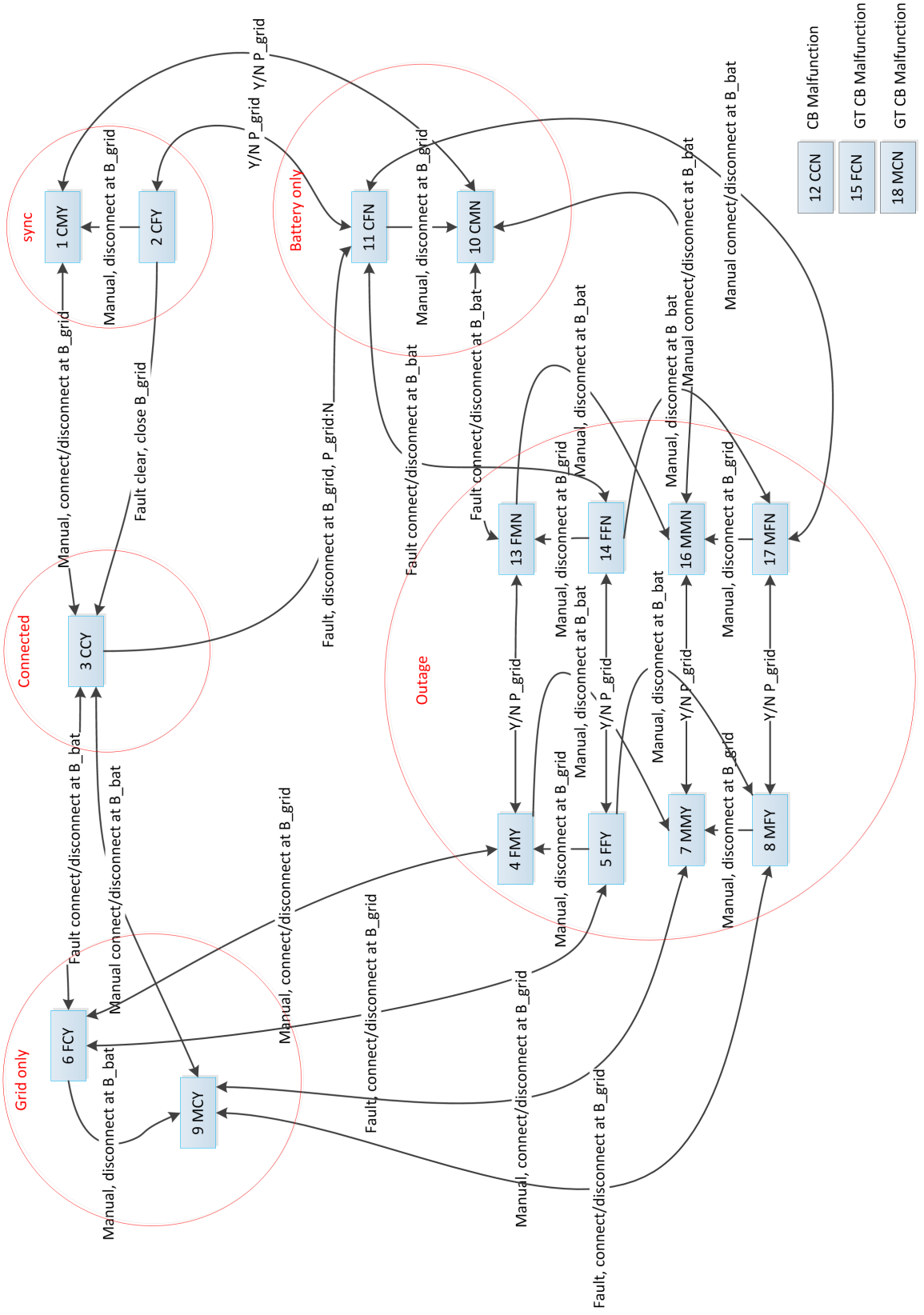

Figure 5.12: Central control unit

5.6 Simulation of Microgrid Operation

In this section, simulations are performed under a variety of fault conditions to demonstrate the different features of the EMS circuit level controller.

5.6.1 Simulation Setup

Matlab R2012b with Simulink is ued to set up a microgrid for simulation. An iMac with 2.5 GHz Intel Core i5 and 4GB ram is used for simulation. This microgrid is a typical setting for residential use, as shown in Figure 5.13. $E_{bat} = 5kWh$, $N_h = 0.3s$, sampling period is $1E^{-6}s$. Number of solar panels is 10.

The microgrid is connected to the utility grid through a transfer switch. Solar array with grid tie inverter are connected to the microgrid bus. Battery packs are connected to the inverter of the EMS system. The electrical panel for household load is connected to the microgrid bus. This simulation is able to test the microgrid at circuit level.

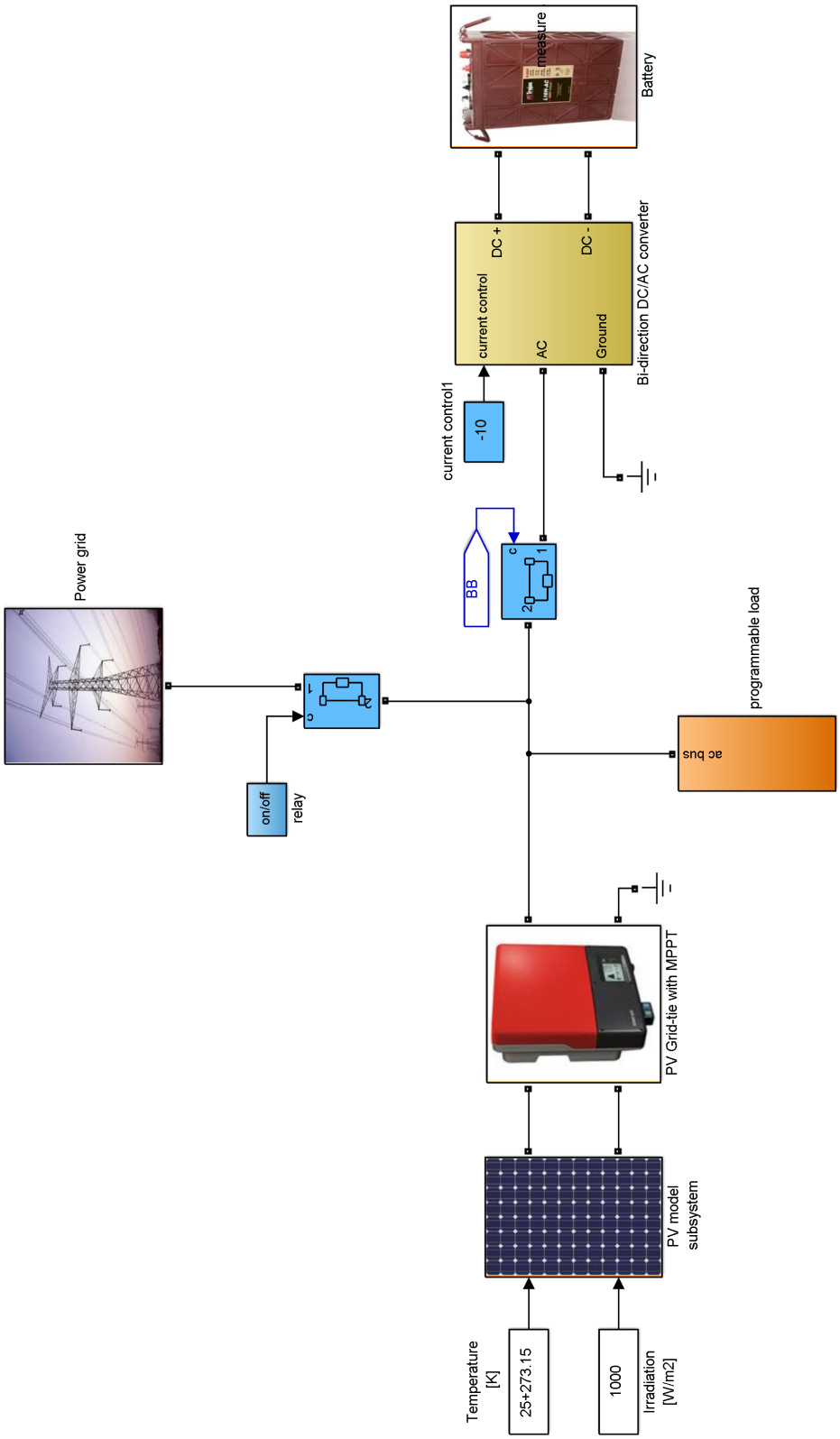

Figure 5.13: System in simulation

5.6.2 Grid Connected Operation

Grid connected operation is the most common operating mode for the EMS system. Assuming fixed battery voltage, power control commands are converted to current control commands. In this mode the current of the EMS is controlled by system level optimization loop. The current control signal in this simulation is 10A(charge), 15A(charge), 15A(discharge), 10A(discharge), 15A(discharge).

As shown in Figure 5.14, the EMS converter can correctly respond to the system level optimization command. It successfully controls the power flow between the utility grid and local microgrid.

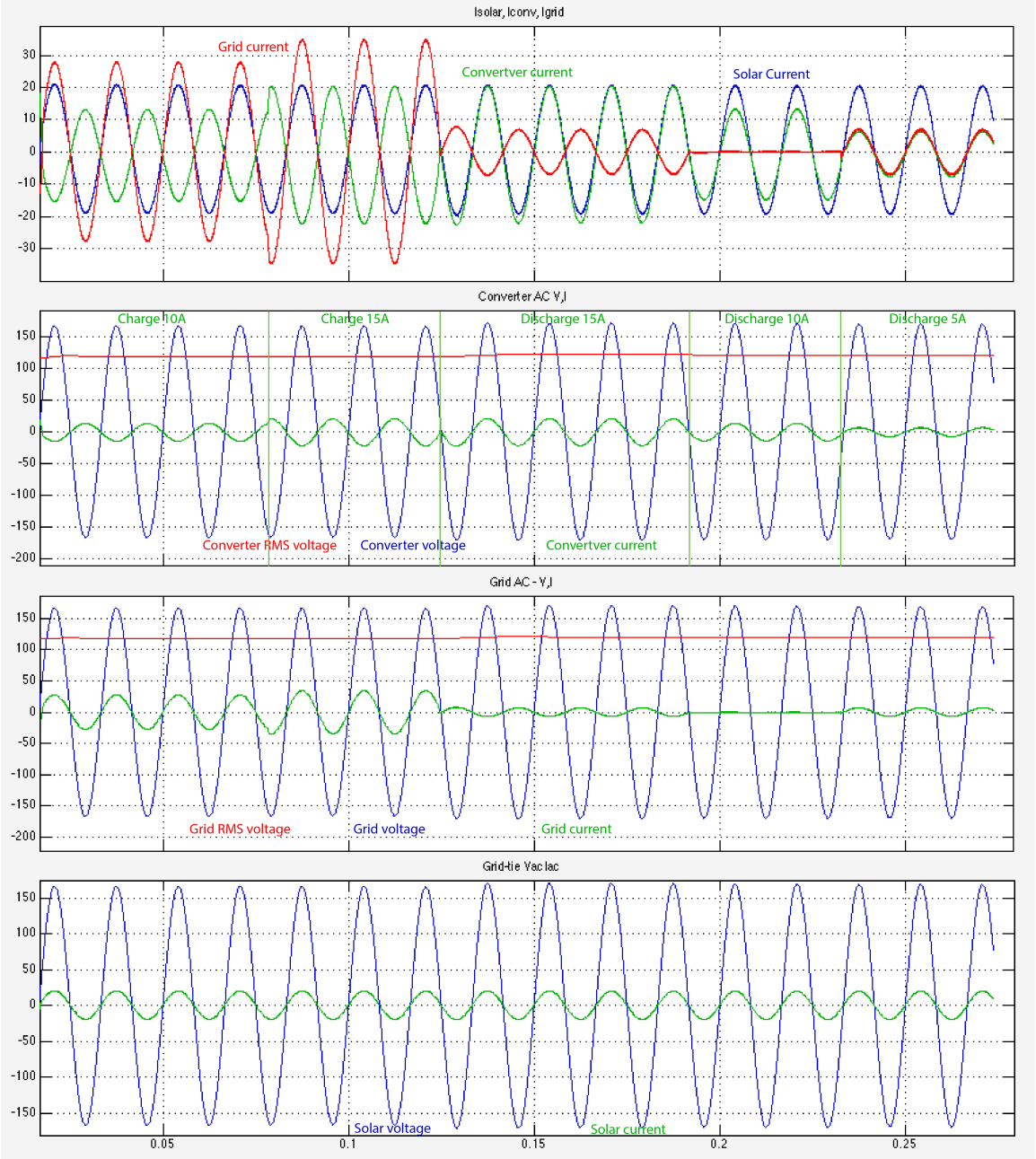

Figure 5.14: Circuit level simulation - grid connected operation, a) current of grid, EMS converter and solar system, b) voltage, current and RMS voltage of the EMS converter, c) voltage, current and voltage RMS value of the grid power profile, d) voltage and current of the solar output power.

5.6.3 Grid Failure

The ability to ride through grid failure or blackout is a key feature of the EMS system. In this simulation, a grid failure occurs which drops its voltage to about 10% of nominal voltage.

As shown in Figure 5.15, the outage happens at time 0.06s, which is detected by the EMS grid relay instantaneously and tripping the transfer switch to isolate the grid off the microgrid. At the same time, the controller of the EMS converter is switched to islanding mode. From the RMS value of the microgrid voltage, this event is invisible to the load and solar array system.

After an undefined length of outage (in this simulation it is 4 cycles), the grid power recovers at 0.13s. During the outage, magnitude and phase difference between the grid voltage and the microgrid voltage may develop. When EMS detects the recovery of utility grid, it starts to synchronize the microgrid voltage to that of the utility grid. At time 0.275s, the microgrid is reconnected to the grid. No current surge is observed at the moment of reconnection, as can be seen in Figure 5.15.

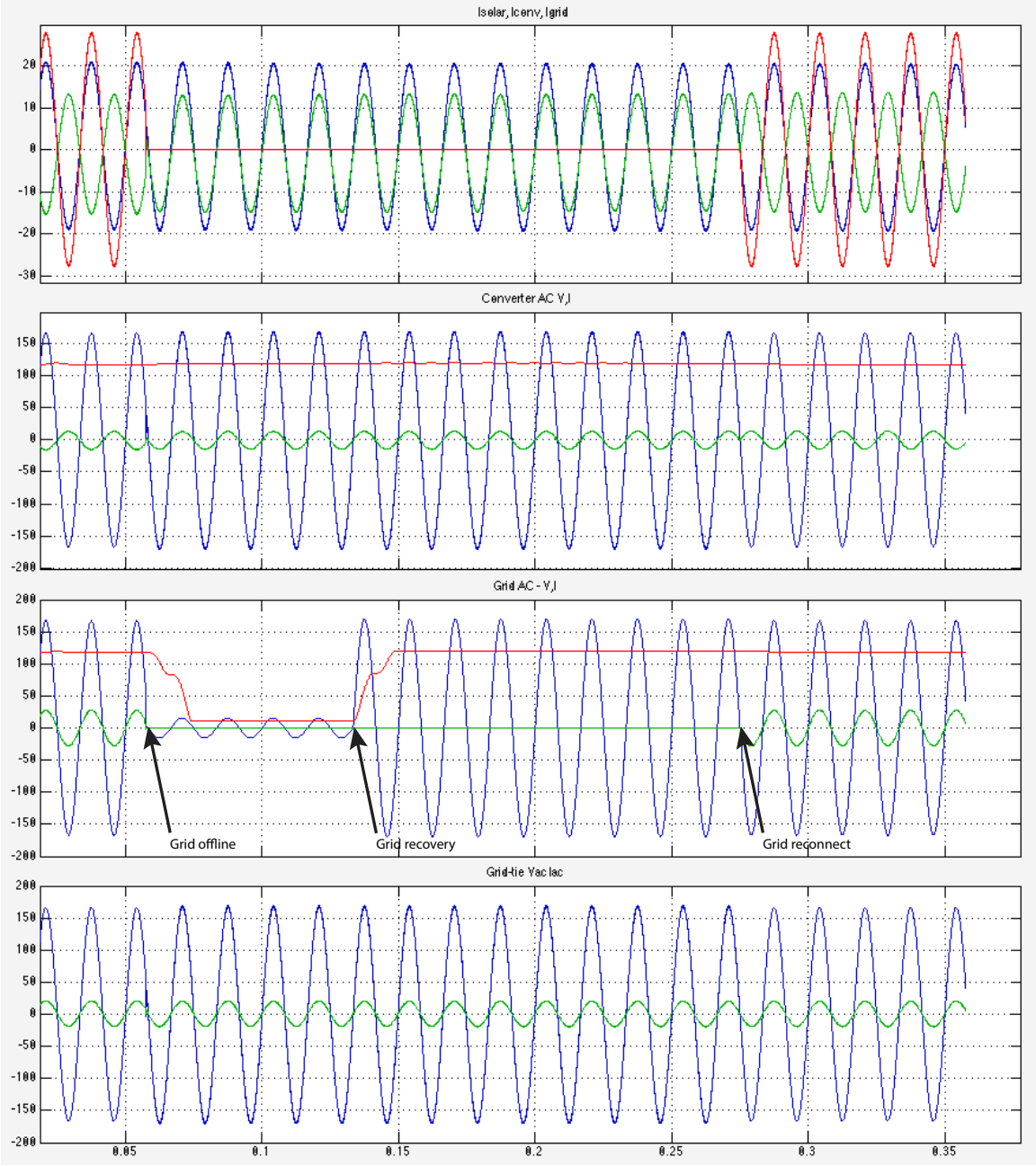

Figure 5.15: Circuit level simulation - grid failure, a) the current of grid, EMS converter and solar system, b) voltage, current and RMS voltage value of the EMS converter. c) voltage, current and RMS voltage value of the grid power profile. d) voltage and current of the solar output power.

5.6.4 EMS Offline

The next scenario considered is the case that EMS goes off-line either because of a equipment failure or scheduled maintenance. The EMS offline event occurs at time 0.07s(see Figure 5.16), which is instantaneously detected by the EMS grid relay and trips the circuit breaker to isolate the EMS converter off the microgrid. The microgrid runs in the grid only mode.

After 0.08s of outage, the EMS converter and battery return to service. The EMS converter is designed in a way that when grid is available, it would start the the synchronization process, making sure the voltage amplitude, frequency and phase stay synchronized with the utility grid. As shown in Figure 5.16 c), at the moment of reconnection, the EMS converter is perfectly synchronized with the grid and there is no current surge.

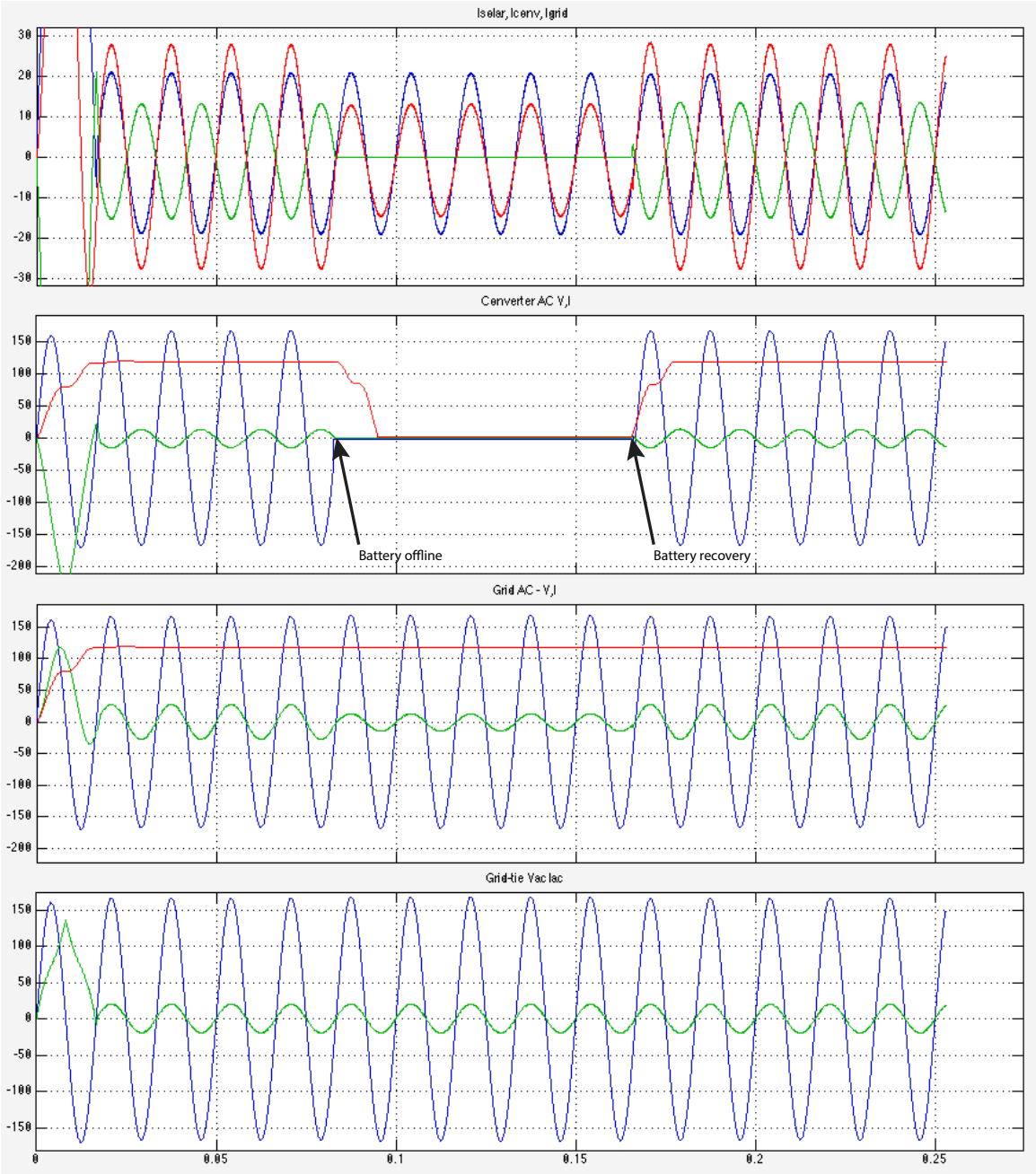

Figure 5.16: Circuit level simulation - EMS offline,a) the current of grid, EMS converter and solar system, b) voltage, current and RMS voltage of the EMS converter, c) voltage, current and voltage RMS value of the grid power profile, d) voltage and current of the solar output power.

5.6.5 Black Start - Battery First

Black start is the process after a total loss of power in the microgrid. It happens either after a long blackout or scheduled event.

During a total power loss, the solar system would not be running along, because there is no voltage reference. In the test case shown in Figure 5.17, the battery system recovers and comes online first. The grid power recovers only after the microgird is running on battery alone. Since the microgrid is already energized, its bus voltage has to be synchronized with the grid before reconnecting to it. The reclosure occurs at time 0.3s in the testing scenario. Due this synchronization, there is no surge current at the time of reclosure.

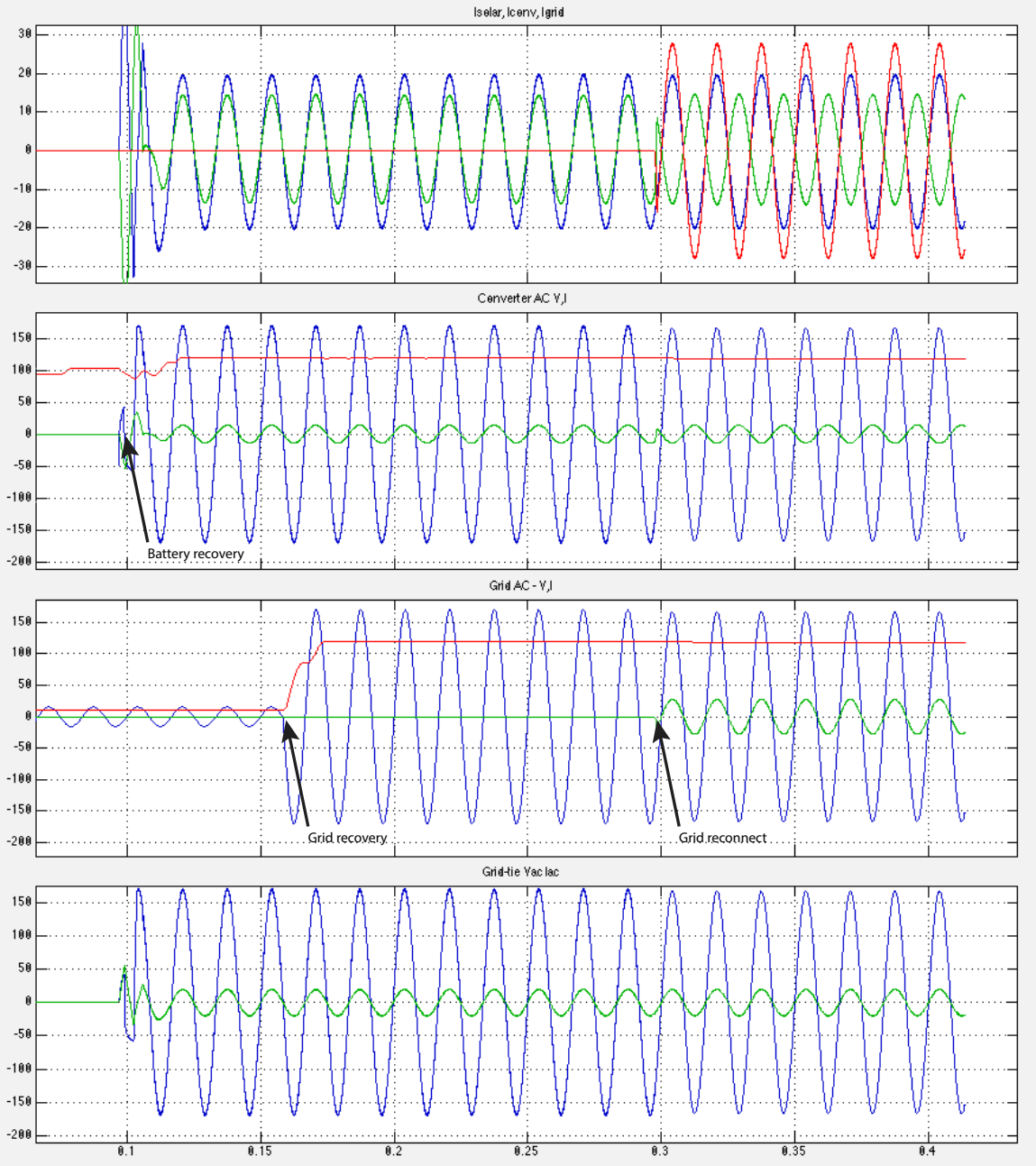

Figure 5.17: Circuit level simulation - EMS black start battery first, a) the current of grid, EMS converter and solar system, b) voltage, current and RMS voltage of the EMS converter, c) voltage, current and voltage RMS value of the grid power profile, d) voltage and current of the solar output power.

5.6.6 Black Start - Grid First

The next scenario of black start assumes that the utility grid recovers before the EMS (see Figure 5.18). The EMS with battery recovers after the system is up and connected to the grid. Since the EMS converter uses the grid voltage as reference, no surge current occurs at the time of reclosure.

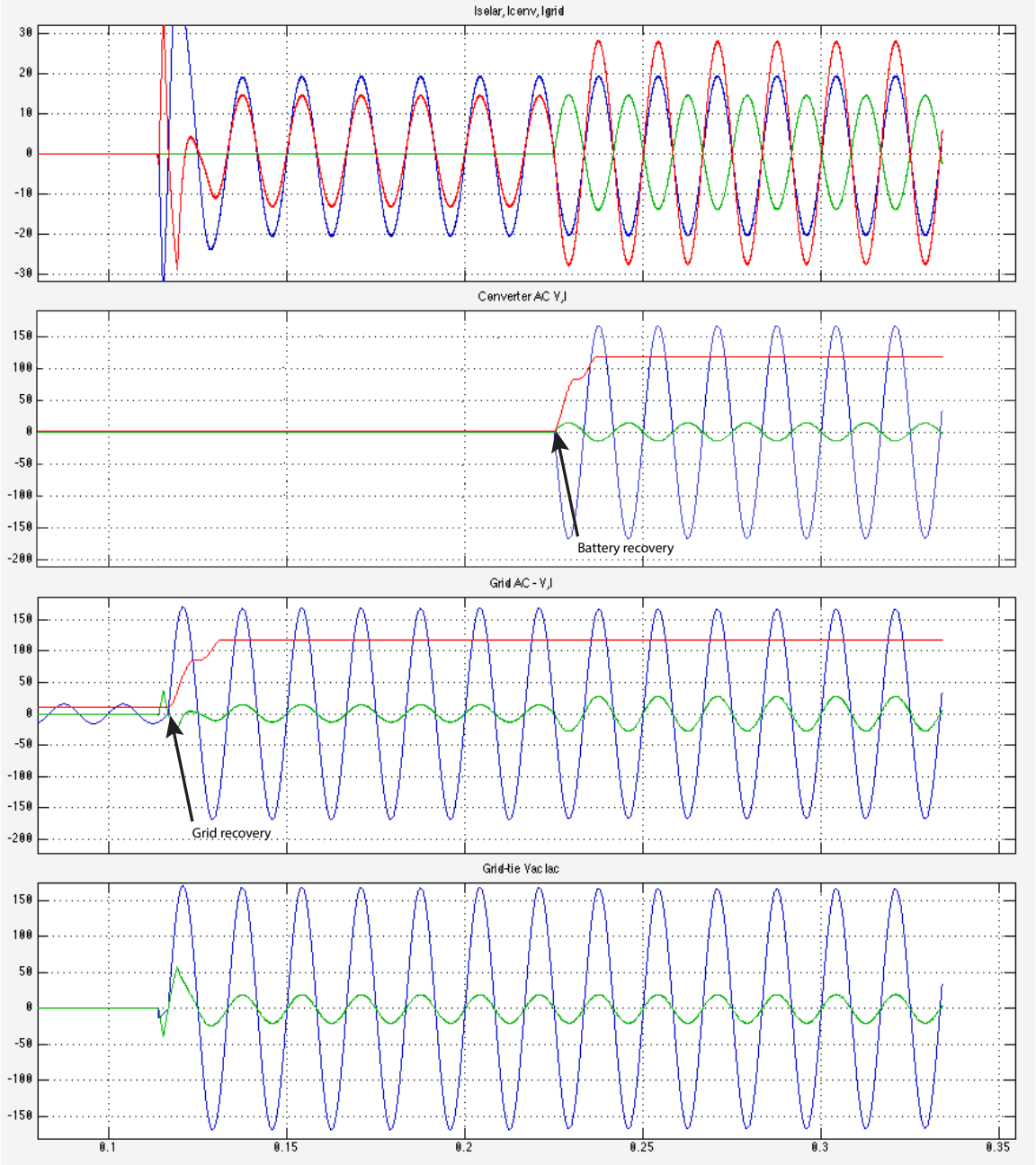

Figure 5.18: Circuit level simulation - EMS black start grid first, a) the current of grid, EMS converter and solar system, b) voltage, current and RMS voltage of the EMS converter, c) voltage, current and voltage RMS value of the grid power profile, d) voltage and current of the solar output power.

Chapter 6

Conclusions and Future Work

6.1 Conclusions

The electric power systems must undergo significant transformation to achieve environmental and energy sustainability. Microgrids will be at the core of this transformation. This thesis was concerned with the control and component sizing for energy management in microgrids with energy storage and renewable energy in residential, commercial and industrial applications.

A hierarchical control approach was proposed for a microgrid with EMS involving an optimization-based high-level power flow controller and a circuit level controller. A complete theoretical presentation of the system level controller, including design, optimization and control of EMS was included. The proposed component sizing optimization is a complete solution of the problem that have not been considered in the literature before. A finite stage machine based controller was presented as one possible option for circuit level control.

A simple system level power flow strategy was proposed in this thesis. The cost

of electricity was minimized by controlling the charge and discharge of an energy storage device such as a battery. Three cases were studied to show the validity of such controller under different building setting, pricing regime and components. Peak demand charge for commercial and industrial customers was reduced by the proposed EMS.

The component sizing optimization for residential, commercial and industrial settings was studied. The proposed approach utilizes the available information such as pricing regime, component rating, capital cost, and power usage profile to determine an optimal size for each component. Theoretical formulation of each optimization problem was presented in the thesis. To verify the proposed component selection algorithm, eight cases were studied for residential, industrial and industrial settings. One case of component sizing optimization for islanded remote community was also considered.

The result of component sizing optimization showed small financial incentive for individual users to install battery backed EMS system with the current pricing regime and using retail price for capital cost of the system components. However, it is not unrealistic to assume that the capital cost of such systems would dramatically come down if in large volumes with increased adoption of such technologies. Also since the utility electricity price is expected to rise, in a some cases very significantly in most jurisdictions in future. A case in point is the province of Ontario which has recently announced an average increase of 33% over the next 3 years (MOE, 2013). The reason for such increases in price is the much needed investments to upgrade an aging power grid and reduce reliance on polluting sources of power such as coal. Integration of microgrids with EMS into the utility grid could enable many new ways

of control, e.g. demand-side control and peak load shaving. This approach could increase the efficiency and improve the reliability of the grid. Although, the benefits are not quantified in this thesis, it is reasonable for utilities to subsidize such system to accelerate deployment of such system. Considering all the above factors, a number of scenarios were studied by assuming future electricity and component pricing to demonstrate potential economic benefits of microgrid with EMS to the consumers.

A microgrid EMS circuit level controller was proposed and simulated in this thesis by employing a finite state machine. This approach ensured a very reliable control algorithm with fast response time. The faults could be detected and cleared in a fraction of a cycle, such the transition between islanded and grid connected operation would be imperceptible to the loads in the microgrid.

6.2 Future Study

There are a number of interesting possible directions for future work based on the research in thesis, as discussed below.

- The EMS optimization algorithm could be further improved by adding a term that represent the cost of each charge and discharge of battery to prevent excessive activities that could shorten the battery life.

- Algorithms can be developed to predict power usage and generation in the microgrid , by for example considering weather forecast information. Such algorithms can be integrated with optimization-based power flow control method for real time energy management in the microgrid.

- Grid level aggregator for microgrid could be studied in the future, in order to

provide services such as power regulation, peak demand generation and spin reserve, to the grid.

Bibliography

Armstrong, M. M., Swinton, M. C., Ribberink, H., Beausoleil-Morrison, I., and Millette, J. (2009). Synthetically derived profiles for representing occupant-driven electric loads in canadian housing. *Journal of Building Performance Simulation*, **2**(1), 15–30.

Armstrong, R. C. (2007). Addressing the global energy challenge.

Arnold, G. (2011). Challenges and opportunities in smart grid: A position article. *Proceedings of the IEEE*, **99**(6), 922–927.

Barklund, E., Pogaku, N., Prodanovic, M., Hernandez-Aramburo, C., and Green, T. (2008). Energy management in autonomous microgrid using stability-constrained droop control of inverters. *Power Electronics, IEEE Transactions on*, **23**(5), 2346–2352.

Borbely, A.-M. and Kreider, J. F. (2001). *Distributed generation: the power paradigm for the niew millennuim*. CRC Press, Boca Raton, FL.

Chakraborty, S., Weiss, M., and Simoes, M. (2007). Distributed intelligent energy management system for a single-phase high-frequency ac microgrid. *Industrial Electronics, IEEE Transactions on*, **54**(1), 97–109.

Chicco, G. and Mancarefla, P. (2009). Distributed multi-generation: A comprehensive view. *RENEWABLE & SUSTAINABLE ENERGY REVIEWS*, **13**(3), 535–551.

De Brabandere, K., Bolsens, B., Van den Keybus, J., Woyte, A., Driesen, J., and Belmans, R. (2007). A voltage and frequency droop control method for parallel inverters. *Power Electronics, IEEE Transactions on*, **22**(4), 1107–1115.

Dimeas, A. and Hatziargyriou, N. (2005). Operation of a multiagent system for microgrid control. *Power Systems, IEEE Transactions on*, **20**(3), 1447–1455.

DING, M., ZHANG, Y., MAO, M., YANG, W., and LIU, X. (2009). Steady model and operation optimization for microgrids under centralized control. *Automation of Electric Power Systems*, **33**(24), 78–82.

DOE (2012). *2010 Commercial Energy End-Use Splits by Fuel Type*. Department of Energy, US, `http://buildingsdatabook.eren.doe.gov/docs/xlspdf/3.1.4.pdf`.

Esram, T. and Chapman, P. L. (2007). Comparison of photovoltaic array maximum power point tracking techniques. *Energy conversion, IEEE transactions on*, **22**(2), 439–449.

Femia, N., Petrone, G., Spagnuolo, G., and Vitelli, M. (2005). Optimization of perturb and observe maximum power point tracking method. *Power Electronics, IEEE Transactions on*, **20**(4), 963–973.

Guerrero, J., Vasquez, J., Matas, J., Castilla, M., and de Vicuna, L. (2009). Control strategy for flexible microgrid based on parallel line-interactive ups systems. *Industrial Electronics, IEEE Transactions on*, **56**(3), 726–736.

Hatziargyriou, N., Dimeas, A., Tsikalakis, A., Lopes, J., Karniotakis, G., and Oyarzabal, J. (2005). Management of microgrids in market environment. In *Future Power Systems, 2005 International Conference on*, pages 7 pp.–7.

HydroOne (2013a). *BUILDING YOUR BILL: PRICES & RATES*. Hydro One Inc., `http://www.hydroone.com/RegulatoryAffairs/RatesPrices/Pages/Default.aspx`.

HydroOne (2013b). *RESIDENTIAL DELIVERY RATES*. Hydro One Inc., `http://www.hydroone.com/RegulatoryAffairs/RatesPrices/Pages/ResidentialDeliveryRates.aspx`.

IESO (2013a). *A GUIDE TO ELECTRICITY CHARGES FOR BUSINESS*. IESO, `https://www.ieso.ca/imoweb/siteShared/electricity_charges.asp?sid=bi`.

IESO (2013b). *IESO market data*. `http://www.ieso.ca/imoweb/marketData/marketData.asp`.

Kariniotakis, G., Soultanis, N., Tsouchnikas, A. I., Papathanasiou, S., and Hatziargyriou, N. (2005). Dynamic modeling of microgrids. In *Future Power Systems, 2005 International Conference on*, pages 7 pp.–7.

Katiraei, F. and Iravani, M. (2006). Power management strategies for a microgrid with multiple distributed generation units. *Power Systems, IEEE Transactions on*, **21**(4), 1821–1831.

Katiraei, F., Iravani, R., Hatziargyriou, N., and Dimeas, A. (2008). Microgrids management. *Power and Energy Magazine, IEEE*, **6**(3), 54–65.

Kyocera (2013). *KYOCERA to Start Exclusive Sales in Japan of New Residential-Use Energy Management System Combining Solar Power with Li-ion Battery Storage Unit*. Kyocera Corporation, `http://global.kyocera.com/news/2012/0102_qpaq.html`.

LaCommare, K. H. and Eto, J. H. (2006). Cost of power interruptions to electricity consumers in the United States (US). *ENERGY*, **31**(12), 1845–1855.

LaRose, B. (2013). *DENSO Develops Vehicle-to-Home Power Supply System for Electric Vehicles*. DENSO Corporation, `http://www.densocorp-na.com/newsroom/show/id/433`.

Lasseter, B. (2001). Microgrids [distributed power generation]. In *Power Engineering Society Winter Meeting, 2001. IEEE*, volume 1, pages 146–149 vol.1.

Lasseter, R. (2002). Microgrids. In *Power Engineering Society Winter Meeting, 2002. IEEE*, volume 1, pages 305–308 vol.1.

Lasseter, R. (2011). Smart distribution: Coupled microgrids. *Proceedings of the IEEE*, **99**(6), 1074–1082.

Li, Y. W. and Kao, C.-N. (2009). An accurate power control strategy for power-electronics-interfaced distributed generation units operating in a low-voltage multibus microgrid. *Power Electronics, IEEE Transactions on*, **24**(12), 2977–2988.

Majumder, R., Ghosh, A., Ledwich, G., and Zare, F. (2009). Load sharing and power quality enhanced operation of a distributed microgrid. *Renewable Power Generation, IET*, **3**(2), 109–119.

MOE (2013). *Ontario's Long-Term Energy Plan*. Ontario Ministry of Energy, `http://www.energy.gov.on.ca/docs/LTEP_2013_English_WEB.pdf`.

Mohamed, F. and Koivo, H. (2007). Online management of microgrid with battery storage using multiobjective optimization. In *Power Engineering, Energy and Electrical Drives, 2007. POWERENG 2007. International Conference on*, pages 231–236.

Mohamed, Y. A. R. I. and El-Saadany, E. (2008). Adaptive decentralized droop controller to preserve power sharing stability of paralleled inverters in distributed generation microgrids. *Power Electronics, IEEE Transactions on*, **23**(6), 2806–2816.

Morais, H., Kádár, P., Faria, P., Vale, Z. A., and Khodr, H. (2010). Optimal scheduling of a renewable micro-grid in an isolated load area using mixed-integer linear programming. *Renewable Energy*, **35**(1), 151–156.

NSN (2013). *Zero CO2 off-grid site solution for E-Plus*. Nokia Solutions and Networks, `http://nsn.com/system/files/document/en_zero_co2_site_solution_for_e-plus_-_whitepaper_versmold_1.3.pdf`.

OEB (2013). *Electricity Prices, Time-of-use (TOU) Prices*. Ontario Energy Board, `http://www.ontarioenergyboard.ca/OEB/Consumers/Electricity/Electricity+Prices`.

Olivier Tremblay, L.-A. D. (2009). Experimental validation of a battery dynamic model for ev applications. *World Electric Vehicle Journal*, **3**.

OPA (2013). *About microFIT*. Ontario Power Authority, `http://microfit.powerauthority.on.ca/about-microfit`.

Parisio, A. and Glielmo, L. (2011). Energy efficient microgrid management using model predictive control. In *Decision and Control and European Control Conference (CDC-ECC), 2011 50th IEEE Conference on*, pages 5449–5454.

Pawel Malysz, Shahin Sirouspour, A. E. (2013). *MILP-based Rolling horizon Control for Microgrids with Battery Storage*. McMaster University.

Pogaku, N., Prodanovic, M., and Green, T. C. (2007). Modeling, analysis and testing of autonomous operation of an inverter-based microgrid. *Power Electronics, IEEE Transactions on*, **22**(2), 613–625.

R. Lasseter, A. Akhil, C. M. and Stephens, J. (2002). *White paper on integration of distributed energy resources the CERTS microgrid concept*. Available: certs.lbl.gov/pdf/50829-app.pdf.

Sao, C. and Lehn, P. (2008). Control and power management of converter fed microgrids. *Power Systems, IEEE Transactions on*, **23**(3), 1088–1098.

SMA (2013). *Sunny Backup*. SMA Solar technology AG, `http://files.sma.de/dl/8016/SBUPSYS-DEN102020.pdf`.

Tsikalakis, A. and Hatziargyriou, N. (2008). Centralized control for optimizing microgrids operation. *Energy Conversion, IEEE Transactions on*, **23**(1), 241–248.

UnitedNation (2013). *Sustainable Energy for All Initiative*. United Nation, `http://www.un.org/wcm/content/site/sustainableenergyforall/home/Initiative`.

USEIA (2012). Primary energy consumption by source and sector, 2010. Technical report, U. S. Energy Information Administration.

Villalva, M., Gazoli, J., and Filho, E. (2009). Comprehensive approach to modeling and simulation of photovoltaic arrays. *Power Electronics, IEEE Transactions on*, **24**(5), 1198–1208.

Wang, C., Xiao, Z., and Wang, S. (2008). Synthetical control and analysis of microgrid. *Automation of Electric Power Systems*, **7**, 024.

Youli, S., Litifu, Z., and Nagasaka, K. (2009). Efficiency of micro grid with storage battery in reliability, economy and environment assessments. *International Journal of Electrical and Power Engineering*, **3**(3), 154–162.

Yubing, D., Yulei, G., Qingmin, L., and Hui, W. (2008). Modelling and simulation of the microsources within a microgrid. In *Electrical Machines and Systems, 2008. ICEMS 2008. International Conference on*, pages 2667–2671.

Zamora, R. and Srivastava, A. K. (2010). Controls for microgrids with storage: Review, challenges, and research needs. *Renewable and Sustainable Energy Reviews*, **14**(7), 2009–2018.